Proceedings of the
Fourth International Symposium on
Vibrations of Continuous Systems

Skiddaw Hotel
Keswick, Lake District, England
July 7-11, 2003

View of Keswick and Derwentwater

CONTENTS

PREFACE

The International Symposium on Vibrations of Continuous Systems is a forum for leading researchers from across the globe to meet with their colleagues and present both old and new ideas on the field. Each participant has been encouraged to either present results of recent, significant research or to reflect on some aspect of the vibration of continuous systems which is particularly interesting, unexpected, or unusual. This latter type of presentation – of which there are several in the program – was proposed to encourage participants to draw on understanding obtained through – in many cases – decades of research.

The location of the Fourth ISVCS is in one of the most beautiful places in Great Britain – the Lake District National Park in north-west England. Here, within 30 miles (50 km) of the coast you can find all of England's highest mountains, topped by Scafell Pike at 3205 feet (977 m), 16 lakes and many picturesque villages, joined by winding mountain roads and footpaths. All of the mountain summits can be reached on foot. For the more adventurous there are spectacular ridge walks, such as Striding Edge on Helvellyn, and classic rock climbs on Great Gable and the Langdale Pikes.

This Proceeding contains short summaries of the presentations to be made at the Symposium and short biographical sketches submitted by many of the participants.

Editor
Ali H. Nayfeh

Reviewing Editors
Charles W. Bert
Peter Hagedorn
Yoshihiro Narita

General Chairman
Arthur W. Leissa

Analysis and Measurement of Flex Circuit Vibration in Hard Disk Drives

Matthew Brake and Jonathan Wickert
Department of Mechanical Engineering
Carnegie Mellon University
Pittsburgh, PA 15213
wickert@cmu.edu

The density of hard disk drives, as measured by the number of data bits stored within a unit area, has grown at a historical rate of about 60% per year. With that trend, greater demands have been placed on the mechanical design of drives in terms of low vibration. In particular, the vibration of flex circuits has been identified as a disturbance which transmits motion to the read/write heads at a high enough frequency that servo performance becomes degraded. A flex circuit connects the stationary electronic components in a hard disk drive to the rotating arm that positions the read/write heads above data tracks on the disk (Figure 1). These structures are formed as a laminate of polyimide, adhesive, and copper conductors (Figure 2), and while previously viewed as a lightweight appendix, they today couple dynamically with the arm and produce undesirable off-track position errors.

The vibration of flex circuits and the roles played by such design parameters as the circuit's finite curvature, laminated structure, free length, and boundary conditions at the arm and electronics block are discussed. Deformation of the circuit is described in the context of the initial unstressed shape, configurations in which stresses set and relax in response to elevated temperature, equilibrium, and small amplitude vibration free and forced vibration about equilibrium. The vibration model (Figure 3) treats arm rotation and planar motion of the circuit in the directions tangent and normal to equilibrium. Non-linearity associated with finite curvature, spring-back, and the arm's geometry and inertia are also incorporated to predict natural frequencies, mode shapes, and coupling factors between the circuit's and the read/write head's motion.

For one case study, Figure 4 depicts the mechanism's lowest four modes. Each element of the figure is annotated to indicate the natural frequency and the ratio η of displacements between the read/write head and the flex circuit. Although the η are only a fraction of a percent in modes two and higher, they have design implications owing to the required precision. A data track on a typical performance drive may be only 500 nm wide, with positioning tolerances of ±25 nm for write and ±50 nm for read operations. In a situation where the flex circuit vibrates at an amplitude corresponding to one thickness (114 μm) and with the coupling ratio being 0.23% in the second mode, the head responds with amplitude 260 nm, some ten times above the drive's write inhibit limit. By using laser interferometry and the test stand shown in Figure 5, the natural frequencies of each mode was measured at 356 Hz, 844 Hz, and 1.23 kHz, values in good agreement with the predictions. Despite layered construction and attachments to the arm and electronics block, the flex circuit presents the light damping ratio of only 1.1% in the second mode.

Figure 6 depicts trends for the coupling ratio in a parameter study of free length. For the (even) modes two, four, and six, η is relatively insensitive to design changes in L. On the other hand, η has a zero crossing for the (odd) modes three and five at nearly the same free length (26 mm). At that design point, the natural frequencies have increased relative to their nominal values, but the displacement ratios for several modes have either been reduced significantly or driven to zero. Such trade-offs may be desirable in certain applications. In short, the distributed parameter vibration model can be used to advantage for optimizing flex circuit designs with respect to vibration transmission. Parameter and optimization studies in the model's other degrees of freedom, and the implications of flex circuit vibration for control system design, are subjects of current investigation.

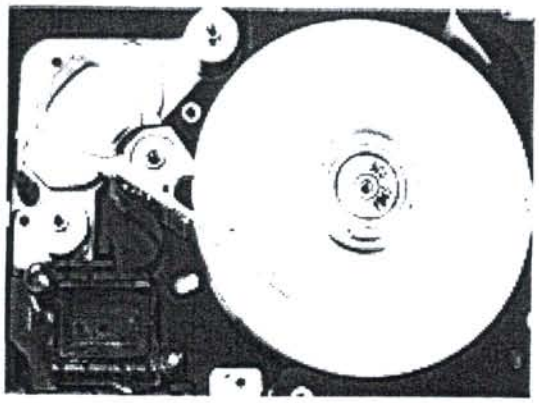

Figure 1: The flex circuit routes electrical leads from the arm and heads to an electronics block.

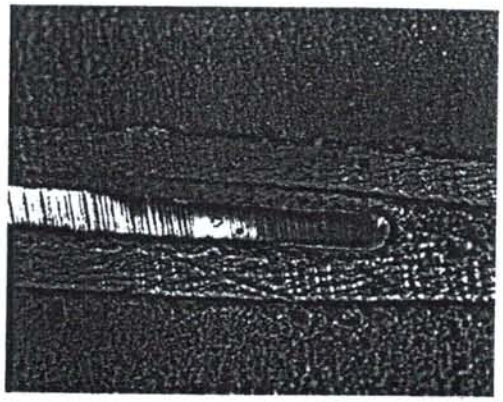

Figure 2: Microscope image of the cross-section depicting the conductor, adhesive, and polyimide.

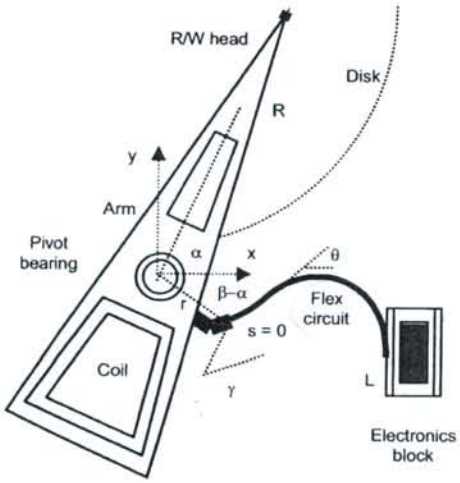

Figure 3: Model for circuit and arm vibration.

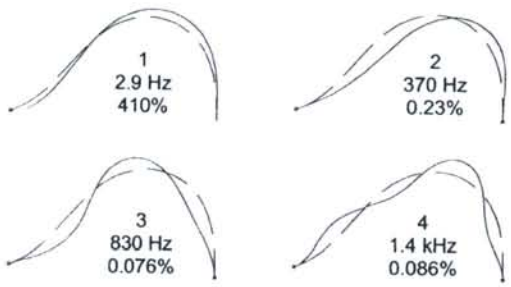

Figure 4: First four arm and flex circuit modes.

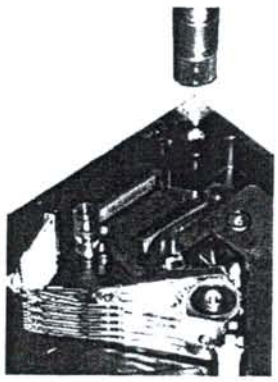

Figure 5: Laser interferometer head and prism for measuring flex circuit natural frequencies.

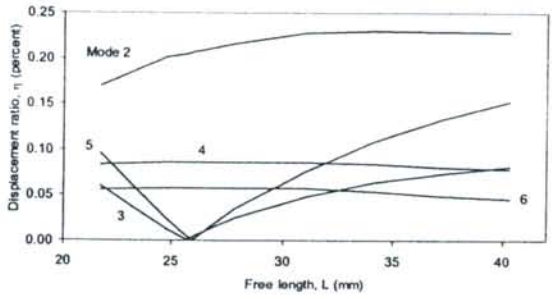

Figure 6: Variation of coupling factors with length.

Vibrations of Layered Plates and Shells via Reissner's Mixed Variational Theorem

Erasmo Carrera
Aerospace Department, Politecnico di Torino,
e.mail: carrera@polito.it

Due to the non-continuous distribution of thermo-mechanical material properties in the thickness direction, multilayered plates and shells exhibit a directional nature of the elastic behavior which is exploited to design material as well as structural properties. Examples of multilayered structures used in modern aerospace, automotive and ship vehicles are laminated constructions made of anisotropic composite materials, sandwich panels, layered structures used as thermal protection or intelligent structural systems embedding piezo-layers. In the recent years, considerable attention is being paid to the development of appropriate two dimensional shell theories that can accurately describe the static and dynamic response of multilayered anisotropic thick structures. Exhaustive overviews are given in the articles by Kapania [1], Noor, Burton and Bert [2] and Soldatos and Timarci [3].

The directional nature of multilayered structures leads to higher transverse shear and normal stress deformabilty with respect to traditional, isotropic cases. Therefore, further requisites become essential towards a reliable modeling of layered structures. Among them, the fulfillment of both continuity of displacement (so called Zig-Zag effect, ZZ) and transverse shear and normal stresses (so called interlaminar continuity, IC) at the interface between two adjacent layers are such a necessary desideratum. In [4] these requisites were referred to by the acronyms C_z^0–requirements which state that both displacements and transverse stress components are C^0–continuous functions in the thickness shell coordinate z.

A comprehensive model of anisotropic multilayered plates and double curved shells fulfilling *a priori* the interlaminar continuity requirements for the transverse shear and transverse normal stress as well as the static conditions on the bounding surfaces of the shell is developed in this paper. To this end, Reissner's Mixed Variational Theorem (RMVT) [5], is employed to derive the equations governing the dynamic equilibrium and compatibility of each layer, while the interlaminar continuity conditions are used to drive the equations at the multilayered level. Both Layer-Wise (LW) and Equivalent Single Layer (ESL) models have been addressed. Following Reddy [6] it is intended that those theories which preserve the number of variables independent of the number of layers are herein denotes as ESLM, while those theories in which the same variables are independent in each layer, are denoted as LWM. Classical displacement formulations based on Principle on Virtual Displacements (PVD) and related Layer-Wise (LW) and Equivalent Single Layer (ESL) models have been derived for comparison purposes. Linear up-to forth order thickness expansions are discussed and closed form exact solution are presented. The evaluations of transverse stress effects have been conducted by comparing constant, linear and higher order distributions of transverse displacement components in the plate thickness directions. No assumptions have been made concerning the terms of type thickness to radii shell ratio h/R. All these modelings are have been written in a unified manner by referring to techniques that have been developed by the Author in earlier works [4].

Table 1. Circular frequency parameter $\omega\sqrt{\frac{a^4\rho}{E_T h^2}}$ of Simply supported square plates Cross-ply skew-symmetric and symmetric laminates (layers of equal thickness); $\frac{E_L}{E_T} = 40$, $\frac{G_{LT}}{E_T} = \frac{G_{Lz}}{E_T} = .50$, $\frac{G_{TT}}{E_T} = .60$, $\nu_{LT} = \nu_{Lz} = \nu_{TT} = 0.25$.

			0/90		
a/h	2	4	10	20	100
LM4	4.703	7.345	10.088	10.859	11.151
LM3	4.680	7.332	10.087	10.859	11.151
LM2	4.668	7.329	10.087	10.859	11.151
LM1	4.136	5.660	6.666	6.874	6.947
EMZC3	4.685	7.444	10.144	10.877	11.152
EMZC2	4.727	7.395	10.119	10.896	11.152
EMZC1	4.672	7.340	10.106	10.878	11.170
EMC4	4.731	7.408	10.124	10.871	11.152
EMC3	4.799	7.527	10.181	10.889	11.153
EMC2	4.711	7.352	10.092	10.861	11.152
EMC1	11.259	7.822	10.367	11.018	11.259
LD4	4.707	7.345	10.088	10.859	11.152
LD3	4.710	7.346	10.088	10.859	10.152
LD2	4.803	7.519	10.178	10.888	11.153
LD1	4.848	7.562	10.215	10.921	11.184
EDZ3	4.780	7.490	10.165	10.884	11.152
EDZ2	4.838	7.545	10.189	11.891	11.153
EDZ1	4.848	7.562	10.215	10.921	11.184
ED4	4.745	7.425	10.132	10.874	11.152
ED3	4.883	7.647	10.235	10.906	11.154
ED2	4.968	7.701	10.254	10.911	11.154
ED1	5.544	8.314	10.545	11.072	11.261

The availability of this large amount of modelings permits one to furnish a quite exhaustive assessment of available 2D theories for vibrational analysis of multilayered, composites plates and shells. Free vibrational response of layered, simply supported plates, cylindrical and spherical shells made of isotropic as well as orthotropic layers has been analyzed in this work.

Two examples of assessments are considered in Tables 1 and 2, which are related to plates and shells, respectively. Acronyms have been used to denote different theories: L/E, denotes LW and ESL variables descriptions, respectively; M and D, denotes formulation based on RMVT and PVD, respectively; Z and C denote inclusions of Zig-Zag Effects and IC, respectively; 1,2,3,4 denote the order of the used expansion in the thickness layer/multilayer direction; d denote discarding of σ_{zz} effects.

Comparison of frequency predictions based upon the implemented two-dimensional models with a number of results spread throughout the specialized literature and obtained via other models reveals that this advanced model provides results in excellent agreement with the ones based on 3-D elasticity theory, and better as compared to the ones, violating the interlaminar stress continuity requirements. Further conclusions are listed below. – The possibility of describing a priori interlaminar continuous transverse normal stress σ_{zz} makes the mixed theories more attractive with respect to other available modelings. – A very accurate description of the vibrational response of highly anisotropic, thick and very plates and shells requires layer-wise description. – Any refinements of classical models are meaningless, unless the effects of interlaminar continuous transverse shear and normal stresses are both taken into account in a multilayered shell theory.

Table 2. Effect of radii to length ratio R/a on $\omega \times a^2\sqrt{\frac{\rho}{h^2 E_T}}$. Comparison to exact solution and to other refined analyses. a/h=10, m=1, n=2 unless given in brackets. Three layered ringed shell 0/90/0, h_1=h_3=$h_2/2$. E_L/E_T=25, G_{LT}/E_T=.5, G_{TT}/E_T=.2, ν_{LT}=ν_{TT}=.25.

R_β/a	5	10	50	100
Exact	10.305^{14}	10.027^{22}	9.834^{24}	9.815
PAR_{ds}	10.496	10.223	10.032^{26}	10.013
HYP_{ds}	10.496	10.226	10.036^{26}	10.018
UNI_{cs}	10.462	10.187	9.996^{28}	9.977
PAR_{cs}	10.329	10.051	9.859^{26}	9.840
HYP_{cs}	10.328	10.050	9.858^{26}	9.839
— *Present Analysis*				
LW4	10.305^{14}	10.027^{22}	9.834^{26}	9.815
EMZC3	10.309^{14}	10.030^{22}	9.837^{26}	9.818
EMZC3d	10.324^{14}	10.043^{22}	9.847^{26}	9.828
EMZC1	10.328^{14}	10.046^{22}	9.850^{26}	9.831
EMZC1d	10.328^{14}	10.046^{22}	9.850^{26}	9.831
ED3	10.453^{14}	10.179^{22}	9.988^{26}	9.969
ED3d	10.470^{14}	10.193^{22}	9.998^{26}	9.979
ED1	11.318^{14}	11.063^{20}	10.879^{20}	10.862
ED1d	11.318^{14}	11.064^{20}	10.880^{20}	10.862

References

[1] R.K. Kapania, 1989, A Review on the Analysis of Laminated Shells. *Journal of Pressure Vessel Technology* , **111**, pp.88-96.

[2] A.K. Noor, S. Burton, C.W. Bert,1996, Computational model for sandwich panels and shells. *Applied Mechanics Review* , **49**, pp 155-199.

[3] K.P. Soldatos, T. Timarci, 1993, A unified formulation of laminated composites, shear deformable, five–degrees–of–freedom cylindrical shell theories. *Composite Structures* , **25**, pp.165-171.

[4] E. Carrera , 2001, Developments, ideas and evaluations based upon the Reissner's mixed theorem in the modeling of multilayered plates and shells, *Applied Mechanics Review* , **54**, 301–329.

[5] E. Reissner, 1984, On a certain mixed variational theory and a proposed applications. *International Journal for Numerical Methods in Engineering* , **20**,pp 1366-1368.

[6] J.N. Reddy, 1997, *Mechanics of Laminated Composite Plates, Theory and Analysis*. CRC Press.

SOME EXACT SOLUTIONS AND ENERGY CONSIDERATIONS FOR VIBRATING PIEZOELECTRIC CONTINUA

Piotr CUPIAL
Institute of Mechanics and Machine Design, Cracow University of Technology
Al. Jana Pawla II-go 37, 31-864 Krakow, Poland. Email: cupial@mech.pk.edu.pl

Piezoelectric elements find wide application in different areas of vibration measurement and generation, as well as in other engineering applications. Nowadays, the interest in these materials has increased due to their use as sensor and actuator elements in smart structures. Piezoelectric elements also hold a promise of application in microelectromechanical systems (MEMS).

Much physical insight into the behavior of vibrating piezoelectric continuous systems can be gained by studying three-dimensional exact solutions. This will be discussed by studying two problems: the longitudinal vibration of a piezoelectric rod poled along its axis and exact three-dimensional vibration of the flexural and through-thickness modes of a rectangular plate polarized normal to its middle plane. The type of problem that needs to be solved is illustrated by the following equation of longitudinal free vibration of a piezoelectric rod poled along its axis (z-axis) and the corresponding electrostatic equation:

$$\begin{cases} \rho A \dfrac{\partial^2 u}{\partial t^2} - \dfrac{\partial}{\partial z}\left[A\left(E\dfrac{\partial u}{\partial z} + \hat{e}_{33}\dfrac{\partial \phi}{\partial z}\right)\right] = 0 \\ \dfrac{\partial}{\partial z}\left[\hat{e}_{33}\dfrac{\partial u}{\partial z} - \hat{\epsilon}_{33}\dfrac{\partial \phi}{\partial z}\right] = 0 \end{cases} \tag{1}$$

to be solved with the following boundary conditions specified at the rod ends:

$$\begin{cases} u = 0 \quad \text{or} \quad E\dfrac{\partial u}{\partial z} + \hat{e}_{33}\dfrac{\partial \phi}{\partial z} = 0 \\ \phi = 0 \quad \text{or} \quad \hat{e}_{33}\dfrac{\partial u}{\partial z} - \hat{\epsilon}_{33}\dfrac{\partial \phi}{\partial z} = 0 \end{cases}$$

Here u is the longitudinal displacement, ϕ -electrostatic potential, A is the cross-sectional area and ρ is the mass density. The other quantities appearing in equations (1) are defined as follows:

$$E = c_{33} - \frac{2(c_{13})^2}{c_{11}+c_{12}}, \qquad \hat{e}_{33} = e_{33} - \frac{2\,c_{13}\,e_{31}}{c_{11}+c_{12}}, \qquad \hat{\epsilon}_{33} = \epsilon_{33} + \frac{2(e_{31})^2}{c_{11}+c_{12}} \tag{2}$$

The elasticity constants (c_{ij}), piezoelectric coefficients (e_{ij}) and the dielectric permittivity (ϵ_{33}), appearing on the right side of expressions (2), are defined in references [1] and [2].

The properties of structures undergoing flexural vibration are well illustrated by considering a 3-D solution of the free vibration of a rectangular plate, as discussed in detail in reference [3]. The full formulation of the problem and a stable numerical algorithm are discussed there. It is pointed out that the algorithm details have been found to be very important in the case when the wavelength along both plate sides is the same, as discussed in detail in reference [3]. The calculated distribution of the mechanical and electrical fields over the plate thickness is

very useful in the construction of approximate plate theories (an alternative approach used in the construction of approximate theories of piezoelectric plates and shells is the asymptotic solution discussed in reference [4]).

Even though analytical solutions provide important information about the behavior of piezoelectric continuous systems, further insight into the effect of electromechanical coupling can be gained using energy considerations. The balance of energy will be discussed for a general 3-D continuum and plots shown of the time variation of different kinds of energy for the case of a vibrating rod and a rectangular plate. As a direct result of the energy balance for the special case of free vibration, one can obtain expressions for Rayleigh's quotient. For the longitudinal vibration of a piezoelectric rod, described by equations (1), the following extension of the classical expression for Rayleigh's quotient is obtained:

$$\omega_n^2 = \frac{\int_0^l A\{E[U_n'(z)]^2 + \hat{e}_{33} U_n'(z)\Phi_n'(z)\}dz}{\int_0^l \rho A U_n^2(z)\,dz} \tag{3}$$

Formula (3) and similar expressions derived for more complex free vibration problems allow efficient analysis of the electromechanical coupling in vibrating piezoelectric elements.

Even though a number of solutions of vibration problems are available for linear piezoelectric continua, very few results exist for non-linear problems. Geometrical non-linearity becomes important when large displacement effects can not be neglected. The general non-linear theory of elastic dielectrics, which includes non-linear piezoelectricity as a special case, is described in references [5] and [6]. Equivalent equations of non-linear piezoelectricity can also be obtained from a more general theory of electromagnetic interaction developed in reference [7]. Even though the general non-linear formulation is well established now, new numerical solutions of the non-linear piezoelectric vibration problems are needed and are being studied now by the author. Some important points of the modeling of non-linear piezoelectric behavior will be briefly discussed. Additional work is also needed for the physical non-linearity brought about by the ferroelectric behavior, characteristic e.g. of many piezoelectric ceramics, and described in references [8] and [9].

References

1. Tiersten, H.F., *Linear Piezoelectric Plate Vibrations,* Plenum Press, New York, 1969.
2. Nowacki, W., *Electromagnetic Effects in Deformable Solids (in Polish),* Polska Akademia Nauk (Polish Academy of Sciences), Warsaw, 1983.
3. Cupial, P., Exact Three-Dimensional Natural Vibration Analysis of a Piezoelectric Rectangular Plate, to appear in the *Proceedings of the Eighth International Conference on Recent Advances in Structural Dynamics*, Southampton, England, 2003.
4. Rogacheva, N.N., *The Theory of Piezoelectric Shells and Plates*, CRC Press, Boca Raton, 1994.
5. Toupin, R.A., The Elastic Dielectric, *J. Rat. Mech. Anal., 5*, 1956, 849-915.
6. Toupin, R.A., A Dynamical Theory of Dielectrics, *Int. J. Engng. Sci.*, **1**, 1963, 101-126.
7. Eringen, A.C. and Maugin, G.A., *Electrodynamics of Continua*, Springer-Verlag, 1990.
8. Jaffe, B., Cook W.R. and Jaffe, H., *Piezoelectric Ceramics*, Academic Press, London, New York, 1971.
9. Kamlah, M., Tsakmakis C., Phenomenological Modeling of the Non-Linear Electromechanical Coupling in Ferroelectrics, *International Journal of Solids and Structures*, Vol.36, 1999, 669-695.

On the Free In-Plane Vibration Analysis of Rectangular Plates by the Method of Superposition

by
D. J. Gorman
Professor Emeritus
Dep,t of Mech. Eng.
University of Ottawa
Ottawa, Canada K1N 6N5

Numerous technical papers related to the free lateral vibration of rectangular plates have appeared in the literature over the decades and more are added every year. The situation with regard to in-plane vibration of these same plates is quite different. This is no doubt due, in large part, to the fact that natural frequencies of in-plane vibration are typically much higher and often beyond the normal range of available excitation frequencies.

It has been drawn to the writer's attention, nevertheless, that there are many realistic situations where such in-plane vibrations play an important role. Examples are the interaction between high frequency acoustic wave excitation and the in-plane vibration of ship hull segments. It has also been reported by people working in these areas that, due to the high frequencies involved, numerical methods, such as the finite element method, do not function satisfactorily when applied to such problems.

As a result of these experiences the writer has been encouraged to explore the obtaining of analytical type solutions to these problems based on the superposition method, a method he has exploited successfully over the years to solve numerous rectangular plate lateral vibration problems.

In this paper the analytical procedure and preliminary computed results are described in detail. As a demonstration problem, the free in-plane vibration of the completely free rectangular plate is analyzed in detail. It is shown that the possible vibration modes fall into three well defined families, as a result of considering symmetry, or anti-symmetry, about the plate central axis.

The work begins by development of the two governing differential equations and expressions for the in-plane stresses, in dimensionless form. It is shown that only one quarter of the actual plate need be analyzed. For each of the mode families a pair of edge-driven forced vibration problems (building blocks) are developed and superimposed. Constants appearing in the combined solution, as a result of Fourier coefficients utilized in representation of the distributed harmonic edge forces, are so constrained as to satisfy the prescribed boundary conditions and thereby generate the eigenvalue matrix from which eigenvalues and free vibration mode shape information is obtained.

Convergence is rapid and excellent agreement is obtained when computed results are compared with those reported in an earlier paper where solution was obtained by

means of a Rayleigh-Ritz approach utilizing a quite complicated set of shape functions [1].

Analogy between the superposition method as employed here and as employed earlier to resolve plate lateral vibration problems becomes apparent. Results are also presented for in-plane vibration of fully clamped and simply supported rectangular plates.

The analytical approach to be taken when seeking solutions to numerous practical problems such as plates with attached masses, plates with fixed point supports, and plates with elastic edge support, etc., are discussed. This will form the subject of future research work. One is able to conclude that the superposition method is ideally suited for resolving vast families of in-plane rectangular plate free vibration problems.

Reference:

[1] Bardell, N. S., Langley, R. S., and Dunsdon, J. M., (1996), 'On the free in-plane vibration of isotropic rectangular plates', Jour. of Sound and Vibration, 191(3), pp 459-467.

Timoshenko Beams of Rectangular Cross-Section

James R. Hutchinson
Department of Civil and Environmental Engineering
University of California, Davis CA 95616

Introduction

In a recent paper [1] a general expression for the shear coefficient in Timoshenko beams was derived using energy principles. Stephen [2] had derived the same expression for the shear coefficient in an entirely different way in 1980. For a rectangular beam that (S-H) shear coefficient is highly dependent on the aspect ratio of the beam. This research investigates the reasons for that behavior by comparing the results for a simply-supported beam with a new series solution that satisfies the three-dimensional linear-elastic equations. Comparisons are also made to both elementary and Mindlin plates. It is found that the Mindlin and three-dimensional solutions match very closely. That good match allows the use of the Mindlin plate solutions as a basis of comparison for the free-free beam. For both simply supported and free beams the use of the S-H coefficient gave a good match only when the aspect ratio was small (< 2) or the wave length was large. A shear coefficient which would cause matching of the three-dimensional and Mindlin solutions would have to be a function of the wave length as well as the aspect ratio. Physical explanations are given for the high dependence on aspect ratio and for the dependence on wave length.

In Ref. [1], Timoshenko beam theory, using the S-H coefficient, was compared to a three-dimensional series solution of the governing equations for the completely free beam. The three-dimensional solution was described in Hutchinson and Zillmer [3]. Because of limitations on the number of terms required in the series, the convergence was not assured. The limitation was caused by the size of the characteristic matrix. The order of the characteristic matrix for the three-dimensional problem was $N_xN_y + N_yN_z + N_zN_x$, where N_x, N_y, and N_z are the number of terms in the x, y and z directions. It was found, however that a series solution could be developed for the simply supported case for which the order of the matrix would be $N_x + N_y$. This solution can then be easily made to converge to any required accuracy.

Beam Solutions

The Timoshenko Beam equations and solutions, as well as the elementary Euler-Bernoulli beam equations and their solutions, appear in most textbooks on structural dynamics. The S-H coefficient for a beam of rectangular cross-section is given in Ref. [1]. The Timoshenko beam equations solved with the above shear coefficient is referred to as the Timoshenko solution in this paper.

Three-Dimensional Solution

The three-dimensional solution for the simply supported beam is formed from a subset of the solution forms derived in Ref. [3]. The assumption of simple supports allows one to directly satisfy boundary conditions on the ends. The remaining boundary conditions requiring satisfaction are:

$$\tau_{xy}(a,y,z) = 0,\ \tau_{xz}(a,y,z) = 0,\ \tau_{xy}(x,b,z) = 0,\ \tau_{yz}(x,b,z) = 0,\ \sigma_x(a,y,z) = 0 \text{ and } \sigma_y(x,b,z) = 0$$

Two series are formed from linear combinations of the solution forms in Ref. [4]. The series are chosen so that the four boundary conditions on shear stress are identically satisfied. The two boundary conditions on normal stress are satisfied by setting:

$$\int_0^b \sigma_x(a,y)\sin\beta y dy = 0 \quad \text{and} \quad \int_0^a \sigma_y(x,b)\cos\alpha x dx = 0$$

where $\alpha = (n - 1)\pi/a \qquad n = 1,2,3...N_x$

and $\beta = (2n - 1)\pi/2b \qquad n = 1,2,3...N_y$

Evaluation of these integrals yields a matrix eigenvalue equation whose order is $N_x + N_y$.

Plate Solutions

The elementary plate has been treated in a number of books and papers. The SS-F-SS-F Mindlin plate was treated by Mindlin et al. [4] in 1956. In that paper, the authors assume a shear coefficient of $\pi^2/12$ and build that into their equations (3) [4]. This drawback is easily remedied by going back to Mindlin's 1951 paper [5] and rederiving these equations. The completely free Mindlin plate was solved by Gorman and Ding [6] in 1996 using

the superposition method. Rather than trying to duplicate their solution, a new solution for this problem was developed. This new series solution compares well with the Gorman and Ding results.

The choice of a best shear coefficient in the Mindlin theory has also received some attention. In his 1951 paper, Mindlin [5] determined the shear coefficient in two different ways. In a 1984 paper, Hutchinson [7] found that by matching the solution for straight crested flexural waves at long wave lengths a shear coefficient of 5/(6 - ν) could be found. In Ref. [7] this shear coefficient was found best for the lower frequency modes of circular plates. It also provided the closest match to the three-dimensional theory developed in this paper.

Results for Simply Supported Beams

Fig. 1 shows the beam of length 2c, width 2a, and depth 2b. In Fig. 2, the values of a shear coefficient, which would make the Timoshenko beam theory match the three-dimensional solution, are shown as dashed lines. The solid line is the S-H coefficient plotted as a function of the width-to-depth ratio. The numbers on the dashed lines indicate the length-to-depth ratio. It can be seen that when the length-to-depth ratio is very small the shear coefficient varies little with the width-to-depth ratio, whereas, for larger length-to-depth ratios the shear coefficient shows much greater variation and approaches the S-H shear coefficient.

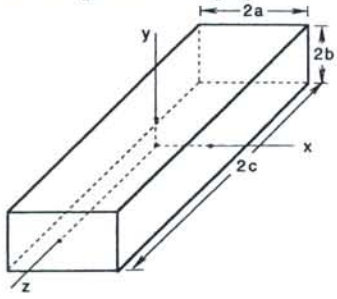

Fig. 1 Coordinates and Dimensions of the beam.

A perhaps better comparison is made with the natural frequencies in Figs. 3 and 4. These figures show the variation of frequency with the width-to-depth ratio for length-to-depth ratios of 10 and 20. The figures show the frequencies as determined by the three-dimensional solution (3D), the Mindlin plate solution (M), the Timoshenko beam solution (TB), the elementary plate solution (EP), and the elementary beam solution (EB). The Mindlin solutions plotted as essentially the same curve as the three-dimensional solutions and are labeled (3D-M).

One very interesting result, which is most evident in Figs. 3 and 4, is that the elementary plate solution shows a frequency variation with the width-to-depth ratio that mimics the frequency variation for the three-dimensional solution. The elementary plate formulation does not allow for any shear deformation or rotary inertia. This leads to the conclusion that the large variation of frequency with the width-to depth ratio is not brought about by the presence of shear deformation and rotary inertia, but rather by plate action. There are several things occurring in plates that aren't usually accounted for in beam theory. One, is the effect of the variation of the displacement v (y direction) as a function of the width coordinate x on the inertia. This effect was accounted for in Ref. [1] by assuming full anticlastic curvature and leads to increased inertia and hence a lowering effect on the frequency. Another plate effect is the twisting effect that produces the twisting moment. This effect was accounted for in Ref. [1] by the assumption of the shear stress distribution found from the three-dimensional solution of the tip loaded cantilever. This assumption gave shear stresses τ_{xz} as well as τ_{yz}. It is the τ_{xz} stress that produces the resultant twisting moment in the plate. This twisting produces a stiffening effect and hence increases the frequency. The combination of these plate effects leads to a rise in the frequency with an increase in the width-to-depth ratio. The plate effects are the main cause of the frequency variation with the width-to-depth ratio.

The plate effects also lead to an understanding of the reasons for the divergence of the Timoshenko beam equations from the three-dimensional solution for large width-to-depth ratios and short wave length-to-depth ratios. For a short wide beam, the end effects are significant. In the central portion of the beam, the variation of the displacement with x will be greatly suppressed and the plate will not be able to take on the full anticlastic curvature. The twisting effect will also be greatly suppressed. To see this more clearly Figs. 5 and 6 show the displacement $v(x,0,0)$ calculated from Mindlin plate theory (M) and from the Timoshenko beam theory (T) using the displacement field assumed in Ref. 1. Fig. 5 is for a length-to-depth ratio of 20 and a width-to-depth ratio of 2. Fig. 6 is also for a length-to-depth ratio of 20 but with a width-to-depth ratio of 10. It can be seen that for the width-to-depth ratio of 2 the displacements match but for a width-to-depth ratio of 10 they differ greatly. The twisting moments were also calculated for these cases and again they matched for the width-to-depth ratio of 2, but were greatly different for a width-to-depth ratio of 10 which is shown in Fig. 7.

Results for Free-Free Beams

In Fig. 8 the values of a shear coefficient, which would make the Timoshenko beam solution match the Mindlin plate solution for the first mode. This figure shows the same type of behavior as for the simply sup-

ported case. Similar results were found for higher modes. Figs. 9 and 10 show the variation of frequency with the width-to-depth ratio for length-to-depth ratios of 10 and 20. Again it can be seen that the elementary plate variation mimics the Mindlin plate variation. All conclusions drawn for the simply supported beam are equally valid for all modes of the free-free beam.

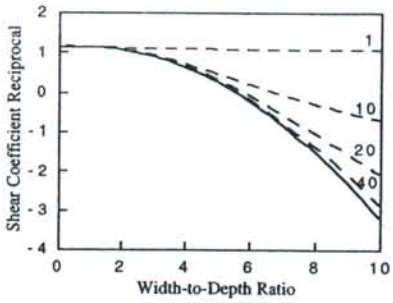

Fig. 2. SS Beam — S-H coefficient.
- - - Coefficients for match, L/D of 1, 10, 20 and 40.

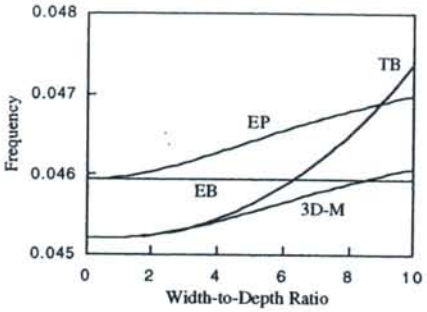

Fig. 3. SS Beam L/D = 10

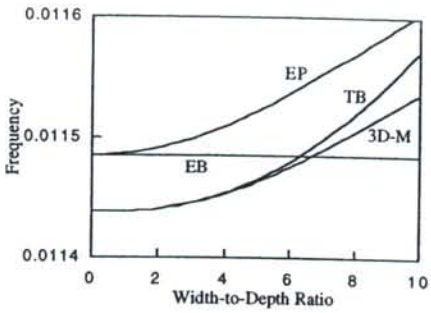

Fig. 4. SS Beam L/D = 20

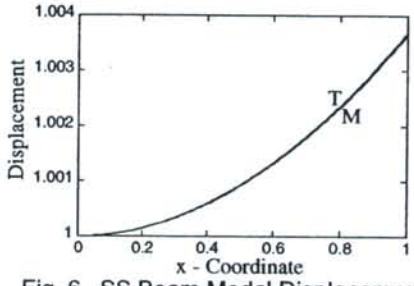

Fig. 6. SS Beam Modal Displacement y = z = 0, L/D = 20, W/D = 2

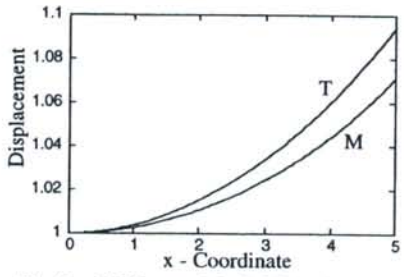

Fig. 7 SS Beam Modal Displacement y = z = 0, L/D = 20, W/D = 10

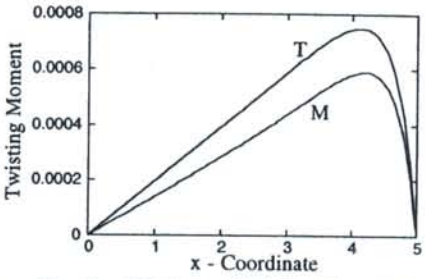

Fig. 8. SS Beam Twisting Moment y = z = 0, L/D = 20, W/D = 10

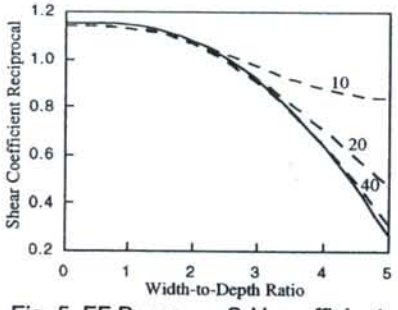

Fig. 5. FF Beam — S-H coefficient.
- - - Coefficients for match, L/D of 10, 20 and 40.

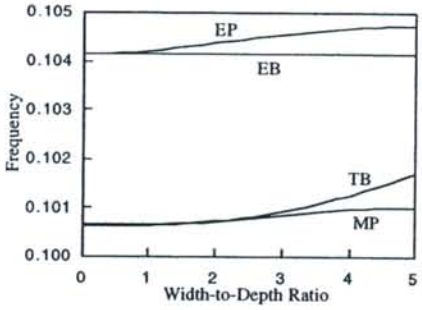

Fig. 6. FF Beam L/D = 10

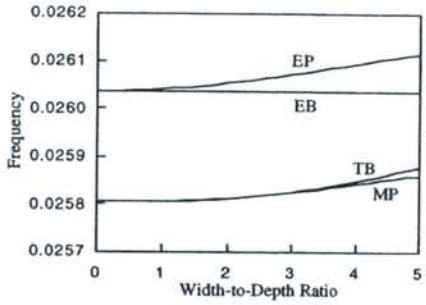

Fig. 7. FF Beam L/D = 20

Dedication

This paper is dedicated to the memory of Scott D. Zillmer 1956-2002

References

[1] Hutchinson, J. R., 2001, "Shear Coefficients for Timoshenko Beam Theory," ASME *J. Appl. Mech.*, **68**, pp. 87-92.

[2] Stephen, N. G., 1980, "Timoshenko Shear Coefficient from a beam Subjected to a Gravity Loading," ASME *J. Appl. Mech.*, **47**, pp. 87-92.

[3 Hutchinson, J. R. and Zillmer, S. D., 1983, "Vibration of a Free Rectangular Parallelepiped," ASME *J. Appl. Mech.*, **50**, pp. 123-130.

[4] Mindlin, R. D., Schacknow, A. and Deresiewicz, H.,1956, "Flexural Vibrations of Rectangular Plates," ASME *J. Appl. Mech.*, **23**, pp. 430-436.

[5] Mindlin, R. D., 1951, "Influence of Rotatory Inertia and Shear on Flexural Motions of Isotropic, Elastic Plates," ASME *J. Appl. Mech.*, **18**, pp. 31-38.

[6] Gorman, D. J. and Ding, Wei, 1996, "Accurate Free Vibration Analysis of the Completely Free Rectangular Mindlin Plate," *Journal of Sound and Vibration*, **189**, pp. 341-353.

[7] Hutchinson, J. R., 1984, "Vibrations of Thick Free Circular Plates, Exact Versus Approximate Solutions," ASME *J. Appl. Mech.*, **51**, pp. 581-585.

Vibration in Wide Woodcutting Bandsaws

Stanley. G. Hutton
Department of Mechanical Engineering
University of British Columbia
Vancouver, B. C., Canada V6T 1Z4
hutton@mech.ubc.ca

Background

Large bandmills are widely used as head rigs for primary breakdown in the lumber industry. Such bandmills may have 10 ft diameter wheels with the bandsaw being of the order of 12in wide. The speed of the bands is of the order of 10,000ft/min. It is very common for such mills to suffer from the problem of washboarding in which a sinusoidal (washboard) pattern is left on the cut boards. This problem is similar to the problem of chatter in metal cutting. The washboarding is caused by high frequency oscillations of the travelling band and experience shows that the washboarding pattern occurs in two distinct forms as shown in Figure 1. There is not a gradual change in the pattern between these two cases, either one or the other is obtained or both together. A further important feature of the washboarding is that it is extremely sensitive to the depth of cut. Below a certain depth of cut no washboarding will occur and above this depth it will always occur.

Figure 2 and 3 show the vibration spectra of the travelling blade measured at a space fixed location beneath the cut for the two types of washboarding pattern. In these spectra the wheels are rotating at 520rpm (corresponding to a linear speed of 8,170 ft/min) and the tooth passing frequency is 933Hz (the number of teeth that pass a space fixed point in one second).

Further parameters of interest are:

a) the band passing frequency (the number of times that a specific point on the band passes a space fixed point) which has the value in this case of 4Hz. If for example there was one bent tooth or a high spot in the blade then the cutting force applied to the blade would experience a variation at the band passing frequency.
b) the wheel rotation frequency which, in this case has a value of 8.7 Hz. As the wheels will not be perfectly round or perfectly balanced it can be expected that there will be some axial excitation of the band at the wheel rotation frequency and its harmonics

In general, therefore, one might expect variations in the cutting forces applied to the blade at:

a) the tooth passing frequency, due to the fact that in general the number of teeth in the cut will be changing at this frequency and also due to the impact of each tooth as it enters the cut;
b) the band pass frequency and its harmonics due to any imperfections in the teeth or band geometry;
c) the wheel rotation frequency and its harmonics.

Excitation Mechanisms

Of interest is the determination the excitation mechanisms that are responsible for the washboarding and an analysis that quantifies this behaviour. Possible mechanisms are:

a) Resonance with forced excitation at the tooth passing frequency
b) Instability due to the regenerative character of the lateral flank cutting force.
c) Instability due to parametric excitation of the axially loaded band

d) Forced vibration due to modulation of the forces at the tooth passing frequency by the band pass frequency

The paper presented will discuss these various mechanisms and draw some conclusions as to the mechanisms actually responsible for the washboarding.

(a) Type I

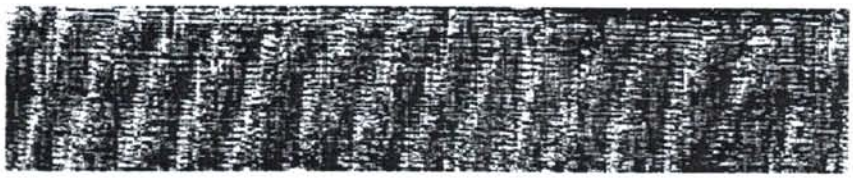

(b) Type II

Figure 1 Bandsaw washboarding patterns

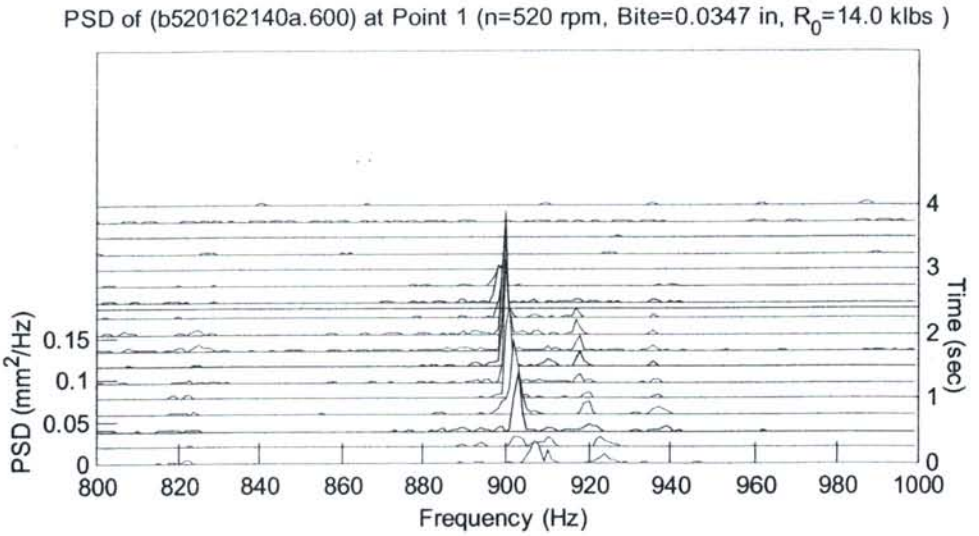

Figure 2 Displacement Power Spectrum of the Blade for Type I Washboarding.

(18G2H2 n=520 rpm, $Bite$=0.035 in, D_{cut}=9.5 in, R_0=14 klbs, Douglas fir, Type I: W_{ext}=0.95, P_x=44 mm, P_y=31 mm, heavy)

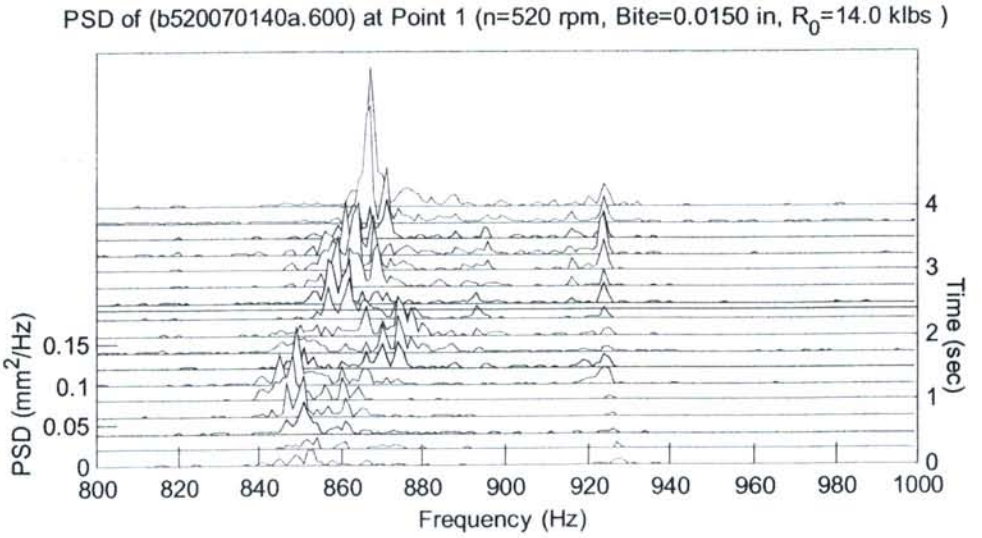

Figure 3 Displacement Power Spectrum of the Blade for Type II Washboarding.

(18G2H2 n=520 rpm, $Bite$=0.015 in, D_{cut}=9.5 in, R_0=14 klbs, Douglas fir, Type II: W_{ext}=1.0, P_x=5.8mm, P_y=29 mm, heavy)

GOOD OLD DYNAMIC STABILITY FUNCTIONS FOR BEAMS CARRYING RIGID BODIES

S. Ilanko
Department of Mechanical Engineering, University of Canterbury, New Zealand

Structural and civil engineers have been using static and dynamic stability functions for the determination of buckling loads and natural frequencies for several decades. In vibration analysis, this method is convenient for determining the "exact natural frequencies" of continuous systems. Their potential use in the analysis of some common mechanical systems such as beams carrying rigid bodies seems to have been largely overlooked by researchers. Several recent journal publications contain derivations of the boundary condition equations from first principles. These problems could have been solved more conveniently using the dynamic stability functions, which give the same result.

Static stability functions [1,2] have been used extensively by civil engineers for calculating the critical loads of frameworks. Dynamic stability functions, based on the method outlined by Velestos & Newmark [3] were published in Table form by Armstrong [4]. Dynamic stability functions that took into account the effect of axial force (geometric stiffness) were presented by Mohsin and Sadek [5]. An experimental study on skeletal frames in partial fulfilment of the requirements of an undergraduate project [6] at the university of Manchester by the author, gave results that were in agreement with the theoretical results using the functions presented in [5]. This method was extended to solve a variety of continuous systems which contain tapered beams, Timoshenko beam-columns and folded plates to name a few, [7-9] by Williams and a number of other researchers. The method involves setting up a dynamic-stiffness matrix that takes into account the stiffness and mass distribution in a structure. The coefficients of this matrix are transcendental functions of the frequency and the natural frequencies may be calculated by searching the roots of the determinantal equation. This may be done by several trial and error search procedures, which should use the Wittrick-Williams algorithm [10,11] to ensure convergence on the required eigenvalue.

The purpose of this paper is to show how the method can be applied to a connected system containing rigid bodies. Dynamic stability functions are stiffness coefficients that give the actions (forces or moments) at the ends of a structural member (beam, bar, shaft etc) due to a prescribed unit displacement (translation or rotation at one of the ends of the structural member). For the present paper, we will confine our investigation to the study of a particular beam system. If one end of a beam of length L and flexural rigidity EI is pinned and the other end is given a rotation θ, then the resulting actions at its ends are expressed in terms of a nominal elastic stiffness factor $k = EI/L$ and dynamic stability functions, S", Q" and q", as shown in Figure 1a. Similarly the actions due to a translation δ of the end that isn't pinned, are expressed in terms of dynamic stability functions, Q", q", T" and t" as shown in Figure 1b.

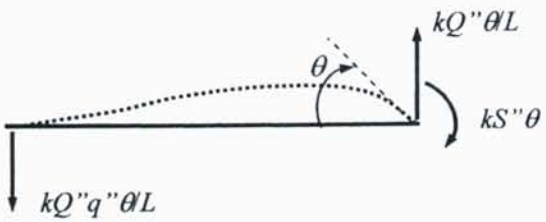

Figure 1a

Figure 1b

Figure 2 shows a system that has been used by the author as an example in his vibration lectures. Results for the special case of $e_1=e_2$ have been published by Kopmaz and Telli [12]. This consists of two Euler-Bernoulli beams that are pinned at one end and rigidly connected to a rigid body at the other end. The centroid of the rigid body is located at distances e_1 and e_2 from the tips of the left and right beams. The body has a mass m_0 and moment of inertia I_0 about its centroid. The beams on the

left and right will be referred to as beam 1 and beam 2 and have the following properties. Mass per unit length, m_1, m_2, flexural rigidities EI_1, EI_2, and lengths L_1, L_2. Non-dimensional frequency parameters for the beams λ_1 and λ_2 are given by $\lambda_i^4 = \dfrac{m_i \omega^2 L_i^4}{EI_i}$ for i=1,2 ...(1)

Let the centre of mass be given a translation Δ and rotation ϕ. This would result in translations of $\Delta - e_2\phi$ and $\Delta + e_1\phi$ of the left and right side beams at the point of attachment. They would both rotate by angle ϕ. Using the dynamic stability functions we can express the moment and force at the ends of the two beams. By Newton's third law of motion, the forces and moments acting on the rigid body are therefore equal and opposite to those on the beams. These actions are shown in Figures 3a,b and c. Using the free-body diagram of the rigid body in Figure 3b, we can find the net force and moment, and by applying Newton's second law of motion we can the derive equations of motion.

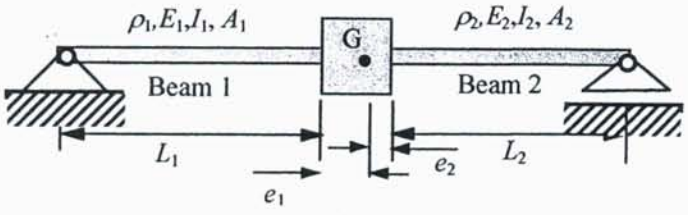

Figure 2

Figure 3a

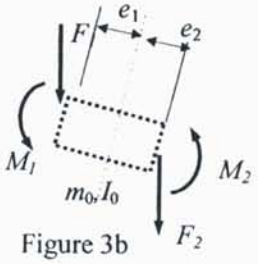

Figure 3b

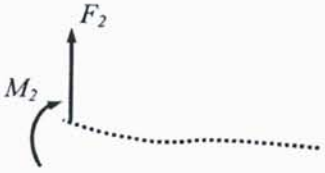

Figure 3c

The net forces in beams 1 and 2 are given by:

$$F_1 = \left(\frac{k_1 Q_1''}{L_1}\right)\phi + \left(\frac{k_1 T_1''}{L_1^2}\right)(\Delta + e_1\phi) \quad ...(2)$$

$$F_2 = \left(-\frac{k_2 Q_2''}{L_2}\right)\phi + \left(\frac{k_2 T_2''}{L_2^2}\right)(\Delta - e_2\phi) \quad ...(3)$$

The moments in beams 1 and 2 are given by:

$$M_1 = (k_1 S_1'')\phi + \left(\frac{k_1 Q_1''}{L_1}\right)(\Delta + e_1\phi) \text{ and} \quad ...(4)$$

$$M_2 = (k_2 S_2'')\phi - \left(\frac{k_2 Q_2''}{L_2}\right)(\Delta - e_2\phi) \quad ...(5)$$

Now let us consider the motion of the rigid-body (see free-body diagram in Figure 3b).Applying Newton's second law of motion in the translational and rotational sense gives the following equations:

$$F_1 + F_2 = -m_0\ddot{\Delta} = \omega^2 m_0 \Delta \quad ...(6)$$

$$M_1 + M_2 + F_1 e_1 - F_2 e_2 = -I_0\ddot{\phi} = \omega^2 I_0 \phi \quad ...(7)$$

Substituting equations (2-5) into equations (6) and (7), and some simplification including non-dimensionalisation of the parameters result in the following matrix equation:

$$[D]\{\delta\} = \{0\} \quad ...(8)$$

where the coefficients of the dynamic stiffness matrix [D] are defined by:

$$D_{1,1} = \gamma^3 T_1'' + \psi T_2'' - \alpha\gamma^3\lambda_1^4; \quad D_{1,2} = D_{2,1} = \gamma^3 Q_1'' - \psi\gamma Q_2'' + \gamma^3\eta_1 T_1'' - \psi\eta_2 T_2''; \quad D_{2,2} = \gamma^3\left(S_1'' + 2\eta_1 Q_1''\right) + \psi\left(\gamma^2 S_2'' + 2\gamma\eta_2 Q_2''\right) + \left(\gamma^3 T_1''\eta_1^2 + \psi T_2''\eta_2^2\right) - \gamma^3\beta\lambda_1^4 \quad \ldots(9a\text{-}d)$$

Here, $\gamma = \frac{L_2}{L_1}$; $\psi = \frac{EI_2}{EI_1}$; $\alpha = \frac{m_0}{m_1 L_1}$; $\beta = \frac{I_0}{m_1 L_1^3}$; $\eta_i = \frac{e_i}{L_1}$ for i=1,2; ...(10a-e)

The dynamic stability functions are [4]:

$$S_i'' = \frac{2\lambda_i \sinh(\lambda_i)\sin(\lambda_i)}{\left(\cosh(\lambda_i)\sin(\lambda_i) - \cos(\lambda_i)\sinh(\lambda_i)\right)} \text{ for } i\text{=1,2;} \quad \ldots(11a)$$

$$Q_i'' = \frac{\lambda_i^2\left(\cosh(\lambda_i)\sin(\lambda_i) + \cos(\lambda_i)\sinh(\lambda_i)\right)}{\left(\cosh(\lambda_i)\sin(\lambda_i) - \cos(\lambda_i)\sinh(\lambda_i)\right)} \text{ for } i\text{=1,2;} \quad \ldots(11b)$$

$$T_i'' = \frac{2\lambda_i^3 \cosh(\lambda_i)\cos(\lambda_i)}{\left(\cosh(\lambda_i)\sin(\lambda_i) - \cos(\lambda_i)\sinh(\lambda_i)\right)} \text{ for } i\text{=1,2;} \quad \ldots(11c)$$

and $\lambda_2 = \lambda_1\gamma\sqrt[4]{\frac{\zeta}{\psi}}$, where $\zeta = \frac{m_2}{m_1}$ ...(12a,b)

The natural frequency parameters are found be solving $|D| = 0$. As expected the solution of this equation agrees with results of [12] which can be generated using a computer program available on www [13]. Natural frequencies of other mechanical systems consisting of skeletal elements, rigid bodies and partial support restraints may also be determined conveniently in this manner. With the use of W-W algorithm, the use of dynamic stability functions remains a convenient method for natural frequencies of continuous systems.

Acknowledgement

The author is grateful to Professor Fred Williams for his comments on the first draft and his continued encouragement and input into this paper.

References

1. Livesley, R.K. and Chandler, D.B.., Stability functions for structural frameworks, Manchester University Press, 1962.
2. Horne, M.R., and Merchant, W., The stability of frames, Pergamon Press, 1965.
3. Veletsos, A.S. and Newmark, H.M., 1957, Natural frequencies of continuous flexural members. Trans. ASCE 122:249-85.
4. Armstrong, I.D., Tables of dynamic stiffnesses and carry-over factors, Civil Engineering Department, Heriot-Watt University, Edinburgh.
5. Mohsin, M.E. and Sadek, E.A., The distributed mass-stiffness technique for dynamical analysis of complex frameworks, The Structural Engineer, Vol 46 (11), 1968.
6. Ilanko, S., Vibration of axially loaded triangulated frameworks, BSc Project Report, Department of Civil Engineering, University of Manchester, 1978.
7. Banerjee, J.R., and Williams, F.W., Exact Bernoulli-Euler dynamic stiffness matrix for a range of tapered beams, Int. J. Num. Meth. Eng., 21, 1985, p2289.
8. Capron, M.D., and Williams, F.W., Exact dynamic stiffnesses for an axially loaded uniform Timoshenko member embedded in an elastic medium, J Sound Vib, 124, 1988, p453.
9. Williams, F.W., Computation of natural frequencies and initial buckling stresses of prismatic plate assemblies, J Sound Vib, 21, 1972, p87.
10. Williams, F.W., and Wittrick, W.H., An automatic computational procedure for calculating natural frequencies of skeletal structures, Int. J. Mech. Sci., 12, 1970, p781.
11. Wittrick, W.H., and Williams, F.W.,Natural vibrations of thin, prismatic, flat-walled structures, IUTAM Symposium, Lie`ge, 1970, P563.
12. O. Kopmaz and S. Telli 2002 *Journal of Sound and Vibration* 252(2), 370-384, doi:10.1006/jsvi.2001.3702.
13. S. Ilanko 2000 Vibration Research Resources Page, www.geocities.com/ilanko/vibration.htm

Simultaneous Optimal Design of Stiffness and Damping of a Flexible Structure Reinforced by FRP Sheets

Yukinori KOBAYASHI, Gen YAMADA and Mitsuaki NAKANISHI
Division of Mechanical Science, Hokkaido University, Sapporo, 060-8628 Japan
E-mail:kobay@eng.hokudai.ac.jp

INTRODUCTION

This paper presents an optimal design of a flexible structure reinforced by fiber-reinforced plastic (FRP) sheets that takes into account both stiffness and damping characteristics. The optimal design of laminated plates for maximum fundamental frequency and maximum buckling load has been investigated by many researchers[(1)~(4)]. We propose an objective function that takes into account both stiffness and damping characteristics. To improve vibration characteristics, the design variables are determined by using an optimization technique. The validity of the present method is verified by numerical examples and by comparison with results of experiments.

MODELING

Figure 1 shows a cantilever steel plate reinforced by FRP sheets. The coordinates (x,y,z) in the middle plane of the plate are taken as shown in the figure. Length and thickness of the steel plate are L_s and t_s and those of an FRP sheet are L_f and t_f, respectively. The principal directions of elasticity are denoted by L and T, and θ is the angle between L and x axes of an FRP. The widths of the steel plate and the FRP sheet are both b. Expressing the loss factor of steel as δ_s, the complex modulus of longitudinal elasticity of steel can be written as $E_s' = E_s(1+j\delta_s)$. The complex modulus of longitudinal elasticity E_L', E_T' of the principal directions and the complex modulus of transverse elasticity G_{LT}' can be obtained by the rule of mixtures.

The whole plate is divided into two parts with different thickness, and each part of the plate is denoted by element 1 and element 2 from the clamped edge. Only element 1 is reinforced by FRP sheets. Denoting the transverse displacements of these elements as W_1 and W_2, we propose displacement functions that satisfy the continuous conditions of displacement and slope at the stepped line located at $x = -L_s/2 + L_f$,

$$\begin{aligned} W_1(x,y) &= \sum_{i=0}^{I}\sum_{l=0}^{I} a_{il}\, x^i (x+\frac{L_s}{2})^2 y^l, \\ W_2(x,y) &= \sum_{i=0}^{I}\sum_{l=0}^{I} b_{il}\, x^i (x+\frac{L_s}{2}-L_f)^2 y^l + W_1 \mid_{x=-\frac{L_s}{2}+L_f} \\ &+ (x+\frac{L_s}{2}-L_f)\frac{\partial W_1}{\partial x} \mid_{x=-\frac{L_s}{2}+L_f}, \end{aligned} \tag{1}$$

where a_{il} and b_{il} are unknown coefficients. For free vibration, the transverse displacement may be expressed as

$$w(x,y,t) = W_n(x,y)\sin(\omega t) \quad (n=1,2), \tag{2}$$

where ω is the frequency in radians/second. Applying the Ritz method, complex eigenvalues ω^2 are obtained as follows:

$$\omega'^2 = \omega^2(1+j\eta), \tag{3}$$

where η is the loss factor corresponding to the natural frequency ω.

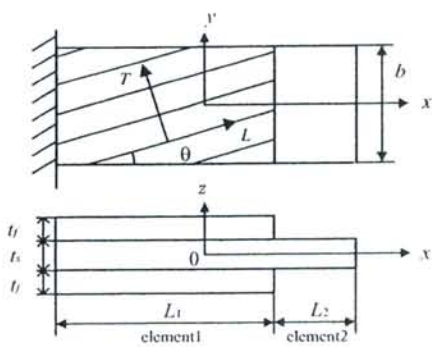

Figure 1: Cantilever plate model

The transverse displacement w can be expressed as

$$w(x,y,t) = \sum_{k=1}^{p} W_{n,k}(x,y)q_k(t) \quad (n=1,2) \tag{4}$$

by using the time function q_k and the mode shape function $W_{n,k}$ given by the Ritz method. The equation of motion is derived by using Lagrange's equation. Assuming that an external force with amplitude F is applied at $(x,y) = (L_s/2, b/2)$, the generalized force Q_k is expressed as

$$Q_k = FW_{2,k}(L_s/2, b/2) = Ff_k. \tag{5}$$

The state equation of the kth mode is expressed in the matrix form

$$\begin{aligned} \dot{\boldsymbol{X}}_k &= \boldsymbol{A}_k\boldsymbol{X}_k + \boldsymbol{B}_kF, \\ \boldsymbol{A}_k = \begin{bmatrix} 0 & 1 \\ -\omega_k^2 & -2\zeta_k\omega_k \end{bmatrix} &, \quad \boldsymbol{B}_k = \{0,\ f_k\}^T,\ \boldsymbol{X}_k = \{q_k, \dot{q}_k\}^T, \end{aligned} \tag{6}$$

where $\zeta_k = \eta_k/2$ is the equivalent viscous damping of the kth mode. Assuming that displacement is measured at $(x,y) = (L_s/2, -b/2)$, the output equation can be written as

$$w_k = \boldsymbol{C}_k\boldsymbol{X}_k = \{c_k,\ 0\}\boldsymbol{X}_k, \tag{7}$$

where w_k is the displacement of the kth mode and $c_k = W_{2,k}(L_s/2,\ -b/2)$.

OPTIMAL DESIGN

In this study, an optimal design is formulated as a general optimal problem such that design variables are determined by minimizing an objective function under constrained conditions. To improve the stiffness and damping characteristics of the initial design structure, we propose the following objective function:

$$J_1 = \int_0^{\omega_{max}} \boldsymbol{X}_1^{*T}(\omega)\boldsymbol{P}\boldsymbol{X}_1^*(\omega)d\omega, \tag{8}$$

where $\boldsymbol{X}_1^*(\omega)$ is obtained by Laplace transformation of Eq.(6) when $k=1$. $\boldsymbol{P}$ is the symmetric, positive definite solution of the algebraic Riccati equation:

$$\begin{aligned} \boldsymbol{A}_1^T\boldsymbol{P} + \boldsymbol{P}\boldsymbol{A}_1 + \tilde{\boldsymbol{C}}_1{}^T\tilde{\boldsymbol{C}}_1 &= 0, \\ \tilde{\boldsymbol{C}}_1 = \{\tilde{c_1},\ 0\}, \quad \tilde{c_1}{}^2 = \int_{-\frac{b}{2}}^{\frac{b}{2}} \{ \int_{-\frac{L_s}{2}}^{-\frac{L_s}{2}+L_f} W_{1,1}^2 dx &+ \int_{-\frac{L_s}{2}+L_f}^{\frac{L_s}{2}} W_{2,1}^2 dx \} dy. \end{aligned} \tag{9}$$

The optimized structure obtained by using Eq.(8) is denoted by OPT 1.

Another optimized structure obtained by using the objective function:

$$J_2 = \int_0^{\omega_{max}} \boldsymbol{X}_1^{*T}(\omega)\tilde{\boldsymbol{C}}_1{}^T\tilde{\boldsymbol{C}}_1\boldsymbol{X}_1^*(\omega)d\omega, \tag{10}$$

is denoted by OPT 2. The value of Eq.(10) decreases even if the damping ratio does not increase, because the response can be reduced across a broad frequency by increasing the stiffness of the structure. The optimized structure obtained by using Eq.(8) under the condition $L_f = L_s$ is denoted by OPT 3. That is, OPT 3 is reinforced by FRP sheets over the whole surface of the steel plate. Moreover, we consider the optimized structure OPT 4 by using

$$J_4 = \frac{\omega_{1,\text{init}}}{\omega_1}, \tag{11}$$

where subscript "init" denotes the initial structure before ompitization. The first natural frequency is maximized in the case of OPT 4.

Table 1: Specification of the plate

E_s	206 GPa	ρ_s	7.86×10^3kg/m^3
E_c	230 GPa	ρ_c	1.8×10^3kg/m^3
δ_s	0.0036	ρ_m	1.3×10^3kg/m^3
ν_s	0.3	ν_c	0.31
ν_m	0.38	t_s	0.6 mm
t_f	0.72 mm	b	130 mm
L_s	600 mm	L_f	400 mm

Table 2: Design pamameters

	OPT 1	OPT 2	OPT 3	OPT 4
L_2(mm)	298	327	600	317
t_f(mm)	0.66	0.60	0.33	0.62
θ	23.9°	16.5°	21.0°	0.0°

Table 3: Numerical results

	init	OPT 1	OPT 2	OPT 3	OPT 4
ω_1(rad/s)	8.82	16.7	18.8	12.4	23.2
ζ_1(%)	0.18	0.86	0.63	0.42	0.22
H_1(dB)	-17.0	-26.8	-28.9	-24.4	-31.5
H_2(dB)	31.8	8.47	9.05	16.8	15.8

Table 4: Experimental results

	init	OPT 1	OPT 2	OPT 3	OPT 4
ω_1(rad/s)	8.82	15.8	18.8	11.6	22.8
ζ_1(%)	0.18	0.96	0.54	0.50	0.24
H_1(dB)	-17.0	-26.6	-29.2	-24.6	-31.5
H_2(dB)	31.8	7.42	10.0	15.8	13.5

Thickness t_f, length L_f and fiber angle θ of the FRP sheet are used as design variables. FRP sheets are symmetrically pasted on both sides of the steel plate as $(\theta/steel/\theta)$. A constrained condition for the mass of the structure is introduced as

$$Mass = \alpha Mass_{\text{init}}, \tag{12}$$

The simple genetic algorithm (GA) is used to seek the minimum value of each objective function. For these structures, parameter α in Eq.(12) is set to 1.2. The simple GA is also used to identify unknown material parameters of FRP in experiments.

RESULTS AND DISCUSSIONS

Table 1 shows the specifications of the initial plate. After optimization using the objecting functions, the design variables are determined as in Table 2. Table 3 and 4 show numerical and experimental results, respectively. Values of H_1 and H_2 are static displacement $H_1 = \boldsymbol{C}_1\boldsymbol{X}_1^*(0)$ and resonance peak of the first natural frequency $H_2 = \boldsymbol{C}_1\boldsymbol{X}_1^*(\omega_1)$. The damping ratio of OPT 1 is the largest of all optimized structures and the natural frequency of OPT 1 is almost twice of the initial design structure in each table. It is verified in the experiments that the stiffness and damping characteristics of OPT 1 are improved effectively.

CONCLUSIONS

The complex eigenvalues of a stepped plate reinforced by FRP sheets were obtained by the Ritz method. Displacement functions that satisfy continuous conditions of displacement and slope at the stepped line were used as admissible functions. The objective function to improve both the stiffness and damping characteristics was proposed. Vibration characteristics of the optimized structure were superior to those of a structure whose fundamental frequency was maximized.

REFERENCES

(1) Bert, C.W., Optimal Design of a Composite-Material Plate to Maximize its Fundamental Frequency, *J. Sound Vib.*, **50**-2 (1977), 229-237.

(2) Miki, M. and Sugiyama, Y., Optimum Design of a Laminated Composite Plates Using Lamination Parameters, *AIAA Journal*, **31**-5 (1993), 921-922.

(3) Fukunaga, H., Sekine, H., and Sato, M., Optimal Design of Symmetric Laminated Plates for Fundamental Frequency, *J. Sound Vib.*, **171**-2 (1994), 219-229.

(4) Narita, Y., and Zhao, X., An Optimal Design for the Maximum Fundamental Frequency of Laminated Shallow Shells, *Int. J. Solids Structures.*, **35**-20 (1998), 2571-2583.

Coupled Belt-Pulley Vibration in Serpentine Drives with Belt Bending Stiffness

Lingyuan Kong and Robert G. Parker
Department of Mechanical Engineering
The Ohio State University

Abstract

Serpentine belt drives with a long, flat, multi-ribbed belt have been widely used in passenger automobiles and heavy duty trucks. Crankshaft torque pulsations due to engine combustion and dynamic accessory torques excite rotational vibration of the pulleys, which can be further transmitted to the belt spans although no direct transverse forces are applied on these belt spans. Large transverse belt vibrations from pulley-belt coupling produce noise, reduce belt life, and cause belt slip. Treating the belt spans as strings [1] can only explain the coupling between the tensioner and the two adjacent belt spans.

Modeling the belt as a moving beam [2,3] provides a mechanism whereby pulley rotation couples to transverse vibration of all spans, including those bounded by fixed centers. This provides an explanation for the span vibrations observed in practice. This mechanism applies at engine idle speeds where parametric excitation mechanisms based on higher frequency excitation do not apply. In this study, free vibration analysis of a continuous/discrete model [2,3] of a prototypical serpentine belt system (Figure 1) is investigated which shows the modal coupling between all spans and pulleys.

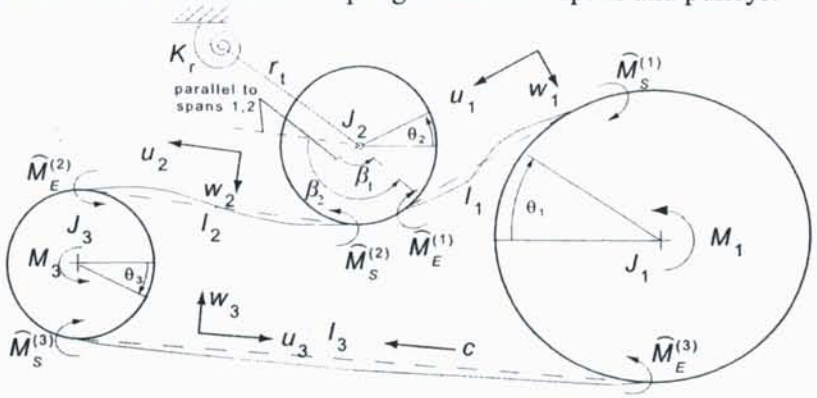

Figure 1. A prototypical three-pulley serpentine belt drive.

Application of Hamilton's principle yields the equations of motion (1)-(9) for the system in Figure 1.

$$m(w_{i,tt} - 2cw_{i,xt} + c^2 w_{i,xx}) - [(P_i + \tilde{P}_i)w_{i,x}]_{,x} + EIw_{i,xxxx} = 0 \qquad i = 1,2,3 \tag{1}$$

$$w_1(0,t) = 0 \quad EIw_{1,xx}(0,t) = \frac{EI}{r_1} \quad w_1(l_1,t) = r_t\theta_t \cos\beta_1 \quad EIw_{1,xx}(l_1,t) = -\frac{EI}{r_2} \tag{2}$$

$$w_2(0,t) = r_t\theta_t \cos\beta_2 \quad EIw_{2,xx}(0,t) = -\frac{EI}{r_2} \quad w_2(l_2,t) = 0 \quad EIw_{2,xx}(l_2,t) = \frac{EI}{r_3} \tag{3}$$

$$w_3(0,t)=0 \quad EIw_{3,xx}(0,t)=\frac{EI}{r_3} \quad w_3(l_3,t)=0 \quad EIw_{3,xx}(l_3,t)=\frac{EI}{r_1} \tag{4}$$

$$J_1\ddot{\theta}_1+\tilde{P}_1r_1-\tilde{P}_3r_1=\tilde{M}_1 \quad J_2\ddot{\theta}_2-\tilde{P}_1r_2+\tilde{P}_2r_2=0 \quad J_3\ddot{\theta}_3-\tilde{P}_2r_3+\tilde{P}_3r_3=\tilde{M}_3 \tag{5}$$

$$J_t\ddot{\theta}_t+k_r\theta_t+[mcw_{1,t}(l_1)+(P_1-mc^2+\tilde{P}_1)w_{1,x}(l_1)+EIw_{1,xxx}(l_1)]r_t\cos\beta_1+(mc^2-\tilde{P}_1)r_t\sin\beta_1$$
$$-[mcw_{2,t}(0)+(P_2-mc^2+\tilde{P}_2)w_{2,x}(0)+EIw_{2,xxx}(0)]r_t\cos\beta_2-(mc^2-\tilde{P}_2)r_t\sin\beta_2=0 \tag{6}$$

$$\tilde{P}_1=\tfrac{EA}{l_1}(-r_2\theta_2+r_1\theta_1-r_t\theta_t\sin\beta_1+\int_0^{l_1}\tfrac{1}{2}w_{1,x}^2dx) \tag{7}$$

$$\tilde{P}_2=\tfrac{EA}{l_2}(-r_3\theta_3+r_2\theta_2+r_t\theta_t\sin\beta_2+\int_0^{l_2}\tfrac{1}{2}w_{2,x}^2dx) \tag{8}$$

$$\tilde{P}_3=\tfrac{EA}{l_3}(-r_1\theta_1+r_3\theta_3+\int_0^{l_3}\tfrac{1}{2}w_{3,x}^2dx) \tag{9}$$

Linearization about the equilibria leads to a conservative gyroscopic system [3]. Solving the corresponding continuous/discrete eigenvalue problem is complicated by the coupled inhomogeneous boundary conditions (2) and (3). For example, to overcome this difficult, a modification of Holzer's method is used in [1] to determine a boundary condition error function akin to a characteristic equation. But due to singularities and numerical ill-behavedness of the characteristic equation, the accuracy and completeness of the calculated natural frequencies can not be guaranteed. Further, this method can not be directly applied to the present model because it needs the explicit form of a traveling string eigenfunction and no such a form exists for a moving beam.

In the work, a spatial discretization is developed for the system with belt bending stiffness and non-trivial equilibria. A key step is to reformulate the span deflections in terms of variables satisfying homogeneous boundary conditions

$$y_1=w_1-\tfrac{r_t}{l_1}x\cos\beta_1\theta_t \quad y_2=w_2+\tfrac{r_t}{l_2}(x-1)\cos\beta_2\theta_t \quad y_3=w_3 \tag{10}$$

$$y_i(0,t)=0 \;\; y_i(1,t)=0 \;\; y_{i,xx}(0,t)=0 \;\; y_{i,xx}(1,t)=0,\; i=1,2,3 \tag{11}$$

Note all span axial coordinates are non-dimensionized to the interval [0,1].

Additional mathematical formulations cast the hybrid system into a structured extended operator form

$$\mathbf{M}\ddot{\mathbf{Y}}+\mathbf{G}\dot{\mathbf{Y}}+\mathbf{K}\mathbf{Y}=\mathbf{F}, \qquad \mathbf{Y}=\{y_1,y_2,y_3,\theta_1,\theta_2,\theta_3,\theta_t\}^T \tag{12}$$

$$<\mathbf{Y},\mathbf{U}>=\int_0^1 y_1\bar{u}_1dx+\int_0^1 y_2\bar{u}_2dx+\int_0^1 y_3\bar{u}_3dx+\sum_{i=1}^{3}\theta_i\bar{\sigma}_i+\theta_t\bar{\sigma}_t \tag{13}$$

where the differential operators **M** and **K** are symmetric and **G** is skew-symmetric, as expected for a conservative gyroscopic system. This form and the trivial boundary conditions for y_i make Galerkin discretization readily applicable with the expansion

$$\mathbf{Y}=\sum_{k=1}^{N_1+N_2+N_3+4}a_k(t)\psi_k(x) \tag{14}$$

where $\psi_k = \{\sin(k\pi x),0,0,0,0,0,0\}^T \quad k = 1,2,...N_1$ for the first span, and $\psi_k = \{0,0,0,1,0,0,0\}$ for the pulley 1. For other spans and pulleys, the basis functions are similar. The ψ_k are global comparison functions where each one describes a deflection of the entire system and satisfies all boundary conditions. They form a complete set. This gives the following equations of motion and eigenvalue problem

$$[\boldsymbol{M}]\ddot{\mathbf{A}} + [\boldsymbol{G}]\dot{\mathbf{A}} + [\boldsymbol{K}]\mathbf{A} = \mathbf{f} \tag{15}$$

$$-\omega^2[\boldsymbol{M}]\rho + i\omega[\boldsymbol{G}]\rho + [\boldsymbol{K}]\rho = \mathbf{0},\ \mathbf{A} = \rho e^{i\omega t},\ \rho = \{a_1, a_2, ...a_{N_1+N_2+N_3+4}\}^T \tag{16}$$

$$M_{ij} = \langle M\psi_j, \psi_i \rangle \quad G_{ij} = \langle G\psi_j, \psi_i \rangle \quad K_{ij} = \langle K\psi_j, \psi_i \rangle \quad f_i = \langle F, \psi_i \rangle \tag{17}$$

The matrices **[*M*]**, **[*K*]**, and **[*G*]** inherit the symmetry/skew-symmetry of the corresponding differential operators in (12). These properties ensure that the eigenvalues are purely imaginary, as required for a conservative gyroscopic system.

The method has several advantages: 1) It is easy to implement because of the simple basis functions; 2) It is efficient, accurate, and reduces computation time; 3) It does not require a user-specified bandwidth to search for natural frequencies; 4) It is numerically robust and free of missing/false natural frequency concerns; 5) Because the method uses Galerkin discretization, all properties of that approach are retained, including convergence of the eigenvalues from above; and 6) Dynamic response analysis is easy to implement using (15). The spatial discretization can be used to solve other hybrid continuous/discrete eigenvalue problems.

New dynamic characteristics of the system induced by the belt bending stiffness are investigated. For appreciable bending stiffness, all modes are spatially distributed and involve transverse deflections of all spans in addition to the pulley rotations, in contrast to zero bending stiffness models where the modes divide into rotational pulley and transverse span modes.

While the natural frequencies generally increase with bending stiffness, the changes are not monotonic. For small bending stiffness, some natural frequencies initially decrease. This unusual phenomenon results because the system equilibrium changes with bending stiffness in a way that tends to increase compliance for deflections about equilibrium.

Belt speed has reduced effect on the natural frequencies as bending stiffness increases within practical ranges. In contrast to the string model where only transverse dominant modes are affected by speed, all natural frequencies change with speed as bending stiffness induced modal coupling increases. Unlike single span moving string and beam models, serpentine drive natural frequencies do not decrease monotonically with speed.

References

[1] Beikmann, R. S., Perkins, N. C., and Ulsoy, A. G., 1996, "Free Vibration of Serpentine Belt Drive Systems," Journal of Vibration and Acoustics, **118**, pp. 406-413.

[2] Kong, L., and Parker, R. G., "Equilibrium and Belt-Pulley Vibration Coupling in Serpentine Belt Drives," *Journal of Applied Mechanics, in press*.

[3] Kong, L., and Parker, R. G., "Coupled Belt-Pulley Vibration in Serpentine Drives with Belt Bending Stiffness," *submitted to Journal of Applied Mechanics*.

Three-Dimensional Vibration Analysis of Bodies of Revolution by the Ritz Method

Arthur W. Leissa
Colorado State University
Fort Collins, Colorado USA

It has long been the desire of analysts to obtain truly three-dimensional (3-D) solutions to problems in mechanics. Until three decades ago, when computers became fast enough, with sufficient capacity, this was possible only in a few special cases, typically having questionable physical meaning; for example, exact solutions of differential equations satisfying unrealistic boundary conditions.

For the free vibration analysis of bodies of revolution, truly 3-D solutions are obtainable more easily, because the modes separate into Fourier components in the circumferential (θ) direction, reducing the problem into ones which are mathematically 2-D. Figure 1 shows a generating cross-section of a typical body of revolution, obtained by rotating it once about the y-axis. For some configurations it is more convenient to use cross-sections laid out in cylindrical coordinates, as shown in Fig.2. These types of cross-sections may be used to create a wide variety of 3-D structural elements of practical, as well as mathematical, interest.

The Ritz method is used to solve these problems. The three displacement components (u_ϕ, u_z, u_θ) are expressed as trigonometric functions in θ, and power series in ϕ and z, with arbitrary coefficients for the series terms. The series are chosen so as to be applicable for fixed or free conditions for each of the displacement components at each of the boundaries. Frequencies (eigenvalues) and mode shapes (eigenfunctions) are obtained in the usual way by minimizing ($V_{max} - T_{max}$). Exact solutions are approached as closely as desired by taking sufficient polynomial terms.

Extensive, accurate results have been obtained in this manner for the frequencies of 3-D bodies of revolution. These shapes are obtained by using various principal radii of curvature (ρ_1 and ρ_2) to the midsurface of the generating element in Fig.1; for example, a plate ($\rho_1 = \rho_2 = \infty$), and spherical ($\rho_1 = \rho_2 = a$), circular cylindrical ($\rho_1 = \infty$, $\rho_2 = r/\sin\phi_o$), toroidal, paraboloidal, ellipsoidal and hyperboloidal shells, thin or thick. One may have constant or variable thickness, h . The meridional boundary angles ϕ_t and ϕ_b at the top and bottom may be chosen so as to obtain shell segments, or closed shells. In addition to shells (hollow bodies), solid bodies may be analyzed.

This presentation summarizes briefly the method of analysis, and gives results taken from a few of the References cited below. Convergence of the solutions is discussed, along with the size of determinants needed to obtain accurate frequencies (exact to four digits). Although a properly constructed 3D finite element computer program could be used, determinants of at least ten times this size would be required to obtain the same accuracy.

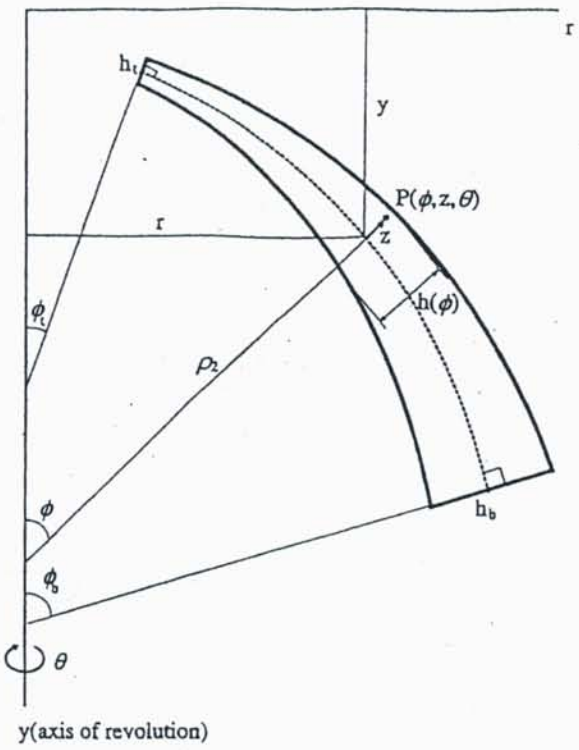

Figue 1. Cross-section of a curvilinear generating element.

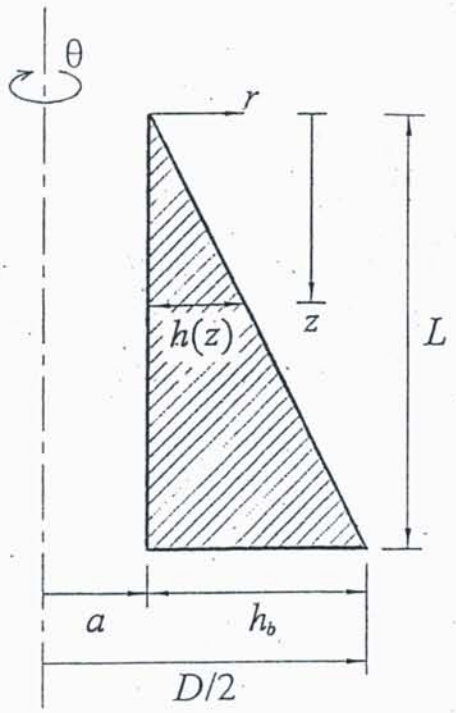

Figure 2. Right triangular cross-section with cylindrical coordinates.

References

"Three-Dimensional Vibrations of Thick, Linearly Tapered, Annular Plates", J.-H. Kang and A.W. Leissa, *Journal of Sound and Vibration,* Vol.217, No.5, pp.927-944, 1998.

"Three-Dimensional Vibration Analysis of Thick Shells of Revolution", A.W. Leissa and J.- H. Kang, ASCE *Journal of Engineering Mechanics,* Vol.125, No.2, pp.1365-1371, 1999.

"Three-Dimensional Vibrations of Hollow Cones and Cylinders with Linear Thickness Variation", J.-H. Kang and A.W. Leissa, *Journal of the Acoustical Society of America,* Vol. 06, No.2, pp.748-755, 1999..

"Three-Dimensional Vibrations of Thick, Circular Rings with Isosceles Trapezoidal and Triangular Cross-Sections", J.-H. Kang and A.W. Leissa, ASME *Journal of Vibration and Acoustics,* Vol.122, No 2, pp.132-139, 2000.

"Three-Dimensional Vibrations of Thick Spherical Shells with Variable Thickness", J.-H. Kang and A.W. Leissa, *International Journal of Solids and Structures,* Vol.37, pp.4811-4823, 2000.

"Three-Dimensional Field Equations of Motion and Energy Functionals for Thick Bodies of Revolution with Arbitrary Curvature and Variable Thickness", J.-H. Kang and A.W. Leissa, ASME *Journal of Applied Mechanics,* Vol. 68, No. 6, pp.953-954, 2001.

"Three-Dimensional Vibration Analysis of Paraboloidal Shells", A.W. Leissa and J.-H. Kang, JSME *International Journal,* Vol.45, No.1, pp.2-7, 2002.

"Three-Dimensional Vibration Analysis of Solid and Hollow Hemispheres having Varying Thickness with and without Axial Conical Holes", J.-H. Kang and H.-J. Shim, *Journal of Vibration and Control* (accepted for publication).

"Three-Dimensional Vibration Analysis of Thick, Circular and Annular Plates with Nonlinear Thickness Variation", J.-H. Kang and J.-I. Oh, *Computers and Structures* (accepted for publication).

""Three-Dimensional Vibration Analysis of Thick Conical Shells", J.-H. Kang, A.W.Leissa and H.-J. Shim (submitted).

"Three-Dimensional Vibration Analysis of Solid Cones with and without an Axial Circular Cylindrical Hole", J.-H. Kang, A.W. Leissa and H.-J. Shim (submitted).

"Three-Dimensional Vibration Analysis of Tapered Rods and Beams with Circular Cross-Section", J.-H. Kang and H.-J. Shim (submitted)

"Three-Dimensional Analysis of Thick Hyperboloidal Shells", J.-H. Kang, A.W. Leissa and H.-J. Shim (submitted)..

Vibration of Nonlinearly Pretwisted Helicoidal Structures

C.W. Lim and **A.Y.T. Leung**

Department of Building and Construction, City University of Hong Kong

Tat Chee Avenue, Kowloon, Hong Kong

E-mails: bccwlim@cityu.edu.hk and Andrew eung@cityu.edu.hk

ABSTRACT

The paper presents a new approach for vibration analysis of helicoidal structures with a large nonlinear pretwist. It also addresses the issue as to what extent the linearized twisting curvature is applicable in the analysis of pretwisted plates. Employing a nonlinear helicoidal model and a natural orthogonal coordinate system, the large nonlinear pretwist is formulated and the energy stored in a distorted helicoil subjected to an external pressure normal to the helicoil axis is derived. By integrating the internal strain energy and external pressure work over the helicoidal domain via a variational principle, a homogeneous system is presented and numerical solutions are obtained. Significant structural responses such as deformation components and resultant, the effects of width and thickness of helicoil on bending are analyzed and discussed. The analysis can be extended to other areas of interest such as turbomachinery blades, drilling structures, motors in micro-electro-mechanical systems (MEMS) and also DNA biomechanics.

Chaotic Oscillations of a Double-Curved Shallow-Shell under Periodic Excitation

Ken-ichi NAGAI, Takao YAMAGUCHI, Shinichi MARUYAMA, Dai YANAGISAWA and Yoshimoto NAKAGAWA
Department of Mechanical Engineering,
Gunma University, 1-5-1 Tenjincho, Kiryu, Gunma 376-8515, JAPAN
nagai@eng.gunma-u.ac.jp

1. Introduction

Both experimental and analytical results are presented for chaotic oscillations of a double-curved shallow shell with rectangular boundary. At the boundary, the shell is simply supported for the deflection, and is elastically constrained for the in-plane displacement. The shell is excited by lateral periodic acceleration. In the analysis, configuration of the shell is assumed to have individual constant curvatures along each edge. The Donnell-Mushtari-Vlasov type equation is used introducing lateral inertia force. Assuming deflection with multiple modes of vibration, basic equation is reduced to nonlinear coupled differential equation by the Bubnov-Galerkin procedure. Chaotic responses are obtained by numerical integration. Both results of the experiment and the analysis are examined as follows; the frequency response curve shows regions where the chaotic response is generated from periodic responses. The chaos is confirmed by the Poincaré projection and the maximum Lyapunov exponent. Contribution of modes of vibration to the chaotic response is analyzed by the Karhuen-Loéve transformation. The analytical results agree well with the experimental ones. Moreover, the chaos of the shell involves more than three modes of vibration simultaneously.

2. Procedure of Analytical Solution

As shown in Figure 1, the rectangular shell with double arcs of curvatures R_x and R_y is subjected to the periodic acceleration $g+a_d\cos\Omega t$. g and a_d correspond to the gravity and the amplitude of excitation, respectively. Ω is exciting frequency. The shell boundary is assumed to be simply supported for deflection. It is also assumed that opposite sides of the shell are constrained by same springs. The springs have non-dimensional elastic coefficients k_x and k_y along x and y direction, respectively. Denoting w and f as non-dimensional total deflection and stress function, governing equation is given by

$$\nabla^4 f = c[\beta^2(w,_{\xi\eta}{}^2 - w,_{\xi\xi} w,_{\eta\eta}) - \alpha_x\beta^2 w,_{\eta\eta} - \alpha_y w,_{\xi\xi}], \tag{1}$$

$$L(w,f) \equiv w,_{\tau\tau} + \nabla^4 w - \alpha_x\beta^2 f,_{\eta\eta} - \alpha_y f,_{\xi\xi} - \beta^2(f,_{\eta\eta} w,_{\xi\xi} - 2f,_{\xi\eta} w,_{\xi\eta} + f,_{\xi\xi} w,_{\eta\eta}) - q_s\delta(\xi-\xi_1)\delta(\eta-\eta_1) - (p_s + p_d\cos\omega\tau) = 0, \tag{2}$$

where $\xi=x/a$ and $\eta=y/b$ are non-dimensional coordinates. $\nabla^2\equiv\partial^2/\partial\xi^2+\beta^2\partial^2/\partial\eta^2$ is the Laplace operator. $\alpha_x=a^2/R_xh$ and $\alpha_y=a^2/R_yh$ are non-dimensional shell curvatures. $\beta=a/b$ is aspect ratio of the length of the rectangular boundary, $(p_s, p_d)=(g, a_d)\rho a^4/D$ $(D=Eh^3/12(1-\nu^2))$ corresponds to non-dimensional load intensities. In-plane displacements $(u, v)=(U, V)a/h^2$ are described by f and w. At the boundary, resultant force is in equilibrium with the spring force.

To solve the equation, first the deflection w is assumed as:

$$w = \sum_m\sum_n \hat{b}_{mn}(\tau)\sin m\pi\xi \sin n\pi\eta, \quad (m, n = 1, 2, 3, \ldots), \tag{3}$$

where $\hat{b}_{mn}$ is unknown time function. $\sin m\pi\xi \sin n\pi\eta$ is the coordinate function which satisfies the boundary condition. Inserting the foregoing equation to the compatibility equation (1), stress function f consists of homogeneous solution and particular solution of the term $\hat{b}_{mn}$. Inserting the solution of f and assumed deflection w into equation (2), and applying the Galerkin procedure the equation is reduced to a set of nonlinear ordinary differential equations in the term of $\hat{b}_{mn}$. Next, static deformation is obtained. Using linear natural modes of vibration, the equation is transformed to standard type of coupled equations as:

$$\tilde{b}_{i,\tau\tau}+2\varepsilon_i\omega_i\tilde{b}_{i,\tau}+\omega_i^2\tilde{b}_i+\sum_j\sum_k\tilde{D}_{ijk}\tilde{b}_j\tilde{b}_k+\sum_j\sum_k\sum_l\tilde{E}_{ijkl}\tilde{b}_j\tilde{b}_k\tilde{b}_l-p_d\tilde{G}_i\cos\omega\tau=0$$
$$(i,j,k,l=1,2,3,\ldots), \quad (4)$$

where $\tilde{b}_i(\tau)$ denotes unknown time function corresponding to the i-th mode. Linear damping is introduced in the equation. Harmonic response is calculated by the harmonic balance method. Chaotic response is computed by numerical integration of the Runge-Kutta-Gill method.

3. Experimental Procedure

A phosphor-bronze sheet of thickness h=0.24 mm is used as a test shell. The test sheet is cut to a square. Side lengths result in a=139.7 mm and b=139.8 mm. The boundary of the shell is connected to inner walls of the square frame by thin flexible films. Strip of the films are wrapped round the edges of shell alternately, and are pasted to the wall. Shell boundary represents simply support for the deflection and elastic constraint for the in-plane displacement. The shell has initial deformation in double-curved shape due to the cutting process, the connection to the frame and the gravity force. The maximum deflection in positive z-direction is approximately 0.3 mm. Consequently, the shell has negative curvatures. The shell is subjected to the periodic acceleration by an electro-magnetic vibration exciter. Multiple sets of laser displacement sensors enable recording simultaneous chaotic responses at different points of the shell.

4. Results and Discussions

Static deformation and natural frequencies of the shell are measured in the experiment. Static deflection under concentrated load is shown in Figure 2. Restoring force of the shell shows characteristics of soft-hardening type including negative gradient. Table 1 shows natural frequencies of small amplitude of vibration. Using the results of restoring force and natural frequencies of the experiment, shell curvatures are approximated as α_x=–6.3 and α_y=–7.5 including the effects of the gravity. Spring coefficients are also identified as k_x=0.1 and k_y=0.01. Analytical results are also shown in Figure 2 and Table 1. Frequency of the lowest mode has large discrepancy due to initial imperfection of the shell. However, higher frequency of the analysis agrees well with the result of the experiment. Figure 3 shows the frequency response curve. Amplitude of responses are plotted by a root-mean-square value w_{rms} to the exciting frequency ω. Notation (m,n): j denotes the type of response. (m,n) is generated mode of vibration, in which integers m and n imply predominant half wave number of the deflection in the x-direction and y-direction, respectively. j indicates the resonance response, for example, j=1 represents a principal resonance and j=1/2 is the subharmonic resonance of 1/2 order. Main chaotic responses are denoted by C_1 and C_2. Regions of the chaos C_1 and C_2 preserve within the ranges $(1.2\sim1.5)\omega_{(1,1)}$ and $(1.6\sim1.9)\omega_{(1,1)}$, respectively. Analytical region of the C_1 is in the domains of $(1.3\sim1.5)\omega_{(1,1)}$, and the region of the C_2 covers $(1.7\sim1.8)\omega_{(1,1)}$. Chaotic responses are generated in the frequency region of the same ratio to the lowest natural frequency. Poincaré maps of the chaotic responses in the C_2 are shown in Figure 4. Each map is recorded by changing phase delay θ from the maximum amplitude of the exciting force. Both results coincide very well in details. As the phase angle shifts, clear formations are observed for folding and stretching of the fractal figure. Moreover, the maximum Lyapunov exponent $\lambda_{\max}$ of the experiment and the Lyapunov dimension d_L of the analysis are shown in Figure 5. $\lambda_{\max}$ is converged to 1.3 as the embedded dimension exceeds e=6, and d_L in the analysis is also converged to a constant value over the number I_c=3 of vibration mode. Therefore, number of modes generated in the chaos is found to be three. Modes that contribute to the chaos are examined by the simultaneous time responses at multiple points. Applying the KL-transformation to the time-data for the analysis, principal components are calculated as shown in Figure 6. The lowest mode (1,1) and the in-phase modes of combined (3,1) and (1,3) make the highest contribution to the chaotic response. The symmetric modes of lower order contribute to the chaotic response of the shell with doubly curved configuration.

References

(1) Nagai, K. and Yamaguchi, T., "Chaotic oscillations of a shallow cylindrical shell with rectangular boundary under cyclic excitaion", High Pressure Technology, ASME,PVP-Vol. 297,(1995),pp.107-115.

(2) Yamaguchi, T. and Nagai, K., "Chaotic vibration of a cylindrical shell-panel with an in-plane elastic-support at boundary", Nonlinear Dynamics Vol.13,(1997), pp.259-277.
(3) Nagai, K. , Kasuga, K. , Kamada, M. , Yamaguchi, T. and Tanifuji, K., "Experiment on chaotic oscillations of a post-buckled reinforced beam constrained by an axial spring", International Journal of Japan Society of Mechanical Engineers Vol.41, (1998), No.3, pp.563-569.
(4) Nagai, K. , Yamaguchi, T. and Murata, T., "Chaotic oscillations of a cylindrical Shell-Panel with Concentrated Mass under Gravity and Cyclic Load", Proceedings of the 3rd International Symposium on Vibrations of Continuous Systems, Grand Teton, WY, U.S.A, July 23-27, 2001, pp.49-51.

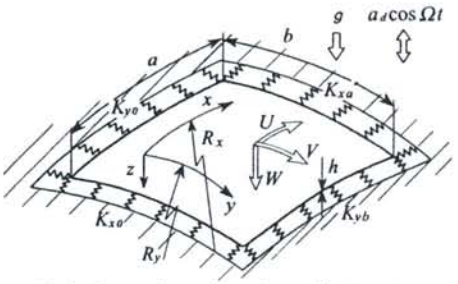

Fig.1 Dynamic model and coordinate system

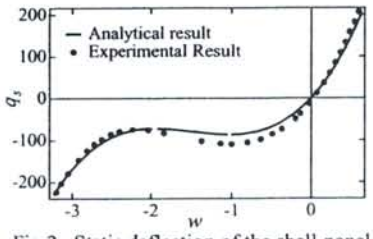

Fig.2 Static deflection of the shell-panel
(measured point ; $\xi = 0.57, \eta = 0.57$)

Table 1 Natural frequency and vibration mode of the shell-panel

Mode (i, j)	Mode symbol	Experimental result ω_{ij}	Analytical result ω_{ij}
(1 , 1)	x, y	24.3	29.9
(2 , 1)		47.7	53.8
(1 , 2)		56.3	54.7
(2 , 2)		81.2	82.1
(3 , 1)		99.8	101
(1 , 3)		110	102

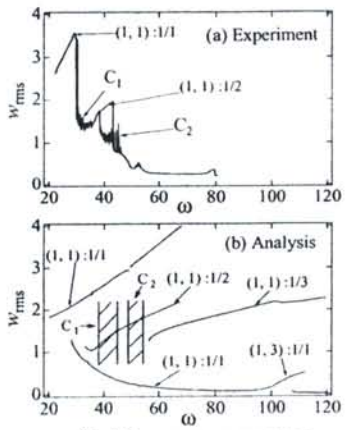

Fig.3 Frequency responses
($p_d = 480$, $\varepsilon_t = 0.01$, $\xi = 0.7$, $\eta = 0.6$)

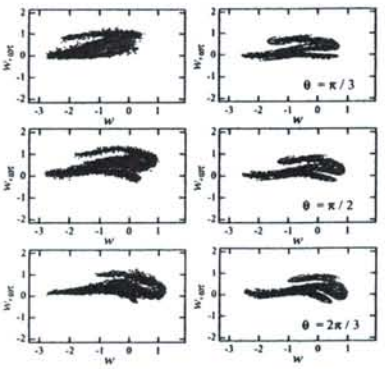

(a) Experiment ($\omega = 47.1$) (b) Analysis ($\omega = 50.0$)

Fig.4 Poincaré maps of chaotic responses
($p_d = 480$, $\xi = 0.7$, $\eta = 0.6$)

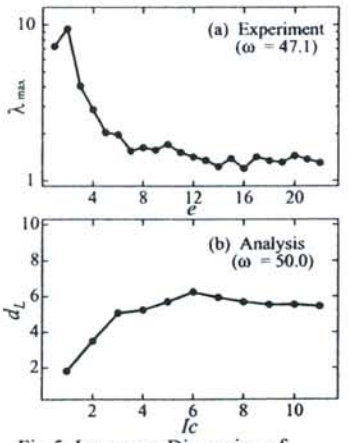

Fig.5 Lyapunov Dimension of the shell-panel ($p_d = 480$)

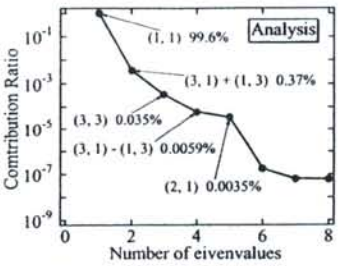

Fig.6 Principal components by KL transformation
($p_d = 480$, $\omega = 50.0$)

Layerwise Optimization (LO) Approach for the Maximum Frequency of Laminated Rectangular Plates

Yoshihiro Narita

Hokkaido Institute of Technology, 7-15 Maeda, Teineku, Sapporo, Japan 006-8585

e-mail: narita@hit.ac.jp

1. INTRODUCION

An original concept of a layerwise optimization (LO) approach was first presented in a paper [1] for free vibration of symmetrically laminated rectangular plates. A set of design variables, which are the fiber orientation angles in the layers, are determined to maximize the fundamental frequencies of the laminated plates. The LO approach is based on a simple physical observation that the outer layer has more stiffening effect than the inner layer in bending of laminated plates and is more influential on determining the natural frequency. This observation is made use of in a LO procedure that the optimal stacking sequence for the maximum natural frequency of laminated plates can be determined sequentially in the order from the outermost to the innermost layer. The numerical examples are given for 8-layer rectangular plates with various uniform boundary conditions, and it is also shown for 24-layer plates that a LO approach is equally effective to plates with many layers.

2. OUTLINE OF THE PROBLEM AND OPTIMIZATION

A symmetrically laminated rectangular plate is considered, where in each layer the major and minor principal material axes are denoted by the L and T axes, respectively. The E_{L} and E_{T} are elastic moduli in the L and T directions, respectively, G_{LT} is the shear modulus and ν_{LT} is the major Poisson ratio. The dimension of the whole plate is given by $a \times b \times h$ (thickness). The total number of layers is denoted by $2N$, where N layers exist in the upper (lower) half of cross-section.

Natural frequency is normalized as a frequency parameter

$$\Omega = \omega a^2 \left(\rho / D_0\right)^{1/2}, \quad \text{with} \quad D_0 = E_T h^3 / 12\left(1 - \nu_{LT}\nu_{TL}\right) \quad \text{(reference bending rigidity)}$$

The frequency parameter Ω for the fundamental (lowest) mode is used as an object function and will be designed to maximize in the present optimization. The design variables are taken to be a set of fiber orientation angles in the N layers of the upper (lower) half of the cross-section $[\theta^{(1)}/\theta^{(2)}/\ldots/\theta^{(k)}/\ldots/\theta^{(N)}]_{\mathrm{S}}$, where $\theta^{(k)}$ is a fiber orientation angle in the k-th layer (k=1:outermost, k=N: innermost) and a subscript "s" denotes symmetric lamination.

When the fiber orientation angles are directly taken for design variables, one inevitably faces intensive computational problems wherein optimum solutions must be determined in multi-dimensional spaces. The LO approach dissolves such conventional mathematical and/or computational problems and reduces the

multi-dimensional search for optimum solutions into a few iterative cycles of one-dimensional search.

For this purpose, a physical observation that "the outer layer has more stiffening effect than the inner layer in bending of laminated plates and is more influential on the natural frequency" is utilized. This physical fact may be interpreted as "the outer layer plays more decisive role in determining the maximum frequency of laminated plates". Based on this consideration, a hypothesis that

The optimum stacking sequence $[\theta^{(1)}/\theta^{(2)}/\ldots/\theta^{(N)}]_{S,opt}$ *for the maximum natural frequency of laminated plates can be determined sequentially in the order from the outermost to the innermost layer*

is proposed and is used in a layerwise optimization (LO) process. In the present study, an optimization algorithm based on the hypothesis is used as an iterative LO procedure.

3. REULTS AND DISCUSSIONS

The elastic constants used in the examples are taken for Graphite/epoxy composite as E_L= 138 GPa, E_T=8.96 GPa, G_{LT}=7.1 GPa and ν_{LT}=0.30. The frequencies were calculated by using the $M\times N$ =10×10 solutions in the Ritz method [2]. The design variables are presented in the usual notation as $[\theta^{(1)}/\theta^{(2)}/\theta^{(3)}/\theta^{(4)}]_s$, where $\theta^{(1)}$ is the fiber orientation angle of the 1st layer (outermost) and $\theta^{(4)}$ is that of the 4th layer (innermost).

The optimum solutions are obtained by the iterative LO procedure for twenty one different cases in boundary conditions. To each set of boundary conditions, the optimum fiber orientation angle $[\theta^{(1)}/\theta^{(2)}/\theta^{(3)}/\theta^{(4)}]_{s,opt}$ and the corresponding maximum fundamental frequency Ω_{opt} are obtained with different number of iterative cycles (NIC) required for convergence. The θ is determined in an increment of θ=5° . To validate optimality of the obtained solutions, comparison is made in Fig.1 to see that the plates with the present optimum solutions $[\theta^{(1)}/\theta^{(2)}/\theta^{(3)}/\theta^{(4)}]_{s,opt}$ actually give higher frequencies than those with other stacking sequences. Typical stacking sequences of the symmetric 8-layered plates are chosen for comparison as [0/0/0/0]s, [0/90/0/90]s, [30/-30/30/-30]s, [45/-45/45/-45]s and [0/-45/45/90]s. The first two (i.e., [0/0/0/0]s are [0/90/0/90]s) are macroscopically specially orthotropic. The next two ([30/-30/30/-30]s and [45/-45/45/-45]s) are alternating angle-ply sequence. The last one ([0/-45/45/90]s) is a quasi-isotropic case. It is observed that all the present optimum solutions (denoted by ■) yield higher frequencies than those of plates with the five typical stacking sequences.

An iterative LO procedure is thus shown to be very effective to improve solution accuracy for 8-layer plates. Since a LO approach depends on the physical observation that the outer layer contributes more than any other layers of the plate to the bending stiffness, one may raise a question on how well the LO procedure works for very thin layers, i.e. laminated plates with many layers. Hence 24-layer plates are considered as a representative of plates with many layers to answer this question. Table 1 shows some examples for Ω_{opt} and $[\theta^{(1)}/\theta^{(2)}/\ldots/\theta^{(12)}]_{S,opto}$ for 24-layer square plates. The results are compared with the frequency parameters for plates with $[0_{12}]$s, $[(0/90)_6]$s, $[(45/-45)_6]$s and $[(0/-45/45/90)_3]$s lay-ups. The present optimum solutions are shown to yield higher values than the reference values and the effectiveness of the LO approach applied to laminated plates with many layers is obvious.

REFERENCES

[1] Y. NARITA 2003 *Journal of Sound and Vibration* (Special Issue in Honor of Prof.Leissa), (to appear). Layerwise Optimization for the Maximum Frequency of Laminated Composite Plates.

[2] Y. NARITA, 2000, Combinations for the Free-Vibration Behaviors of Anisotropic Rectangular Plates under General Edge Conditions, *J. Appl. Mech.*, 67, pp.568-573.

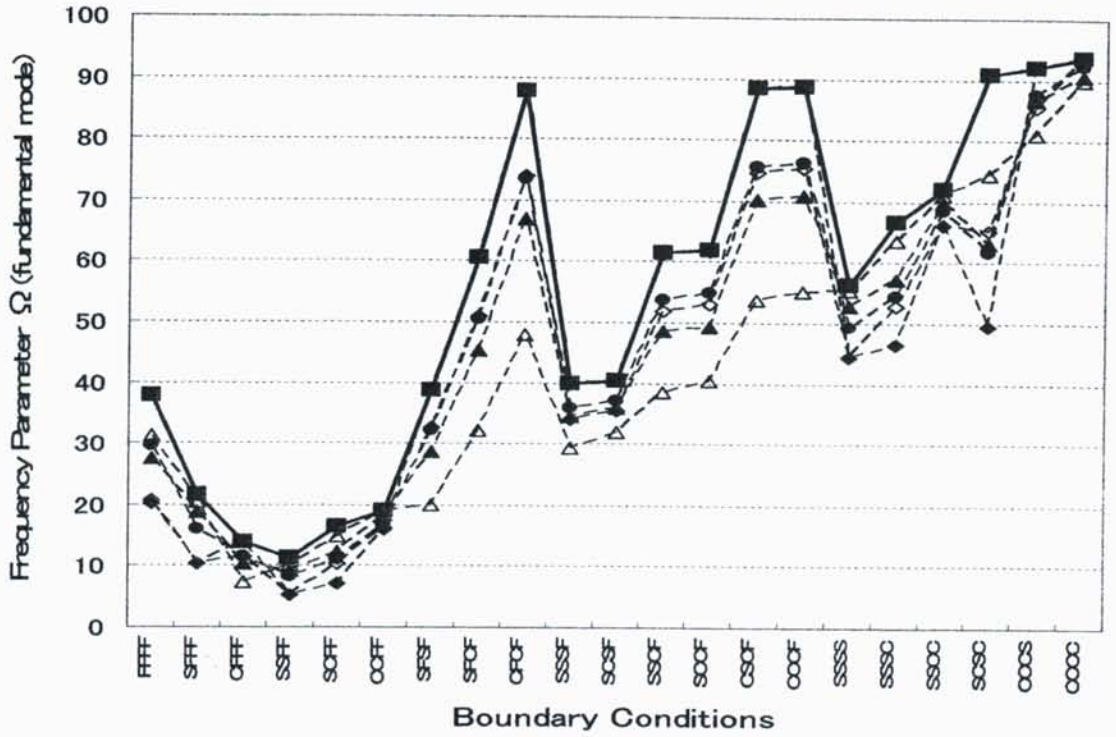

Fig.1 Comparison between the optimum frequency and frequencies of symmetric 8-layer square plates with various stacking sequences (a/b=1, ■: optimum frequency, ◆: [0/0/0/0]s, ◇: [0/90/0/90]s, ▲: [30/-30/30/-30]s, △: [45/-45/45/-45]s, ●: [0/-45/45/90]s)

Table 1 Converged optimum solutions and reference frequencies for typical lay-ups of symmetrically laminated 24-layer square plates (a/b=1, Increment is θ=5°).

B.C.	Ω_{opt}	Ω $[0_{12}]$s	$\Omega[(0/90)_6]_2$	$\Omega[(45/-45)_6]_2$	$\Omega[(0/-45/45/90)_3]_2$
	$[\theta^{(1)}/\theta^{(2)}/\theta^{(3)}/\theta^{(4)}/\theta^{(5)}/\theta^{(6)}/\theta^{(7)}/\theta^{(8)}/\theta^{(9)}/\theta^{(10)}/\theta^{(11)}/\theta^{(12)}]_{s,opt}$				
SSFF	11.30	5.053	5.201	10.79	8.772
	[-45/45/-45/-45/45/-45/45/-45/-45/-45/45/45]s, (NIC=1)				
SSSS	56.53	44.31	44.31	56.39	50.62
	[45/-45/-45/45/-45/45/45/-45/-45/45/45/45]s, (NIC=1)				
CCCC	93.67	93.61	93.67	90.94	92.56
	[90/0/0/90/0/90/90/0/90/0/90/0]s, (NIC=1)				

AN ANALYTICAL-NUMERICAL COMBINED METHOD FOR CAR DISC VIBRATION AND SQUEAL

Huajiang Ouyang and John E Mottershead
Department of Engineering, the University of Liverpool
Liverpool, L69 3GH, United Kingdom

1. Introduction

Car disc brakes often generate unwanted vibration and noise. One type of noise in the frequency range above 1 kHz, called squeal, is very unpleasant. Squealing brakes are difficult and expensive to correct. Customers become concerned about the quality and reliability of the vehicle when it has got a squealing disc brake. High warranty cost has been incurred to the manufacturer. It is recognized that the brake-emanated vibration and noise is caused by the dry friction at the disc and pads interface. To achieve good braking performance, the pads must possess a high friction coefficient. However, high friction materials invariably promote noise occurrence. Thus it is very challenging to design car disc brakes that have both good braking and noise performance.

The first concerted effort to study disc brake squeal was conducted in MIRA in late 1950's. Since then, great progress has been made towards the understanding of disc brake squeal and the improved design of disc brakes. However, disc brake squeal is still an unsolved problem. There are considerable difficulties in the study of disc brake squeal.

First of all, the friction at the disc and the pads interface is not well understood. Its behaviour is influenced by the temperature and humidity, in addition to forces and deformations. Secondly, there exists dynamic contact between the disc and pads, which poses a nonlinear problem. Furthermore, the contact interface is moving. Therefore, it is a moving load problem as well. Finally, a disc brake is a very complicated system. The computing load involved can be formidable.

This paper describes the methodology established at the University of Liverpool and presents some of the latest results of the dynamic stability of the disc brake system. It is an analytical-numerical combined approach. As such, the work fully fits the two themes of this symposium — vibrations of continuous systems. It is thought that there are four aspects of modeling issues, which will be elaborated in this paper.

2. The System Model

A car disc brake system consists of a rotating disc and non-rotating, stationary pads, carrier bracket, calliper and mounting pins. The pads are loosely housed in the calliper and located by the carrier bracket. The calliper itself is allowed to slide fairly freely along the two mounting pins in a floating calliper design. A typical floating-type vented disc brake system is shown in Figure 1.

Figure 1. A car disc brake of floating calliper design

The disc is mounted to the car wheel and thus rotates at the same speed as the wheel. When the disc brake is applied, the two pads are brought into contact with the disc surfaces. Most of the kinetic energy of the travelling car is converted to heat through friction. But a small part of it becomes sound energy and generates noise. Since a squealing brake is difficult and expensive to correct, ideally the noise issue should be resolved at the design stage. Modelling and simulating vibration and squeal is an important way of understanding the problem and designing quieter disc brakes.

The authors conceptually divide a whole disc brake system into two parts: the rotating disc approximated as a thin, annular plate, and the non-rotating, stationary, components described by many thousands of finite elements. This separation also facilitates the formulation of the vibration and squeal as a moving load problem.

3. The Contact Model

During operation, the contact between the disc and pads is not complete. In addition, the contact area varies with time. This is a dynamic contact problem. In this study, a nonlinear static contact analysis is carried out for the sliding contact interface to establish the static contact area and pressure distribution. Both sets of information is used to define the material properties of the friction film at the disc and pads interface. Thus the dynamic contact is simplified as a static contact. If the former is pursued, the sheer amount of computation is overwhelming and thus has not been conducted at this stage.

4. The Friction Model

It is the friction that causes the unwanted disc vibration and squeal. Therefore, the friction model is fundamentally important. Because of other complexities, only the simple Coulomb friction law is used. However, the friction occurring at the disc and pads interface contributes to the non-conservative forces in a very special way, that is, as a friction couples acting onto the disc. This way of incorporating friction forces, usually referred to as a squeal mechanism, is based on the North's original idea. It will be

demonstrated through numerical results that this squeal mechanism indeed can bring the whole disc brake system into dynamic (flutter) instability.

5. The Dynamics Model

The finite element model for the car disc brake under present investigation has about one hundred and eighty thousand degrees-of-freedom. It is time consuming to compute the frequencies and modes and it is quite unnecessary to use such a detailed model. Each stationary component of the disc is treated as a substructure and the Craig-Bampton dynamic reduction is used to reduce each component finite element model. Different numbers of retained modes and nodes are tried and compared with a full model.

The rotating engagement between the disc and pads is treated as a moving load problem. It is felt that by bringing in the moving load element into the model, the model should represent a real disc brake in a better way. However, this adds much extra complexity.

Through the displacement continuity at the disc and pads interface, a complex-valued, asymmetric eigenvalue formulation is established. If an eigenvalue has a positive real part, the corresponding imaginary part is considered an unstable frequency. Numerically predicted unstable frequencies are taken to mean squeal frequencies in reality.

6. Results and Discussion

It can be appreciated that there are a number of uncertain system parameters and locations, in particular at some contact interfaces. Consequently, a form of tuning based on experimental data is conducted at first. Then the system eigenvalues under normal operating conditions are computed and listed in tables.

A large collection of experimental data from modal testing and laser holography have been obtained. Some of them are presented to show that the established methodology indeed works and the systems parameters used represent the system satisfactorily.

7. Conclusions

Friction-induced vibration and squeal of disc brake are studied in the paper. The rotating disc is represented by a Kirchoff plate while the stationary components are modeled by a large finite element model. A distinct squeal mechanism based on North's friction couple is incorporated into the model and combined with a moving load treatment. Numerically predicted unstable frequencies are close to experimentally established squeal frequencies in general. The method and program established is a valuable tool for disc brake design.

References

To be given in the full paper and the talk.

NONLINEAR DYNAMICS AND STABILITY OF AXIALLY LOADED CIRCULAR CYLINDRICAL SHELLS

F. PELLICANO
Dip. di Ingegneria Meccanica e Civile, Università di Modena e Reggio Emilia, V. Vignolese, 905, Modena, I - 41100 ITALY
E-MAIL: frank@unimo.it
M. AMABILI
Dip. di Ingegneria Industriale, Università di Parma, Area delle Scienze, 181/A, Parma, 43100 ITALY
E-MAIL: marco@me.unipr.it

ABSTRACT
The dynamic stability of simply supported, circular cylindrical shells under periodic axial loads is analysed. Nonlinearities due to finite-amplitude shell motion are considered by using the Donnell's nonlinear shallow-shell theory. A finite length, simply supported shell is considered; the boundary conditions are satisfied, including the contribution of external axial loads acting at the shell edges. The effect of a contained liquid on the dynamic stability is investigated.

1. INTRODUCTION
The fundamental investigation on the stability of circular cylindrical shells is due to Von Karman and Tsien (1941), who analysed the static stability (buckling) and the postcritical behaviour of axially loaded shells.
Koval (1974) used the Donnell's nonlinear shallow-shell theory to study the effect of a longitudinal resonance in the parametric transversal instability of a circular shell. Hsu (1974) used the Donnell's linear shallow-shell theory to analyse the parametric instability of a circular cylindrical shell. The same problem was studied by Nagai and Yamaki (1978) using the Donnell's linear shallow-shell theory, considering different boundary conditions. Popov *et al.* (1998) analysed the parametric stability and the postcritical behaviour of an infinitely long circular cylindrical shell, dropping the boundary conditions. The effect of internal resonances between asymmetric modes was analysed in detail. Gonçalves and Del Prado (2000) analysed the dynamic buckling of a perfect circular cylindrical shell under axial static and dynamic loads. Donnell's nonlinear shallow-shell theory was used and the membrane theory was considered to evaluate the in-plane stresses.
In the present paper, the dynamic stability and postscritical dynamics of a circular cylindrical shell subjected to periodic axial loads is analysed. The Donnell's nonlinear shallow-shell theory is used; the effect of a contained fluid is considered and simply supported boundary conditions are satisfied. The dynamics of axisymmetric modes is considered, avoiding the approximation of the membrane theory for the in-plane stress evaluation. The dynamical system obtained through a Galerkin procedure is analysed with numerical techniques.

2. GOVERNING EQUATIONS
The Donnell's nonlinear shallow-shell theory is used. The equation of motion for finite-amplitude, flexural vibrations of a thin, circular cylindrical shell is given by (Evensen, 1967; Amabili *et al.* 1998; Amabili *et al.* 1999a)

$$D\nabla^4 w + c\,h\,\dot{w} + \rho\,h\,\ddot{w} = f + p + \frac{1}{R}\frac{\partial^2 F}{\partial x^2} + \left(\frac{\partial^2 F}{R^2\,\partial\theta^2}\frac{\partial^2 w}{\partial x^2} - 2\frac{\partial^2 F}{R\,\partial x\,\partial\theta}\frac{\partial^2 w}{R\,\partial x\,\partial\theta} + \frac{\partial^2 F}{\partial x^2}\frac{\partial^2 w}{R^2\,\partial\theta^2}\right), \tag{1}$$

with the compatibility equation

$$\frac{1}{E\,h}\nabla^4 F = -\frac{1}{R}\frac{\partial^2 w}{\partial x^2} + \left[\left(\frac{\partial^2 w}{R\,\partial x\,\partial\theta}\right)^2 - \frac{\partial^2 w}{\partial x^2}\frac{\partial^2 w}{R^2\,\partial\theta^2}\right], \tag{2}$$

where $D = E\,h^3/\left[12(1-\nu^2)\right]$ is the flexural stiffness, E the Young's modulus, ν the Poisson ratio, h the shell thickness, R the mean shell radius, ρ the mass density of the shell, c the damping coefficient, F is the in-plane stress function, p is the pressure acting on the shell surface due to the fluid-structure interaction and f is a distributed external load. Moreover, simply supported boundary conditions are considered and the continuity in θ is imposed. The axial load is: $\widetilde{N}_x(t) = -N + N_D\cos\omega t$.

The radial displacement w is expanded by using the linear shell eigenmodes as basis; in particular, the flexural response may be written as follows:

$$w(x,\theta,t)=\sum_{n_1=1}^{N_1}\sum_{m=1}^{N_1}\left[A_{m,(n_1 n)}(t)\cos(n_1 n\theta)+B_{m,(n_1 n)}(t)\sin(n n_1\theta)\right]\sin(\lambda_m x)+\sum_{m=1}^{M}A_{2m-1,0}(t)\sin(\lambda_{2m-1}x),$$

(4)

where $\lambda_m = m\pi/L$, t is the time; $A_{m,j}(t)$, $B_{m,j}(t)$ and $A_{m,0}(t)$ are unknown functions of t and $j = n_1 n$. In the numerical calculations, N_1 and M will be assigned equal to 3 and 5, respectively. Expansion (4) is suggested by the presence of quadratic and cubic nonlinearities.

3. FLUID-STRUCTURE INTERACTION

The shell is assumed to be empty or completely fluid-filled. An incompressible inviscid fluid is considered and the effect of the dynamic pressure acting on the shell surface is linearized. The fluid velocity field can be described in terms of the velocity potential Φ:

$$\nabla^2\Phi=\frac{\partial^2\Phi}{\partial x^2}+\frac{\partial^2\Phi}{\partial r^2}+\frac{1}{r}\frac{\partial\Phi}{\partial r}+\frac{1}{r^2}\frac{\partial^2\Phi}{\partial\theta^2}=0\,.$$

(5)

The fluid velocity field is given by $\mathbf{v}=-\nabla\Phi$.

3. NUMERICAL RESULTS

A numerical analysis is performed on a test shell, studied in (Popov *et al.* 1998; Gonçalves and Del Prado, 2000), having the following characteristics: $h = 2\times10^{-3}$ m, $R = 0.2$ m, $L = 0.4$ m, $E = 2.1\times10^{11}$N/m^2, $\nu = 0.3$, $\rho = 7850$ kg/m^3; in the case of fluid-filled shell, $\rho_F = 1000$ kg/m^3. The fundamental frequency of the empty shell is equal to $2\,\pi\times503.7$ rad/s and is obtained for m=1 and n=5. When the shell is excited by an axial periodic load, two kind of excitations are present on the modal equations: (*i*) a direct excitation of the axisymmetric modes due to the Poisson's effect; (*ii*) a parametric excitation of all modes.

In the present problem, when $\omega/\omega_{1,5}$=1.9, the frequency of excitation is close to the principal parametric resonance of the fundamental mode. In Figure 1 the maximum amplitude of periodic oscillation is represented for fundamental mode $A_{1,5}$, versus the dynamic load N_D/N_{cr}; where $N_{cr}=Eh^2/\left(R\sqrt{3(1-\nu^2)}\right)$ is the classical critical load per unit length in the circumferential direction. Increasing the dynamic excitation level N_D, a period doubling bifurcation, due to a parametric instability, is found for N_D/N_{cr} = 0.46. Before the bifurcation the shell vibrates with the same frequency of excitation (1T oscillation), and the dynamics is due to the axisymmetric modes only. After the period doubling bifurcation a sub-critical branch 2 can be observed. For the same problem, in Ref. (Popov *et al.* 1998) the parametric instability has been found at N_D/N_{cr}=0.39, the difference can be addressed to the use of the membrane theory in (Popov *et al.* 1998).

N_D/N_{cr}	$\omega/\omega_{1,5}$	ζ	Presence of fluid
0.448	1.9	0.089	No
0.86	1.9	0.089	Yes
0.416	2	0.089	No
0.722	2	0.089	Yes
0.492	2.1	0.089	No
0.724	2.1	0.089	Yes
0.24	1.9	0.016	No
0.46	1.9	$\zeta_{1,5}$=0.089 (Kelvin-Voigt damping model)	No

Table 1. Critical dynamic load: the damping ratio is constant on all modes if not specified.

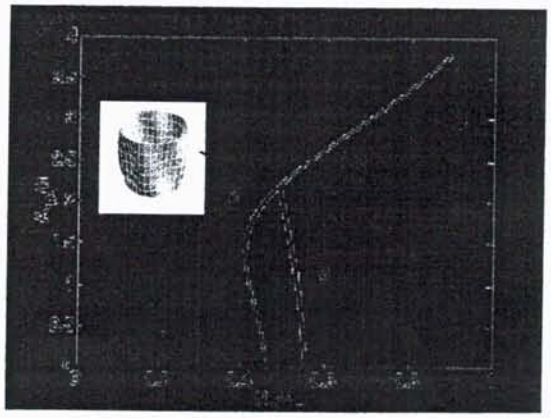

Fig. 1. Dynamic instability (empty shell). Static load N/N_{cr}=0, ζ=0.089. $\omega/\omega_{1,5}$=1.9. '—' stable solution, '—' unstable solution, 'PD' Period Doubling

In order to quantify the effect of a contained fluid and the damping, the dynamic critical loads are computed for different excitation frequencies, damping ratios and considering empty and water-filled shells; the results are reported in Table 1. It is of interest that the presence of a contained fluid enlarges the critical load; this safety effect is due only to the inertial effect of fluid.

Periodic and non-stationary responses are now analyzed in detail by means of direct simulations and bifurcation diagram of Poincaré maps. The case of an empty shell is shown in Figure 2; the following parameters are considered: N/N_{cr}=0.6, N_D/N_{cr}=0.01; ζ=0.0008. The diagram is obtained by decreasing the excitation frequency. A 1% perturbation of the natural frequency of the companion mode is used in order to simulate a small imperfection. At $\omega/\omega_{1,5(0)}$=1.251 the parametric instability of the companion mode $B_{1,5}$ is met; indeed, because of the small perturbation, the natural frequency of the companion mode is 1% higher than the natural frequency of mode $A_{1,5}$. At $\omega/\omega_{1,5(0)}$=1.207 the mode $A_{1,5}$ is excited and, for $\omega/\omega_{1,5(0)}$=1.157, mode $B_{1,5}$ collapses to the trivial solution. In the region $\omega/\omega_{1,5(0)}\in$(0.996,1.077) alternate periodic and quasi-periodic orbits can be found. At $\omega/\omega_{1,5(0)}$=0.975 a sudden jump to a chaotic orbit is found. At $\omega/\omega_{1,5(0)}$=0.929 a jump to an orbit around the bifurcated static position takes place; the amplitude of oscillation is quite large (not shown), i.e. the shell collapses.

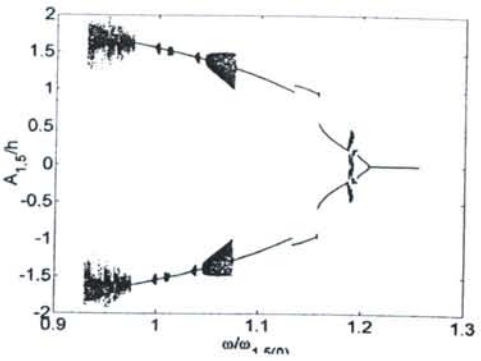

Figure 2. Bifurcation diagram (empty shell): dynamic load N_D/N_{cr}=0.01, static load N/N_{cr}=0.6; ζ=0.0008. 1% perturbation on the linear frequencies.

CONCLUSIONS

The parametric instability and the postcritical behaviour of a circular cylindrical shell subjected to dynamic axial loads are analysed. The Donnell's nonlinear shallow-shell theory has been used, and partial differential equations have been deiscretized by means of the Galerkin procedure, using a relatively large set of modes in the expansion. The combined effect of a static axial preload and dynamic loading is considered, in order to investigate the stability bounds and post-critical behaviour. Dynamic stability bounds for empty shells are compared with the results present in literature. The contained liquid gives rise to an increment of the linear damping and an added mass effect, which reduces the linear natural frequencies of vibration. The contained liquid causes also interesting variations in the dynamic stability bounds.

ACKNOWLEDGEMENTS

This work was partially supported by the COFIN 2000 grant of the Italian Ministry for University and Research (MURST), the CNR Agenzia 2000 grant and N.A.T.O. Cooperative Linkage Grant Project (N. PST.CLF. 977350).

REFERENCES

Amabili, M., Pellicano, F., Païdoussis, M. P., 1998. Nonlinear Vibrations of Simply Supported, Circular Cylindrical Shells, Coupled to Quiescent Fluid. J. of Fluids and Structures 12, 883-918.

Amabili, M., Pellicano, F., Païdoussis, M. P., 1999a. Non-Linear Dynamics and Stability of Circular Cylindrical Shells Containing Flowing Fluid. Part I: Stability. J. of Sound and Vibration 225, 655-699.

Evensen, D. A., 1967. Nonlinear Flexural Vibrations of Thin-Walled Circular Cylinders. NASA TN D-4090, Government Printing Office, Washington DC.

Gonçalves, P.B. and Del Prado, Z.J.G.N., 2000. The Role of Modal Coupling on the Non-Linear Response of Cylindrical Shells Subjected to Dynamic Axial Loads. In: Proc. of the Symp. on Nonlinear Dynamics of Shells and Plates, ASME Int. Mech. Eng. Congr. and Exp. (AMD Vol. 238), pp. 105-116, Orlando, USA.

Hsu, C. S., 1974. On Parametric Excitation and Snap-Through Stability Problems of Shells. In: Thin-Shell Structures. Theory Experiments and Design. Y.C. Fung and E.E. Sechler Eds. Englewood Cliffs, Prentice-Hall, New Jersey.

Koval, L.R., 1974. Effect of Longitudinal Resonance on the Parametric Stability of an Axially Excited Cylindrical Shell. J. of Acoustic Society of America 55(1), 91-97.

Nagai, K. and Yamaki N., 1978. Dynamic Stability of Circular Cylindrical Shells Under Periodic Compressive Forces. J. of Sound and Vibration 58(3), 425-441.

Popov, A.A., Thompson J.M.T., McRobie, F.A., 1998. Low Dimensional Models of Shell Vibrations. Parametrically Excited Vibrations of Cylindrical Shells. J. of Sound and Vibration 209, 163-186.

Von Kármán, T. and Tsien, H.S., 1941. The Buckling of Thin Cylindrical Shells under Axial Compression. J. of the Aeronautical Sciences 8(8), 303-312.

THEORETICAL AND EXPERIMENTAL MODAL ANALYSIS OF THE MODES OF DOUBLE EIGENFREQUENCIES IN ULTRASONIC MOTORS BY A HARMONIC EXCITATION OF THE PIEZOCERAMIC ELEMENTS

W. Seemann
Institute of Mechanics, University of Karlsruhe

In recent years ultrasonic motors have become very popular. In these motors the motion is generated not by electrodynamic forces like in conventional motors but instead one part of the system –the stator-- is excited by piezoceramic elements in such a way that some points of the stator move on elliptic trajectories. In rotational motors a ring is pressed to these points so that due to frictional forces the ring begins to rotate. One principle of an ultrasonic motor is the travelling wave motor in which bending waves may be used to generate the elliptic motion. The bending waves themselves are excited by piezoceramic elements which are bonded to the stator. A travelling wave may be generated if two groups of piezoceramics are excited both with a temporal and spatial phase shift. In order to get large amplitudes the two modes have to be excited in resonance. As the excitation frequency is the same for the two modes, the resonance frequencies of both modes should be equal or nearby.

For rotational motors this requirement may be fulfilled due to the rotational symmetry. For stators of linear motors, however, production uncertainties may lead to large differences between the eigenfrequencies of the two corresponding modes. One idea is to manipulate the stator after the production process in order to shift the resonance frequencies. This, however necessitates that the position of the mode shapes are known. In theory the mode shapes can be determined for example by a finite element analysis. As in the finite element model the eigenfrequencies should be identical every function which is a combination of the two corresponding mode shapes is also a mode. In reality, the two corresponding eigenfrequencies differ to a certain amount and therefore, the modes are spatially fixed in the system and in general they differ from those obtained by FEM.

The lecture presents some ideas how the eigenfrequencies and the modes of the real system can be determined experimentally. First the stator of the ultrasonic linear motor is modeled as a periodic system. The excitation of the two modes is done by piezoceramic elements which are bonded in such a way that each group excites one of the modes. In order to obtain eigenfrequencies which differ from each other, an asymmetry is introduced in the theoretical model. Results are obtained depending on the amount and position of the asymmetry. Also in the theoretical model the effect of the temporal phase shift is investigated. If the two piezoceramic groups are excited harmonically with a temporal phase shift of 90 degrees for the symmetric system a pure travelling bending wave is obtained. If there is an asymmetry the phase shift of the vibration may be different from the phase shift of the electrical excitation and if damping is taken into consideration the situation even gets more complicated.

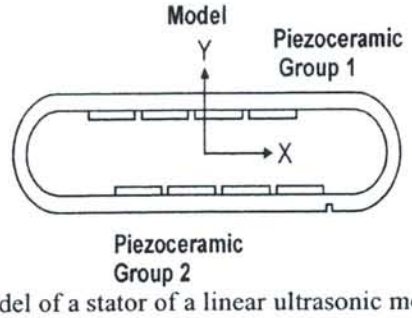

Model of a stator of a linear ultrasonic motor

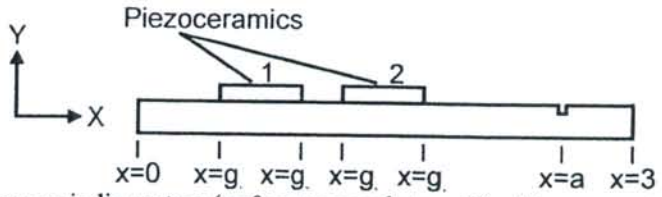

Model as a periodic system (x=0 corresponds to x=3) with asymmetry at x=a

THE FREE VIBRATION ANALYSIS OF LAMINATED ELLIPTIC PLATES BY A MESHLESS METHOD

Anand V. Singh
Department of Mechanical and Materials Engineering, The University of Western Ontario, London, Ontario, Canada
email: avsingh@eng.uwo.ca

Introduction. The earliest investigation on the vibration of elliptic plate dates back to 1802 by Chladni and nearly one and one half century later Mary Waller [1] published in 1950 the comparison of her experimental results with those of Chladni. During the fifties of the last century, some researchers obtained frequency equation for the vibration of elliptic plate in terms of Mathieu's functions. Leissa [2] published a paper on the free vibration of a simply supported elliptical plate using the Rayleigh-Ritz method. In this study, he reported experimental work done on the vibration of free elliptical plate by Mary Waller in 1950 and many other distinguished researchers who obtained frequency equation using the Mathieu's function. The free transverse vibration of elliptical plates with rectangular orthotropy and completely free edges was analyzed by Narita[3] who also used the Ritz method by considering complete power series as a trial function and obtained the natural frequencies for a range of aspect ratios. He continued along the same line to analyze orthotropic elliptical plates resting on arbitrarily distributed point supports [4]. Recently, Hosokawa et al. [5] published a paper that involved both a numerical solution for the free vibration analysis of clamped anti-symmetrically laminated elliptical plates and the experimental study of the same.

In the present study, a modified version of the Rayleigh-Ritz method is used to study the free vibration analysis of fiber reinforced laminated elliptical plate, the domain of which is first mapped into a circular domain and then further mapped into a square using natural coordinates and cubic interpolating functions. The geometry is represented by a set of sixteen nodes in the model. In a similar manner, for the displacement fields, a different set of nodal points is introduced and the shape functions are then obtained using considerably higher order polynomials than those used for the geometric shape functions. By keeping the plate geometry unchanged, the convergence in the solution is obtained by increasing the order of the displacement shape functions.

Formulation. The numerical method, which is a kind of subparametric finite element is based on the first order shear deformable plate theory also known as the Reissner-Mindlin Theory of plates. The displacement components along the Cartesian axes at an arbitrary point in the plate are denoted by u', v' and w' respectively. Under this scheme, the displacement components are expressed in terms of the displacement components at the middle plane of the plate and also the components of rotation of the normal to this plane as: $u' = u + z\beta_1$, $v' = v + z\beta_2$, $w' = w$. Here, symbols u, v, w denote the displacement components along x, y, and z axes respectively; β_1 and β_2 are components of rotation of the normal to the middle plane of the plate; and z is the distance measured from the reference plane in the direction perpendicular to the plate. The primed indices correspond to an arbitrary point (x, y, z) in the plate whereas the unprimed ones are associated with the corresponding parameter at the middle plane $(x, y, 0)$. For the flexural modes of the plate vibration, it is appropriate to assume $u = 0$ and $v = 0$, i.e. no stretching of the middle plane. The shear correction factor $(k = 5/6)$ is used in this method to compensate for the parabolic distribution of the transverse shear stress along the thickness. The ellipse having a and b as the major and minor axes respectively in x-y plane can be mapped into a circle in the s-t plane by using $s = x/a$ and $t = y/b$. The differentials are also modified accordingly as: $dx = a\,ds$ and $dy = b\,dt$. Using

this, it is very simple to note that $\partial/\partial x = (1/a)\partial/\partial s$, $\partial/\partial y = (1/b)\partial/\partial t$ and the infinitesimal area $dA = dx\,dy = a\,b\,ds\,dt$. In the following, the geometry is defined in s-t coordinate system with the help of the natural coordinates.

The geometry of a plate being studied is bounded by a quadrilateral region with curved edges in the s - t plane. This region is considered to represent the middle surface of the plate of which the thickness (h) is assumed to be uniform across the region and small in comparison with the dimensions along s and t axes. Furthermore, the natural co-ordinates ξ and η, bounded by $-1 \le (\xi \text{ or } \eta) \le +1$, together with the shape functions $N_j(\xi,\eta)$ *for* $j = 1,2,3,.....8$ are used in this study to interpolate the coordinates (s,t) of an arbitrary point inside the quadrilateral region.

$$s(\xi,\eta) = \sum_{j=1}^{16} N_j(\xi,\eta)\, s_j \qquad t(\xi,\eta) = \sum_{j=1}^{16} N_j(\xi,\eta)\, t_j \tag{1}$$

Hereafter, all the functional forms of the plate quantities are expressed in terms of the natural co-ordinates ξ and η. The Jacobian matrix $[J(\xi,\eta)]$ and its determinant $|J(\xi,\eta)|$ are used in the derivation of the plate equations. As mentioned earlier, the interpolating functions of much higher order than those used above for the geometry are considered for the displacement fields. For this, a different set of displacement nodes are introduced and each node is assigned three degrees of freedom pertaining to w, β_1 and β_2 respectively. The displacement and rotation components are represented by the following.

$$w = \sum_{j=1}^{n} \psi_j(\xi,\eta)\, W_j \qquad \beta_1 = \sum_{j=1}^{n} \psi_j(\xi,\eta)\, \Phi_j \quad \beta_2 = \sum_{j=1}^{n} \psi_j(\xi,\eta)\, \Theta_j \tag{2}$$

The interpolating functions $\psi_j(\xi,\eta)$ in eq. (2) are deduced in the same manner as $N_j(\xi,\eta)$ in eq. (1). Indices W_j, Φ_j and Θ_j correspond to w, β_1 and β_2 respectively, at the jth displacement node. Complete polynomials in each ξ and η are used in the displacement interpolation. To achieve this, nodes are introduced at the four edges as well as in the interior of the plate geometry. If p and q denote respectively the orders of the polynomials in ξ and η, the number of displacement nodes needed is $n = (p+1)(q+1)$.

Numerical Example. To validate the numerical procedure described briefly, an anti-symmetrically laminated clamped elliptic plate with the stacking sequence of $30°/-30°/30°/-30°$ is considered and analysed using $p = q = 11$. The plate parameters are denoted by: a = major axis, b = minor axis, h = thickness, ρ = mass density, ω = circular frequency in radian per second, D = flexural rigidity, etc. The condition applied at the boundary is: $w = \beta_1 = \beta_2 = 0$. The natural frequency parameter $\Omega = \omega\sqrt{D/\rho h b^4}$ are calculated for the first four modes of the laminated plate and presented in the Table for three different materials, viz. E-Glass/Epoxy, Boron/Epoxy and Graphite Epoxy. Also included in this table are the values of the natural frequencies obtained earlier by Hosokawa et al. [5]. The present method has used the first order shear deformation theory of plates, whereas the work by Hosokawa is based on the classical thin plate theory. The two sets of results are found to be in good agreement with each other. When the calculations were performed for an isotropic circular plate with $b/a = 1.0$ and also for an isotropic elliptical plate with $b/a = 2.0$, the results prom the present method were found to match almost exactly with the results from others researchers.

References:

[1] Waller, M. D., 1950, "Vibration of free elliptical plates," Proceedings of the Physical Society (London) Series B 63, pp. 451-455.
[2] Leissa, A. W., 1967, "Vibration of a simply supported elliptic plate," J. Sound and Vibration, 6(1), pp. 145-148.
[3] Narita, Y., 1985, "Natural frequencies of free orthotropic elliptical plates," J. of Sound and Vibration, 100, pp. 83-89.
[4] Narita, Y., 1986, "Free vibration analysis of orthotropic elliptical plates resting on arbitrarily distributed point supports," J. of Sound and Vibration, 108, pp. 1-10.
[5] Hosokawa, K., Yamada, Y. and Sakata, T., 1998, "Free vibration analysis of clamped antisymmetrically laminated elliptical plates," ASME J. of Applied Mechanics, 65, pp. 341-345.

Table 2. Dimensionless Natural Frequencies $\Omega = \omega\sqrt{D/\rho h b^4}$ of four layered elliptical plates with the stacking sequence of $30°/-30°/30°/-30°$.

E-Glass / Epoxy: $E_1 = 60.7\,GPa$, $E_2/E_1 = 0.40857$, $G_{12}/E_1 = 0.19753$, $\nu_{12} = 0.23$								
a/b	Mode 1		Mode 2		Mode 3		Mode 4	
	Present	Ref. [5]	Present	Ref.[5]	Present	Ref.[5]	Present	Ref [5]
1.0	8.2789	8.1294	15.523	15.945	18.760	17.826	25.596	26.337
1.2	6.7646	6.7302	13.364	13.562	14.749	14.429	22.370	22.387
1.5	5.6297	5.6750	10.178	10.150	13.051	13.242	16.544	16.273
2.0	4.8482	4.9364	7.5378	7.6033	11.277	11.204	12.061	12.331
2.5	4.5174	4.6173	6.3661	6.4693	8.8710	8.8890	11.603	11.911
3.0	4.3389	4.4432	5.7383	5.8542	7.5953	7.6393	10.081	9.8241
4.0	4.1483	4.2573	5.0951	5.2120	6.3422	6.3625	8.0735	7.7235
Boron / Epoxy: $E_1 = 209\,GPa$, $E_2/E_1 = 0.09091$, $G_{12}/E_1 = 0.1 = 030622$, $\nu_{12} = 0.21$								
a/b	Mode 1		Mode 2		Mode 3		Mode 4	
	Present	Ref. [5]	Present	Ref.[5]	Present	Ref.[5]	Present	Ref [5]
1.0	6.8395	6.2734	10.855	11.226	16.347	14.619	16.860	17.409
1.2	5.2810	4.9732	9.0291	9.6750	12.594	10.956	14.210	15.393
1.5	4.0627	3.9353	7.2922	7.9485	9.4360	8.4029	11.855	12.609
2.0	3.1954	3.1607	5.3680	5.6024	7.6755	7.4049	8.4682	8.6595
2.5	2.8336	2.8165	4.3294	4.5110	6.4220	6.6178	7.0679	6.9295
3.0	2.6476	2.6320	3.7582	3.9107	5.2736	5.4752	6.7543	6.6586
4.0	2.4612	2.4445	3.3182	3.2924	4.1305	4.2958	5.4111	5.4693
Graphite / Epoxy: $E_1 = 138\,GPa$, $E_2/E_1 = 0.06493$, $G_{12}/E_1 = 0.05145$, $\nu_{12} = 0.30$								
a/b	Mode 1		Mode 2		Mode 3		Mode 4	
	Present	Ref. [5]	Present	Ref.[5]	Present	Ref.[5]	Present	Ref[5]
1.0	6.8457	6.2489	10.926	11.080	16.331	14.650	16.858	17.199
1.2	5.2933	4.9359	9.0562	9.5392	12.633	10.941	14.115	15.243
1.5	4.0754	3.8923	7.2609	7.9018	9.5144	8.2838	11.776	12.582
2.0	3.2018	3.1198	5.3307	5.5419	7.7278	7.3067	8.4658	8.6120
2.5	2.8337	2.7800	4.3030	4.4518	6.4110	6.5558	7.0885	6.8440
3.0	2.6433	2.5992	3.7373	3.8560	5.2600	5.4113	6.7558	6.5809
4.0	2.4530	2.4162	3.3167	3.2463	4.1182	4.2377	5.4157	5.4042

THEORETICAL PREDICTION OF LIMIT CYCLE OSCILLATIONS FOR AIRCRAFT IN TRANSONIC FLOW

Earl H. Dowell[1]

Duke University, Durham, North Carolina 27708-0300

ABSTRACT

Limit cycle oscillations have been observed in flight in various military aircraft including the F-16, F-18 and B-1 as well as commercial aircraft due to the interaction between the dynamics of the flexible structure and the surrounding aerodynamic flow. Limit cycle oscillations also have been observed in wind tunnel models and when the governing nonlinearity is in the structural model, e.g. freeplay or geometric strain-displacement effects, good correlation has been obtained with theoretical models. However nonlinear aerodynamic effects such as large shock wave motion or separated flow have proven to be more difficult to model theoretically and no definitive correlation between theory and experiments has yet been achieved.

In this presentation, recent advances in theoretical prediction of nonlinear effects in the aerodynamic flow interacting with the flexible structure are presented for three configurations where experimental data are available. These are the supercritical airfoil, NLR 7301, tested at the German transonic wind tunnel facility in Gottingen; the AGARD 445.6 wing tested at the Transonic Dynamics Tunnel at the NASA Langley Research Center; and the operational aircraft, F-16, flight tested at Eglin Air Force Base. Initial correlations between theory and experiment are shown which are encouraging. These are the beginnings of a more extensive planned validation and verification process.

---

[1]J.A. Jones Professor, Department of Mechanical Engineering and Materials Science and Director of the Center for Nonlinear and Complex Systems. Dean Emeritus, Pratt School of Engineering.

Dynamics of a flexible cable loop

L.N. VIRGIN
School of Engineering and
Center for Nonlinear and Complex Systems
Duke University, Durham, NC 27708-0300.
and
R.H. PLAUT
Charles E. Via, Jr. Department of Civil and Environmental Engineering
Virginia Polytechnic Institute and State University, Blacksburg, VA 24061-0105.

Abstract

This paper considers the stability and dynamics of a very flexible cable *loop* structure. There is a subtle interplay between gravitational loading (achieved through changing length and hence self-weight) and (linear) free vibrations. The cable stiffness exhibits a softening nonlinearity which leads to an unstable symmetric bifurcation as the cable changes from an upright position and then droops heavily, and suddenly, to one side. The qualitative nature of the behavior is captured by a relatively simple model, and comparisons are made with an analysis of the continuous system. Both pre- and post-buckling dynamics are included in the study together with some preliminary experimental results.

The model

Consider the simple loop structure shown in Figure 1 consisting of a plastic-coated steel coil cable. By varying the length (say, through feeding in more material through one of the built-in ends) we can observe some interesting dynamics and stability (Ioos and Joseph [1] attribute this model to T.B. Benjamin in their book). The softening nature of the rod causes the system to exhibit an unstable-

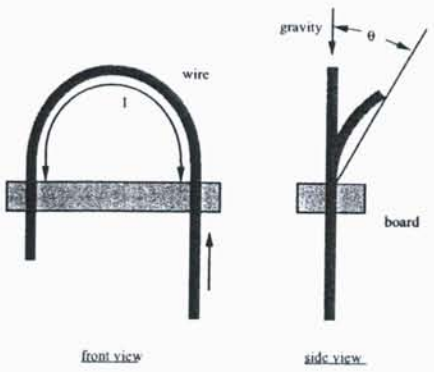

Figure 1: *Schematic of the rod.*

symmetric bifurcation which subsequently stabilizes for large deflections. In purely qualitative terms we can write down the *form* of the potential governing this behavior as

$$V = \frac{1}{720}q^6 - \frac{1}{24}q^4 - \frac{1}{2}\lambda q^2, \tag{1}$$

where λ is associated with the cable length, and θ is associated with the lateral deflection of the loop. The corresponding equilibrium conditions are then given by [2]

$$V' = \frac{1}{120}q^5 - \frac{1}{6}q^3 - \lambda q = 0, \tag{2}$$

which can be solved to give the equilibrium paths:

$$\begin{aligned} q &= 0 \\ \lambda &= -\frac{1}{6}q^2 + \frac{1}{120}q^4. \end{aligned} \tag{3}$$

The stability of these paths depends on the second derivative of potential energy:

$$V'' = \frac{1}{24}q^4 - \frac{1}{2}q^2 - \lambda, \tag{4}$$

and evaluating this expression along the equilibrium paths of equation (3) we get

$$\begin{aligned} V''_f &= -\lambda \\ V''_p &= \frac{1}{24}\left[10 \pm \sqrt{100 + 120\lambda}\right]^2 \\ &\quad -\frac{1}{2}\left[10 \pm \sqrt{100 + 120\lambda}\right] - \lambda, \end{aligned} \tag{5}$$

where the subscripts f and p denote fundamental and post-buckled, respectively.

The equilibria for this system are shown in Figure 2(a) where we observe a stable-symmetric bifurcation (super-critical pitchfork) which subsequently restabilizes, i.e., as the length of the rod is increased the loop grows in its upright (trivial) equilibrium until it droops over (to one side or the other). This process is dynamic since there is no locally adjacent stable configuration.

For small amplitude vibrations about these nonlinear equilibrium paths we can make use of Rayleigh's method to relate the natural frequency to the underlying potential energy. This is plotted in Figure 2(b), in which we observe the decay in the natural frequency prior to initial buckling. The system will naturally settle onto a remote post-buckled equilibrium (i.e., heavily drooped over) with a new natural frequency.

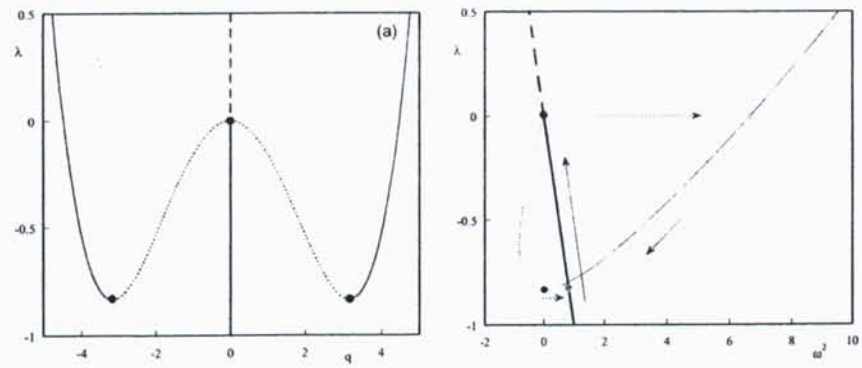

Figure 2: *Equilibrium and dynamics of the cable.*

This study has been developed in a number of directions:

- *Initial Imperfections* - symmetric structures inevitably have some initial geometric imperfection which tends to have a relatively important influence on instability, i.e., the inherent symmetry of the system is broken. The governing potential can be easily augmented to take account of this.
- *Damping* - the inevitable presence of a little energy disspation will cause the system to become overdamped just prior to buckling. For example, with $\beta = 0.1$ oscillations would cease when $\lambda = -0.0025$.

- *Nonstationarity* - incorporating the inertia terms, integrating the equation of motion can be achieved while sweeping through the control parameter (the length of the rod). An example of this is shown in Figure 3 including a reverse sweep to highlight hysteresis.

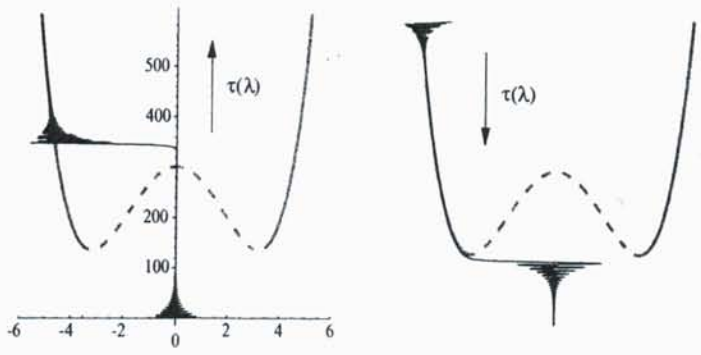

Figure 3: *A slow sweep through the butterfly bifurcation.*

- A classical mechanics solution can also be obtained based on a conventional vectorial approach [3]. Some configurations are shown in Figure 4 for three different lengths (three snapshots of time) as the loop starts to droop (dynamically) from the upright position.

Figure 4: *Some equilibrium shapes based on the continuum model.*

References

1. G. Iooss and D.D. Joseph (1990) *Elementary Stability and Bifurcation Theory*, Springer.
2. J.M.T. Thompson and G.W. Hunt (1984) *Elastic Instability Phenomena*, Wiley.
3. R.H. Plaut and L.N. Virgin (2002) "Dynamics and stability of a flexible cable loop with a softening stiffness characteristic" (*in preparation*).

Nonlinear Longitudinal Vibrations of Transversely Polarized Piezoceramics

Utz von Wagner and Sandeep Kumar Parashar

Department of Applied Mechanics, Technische Universität Darmstadt, Hochschulstrasse 1, 64289 Darmstadt, Germany

1 Introduction

Characteristic nonlinear vibration behavior can be found when piezoceramic actuators are excited even by weak electric fields. In this presentation the authors attempt to model this behavior using higher order dissipative and nondissipative terms respectively in the constitutive equations. Hamilton's principle is used to obtain the equation of motion. The partial differential equation is directly attacked to get the solution and as an alternative approach Rayleigh-Ritz method is also used. The results of these two different approaches are compared.

2 Experiments

Experimental studies of piezoceramics subjected to weak electric field have revealed typical nonlinear vibration behavior, e.g. dependence of the resonance frequency on the amplitude, superharmonics at twice and three times of the excitation frequency and a nonlinear relationship between excitation voltage and vibration amplitude [2]. Figure 1 shows a free piezoceramic beam, which is transversely polarized in z-direction. In the experiment, longitudinal vibration of the piezoceramic is excited at different excitation voltages using the d_{31}-effect near to the first resonance. The displacement amplitude is measured with the help of a laser-vibrometer and the current is measured using shunts. The experimental results plotted in Figure 2 clearly show the nonlinear vibration behavior of this piezoceramic.

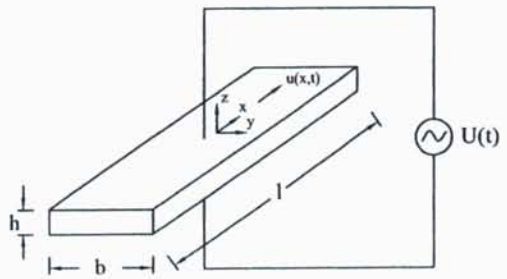

Figure 1: Experiment: transversally polarized piezoceramic actuator.

3 Nonlinear Modelling

To model the nonlinear vibration behavior, linear constitutive relations of piezoceramics are modified in the following manner

$$T_{xx} = E^{(0)} S_{xx} - \gamma_0 E_z + E_d^{(0)} \dot{S_{xx}} + E^{(1)} S_{xx}^2 + E_d^{(1)} (\dot{S_{xx}^2}) + E^{(2)} S_{xx}^3 + E_d^{(2)} (\dot{S_{xx}^3}), \tag{1}$$

where T_{xx} and S_{xx} denote the stress and the strain respectively in x-direction. $E^{(0)}$ and γ_0 are the elastic modulus and the piezoelectric coupling factor for the one-dimensional longitudinal vibration. $E^{(1)}$ and $E^{(2)}$ are the parameters of the quadratic and cubic nonlinear nondissipative elastic terms while $E_d^{(1)}$ and $E_d^{(2)}$ are the corresponding dissipative terms.

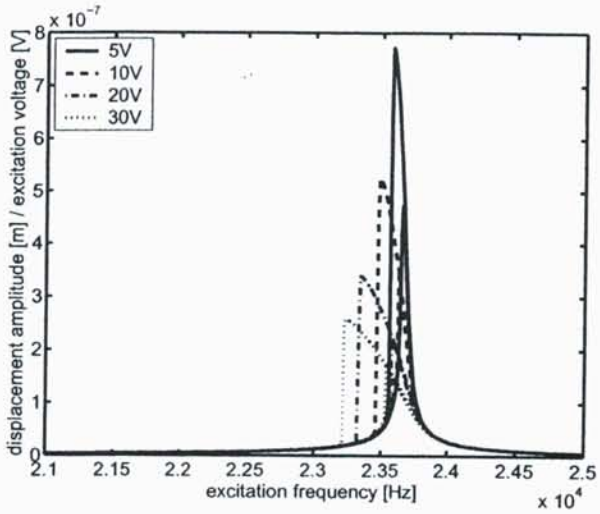

Figure 2: Experiment: displacement amplitude response close to first resonance.

4 Direct solution of the field equation

Using Hamilton's principle, the equation of motion

$$-\rho\ddot{u} + E^{(0)}u'' + 2E^{(1)}u'u'' + 3E^{(2)}u'^2u'' + E_d^{(0)}\dot{u}'' + 2E_d^{(1)}u''\dot{u}' + 2E_d^{(1)}u'\dot{u}'' + 3E_d^{(2)}u'^2\dot{u}'' + 6E_d^{(2)}u'u''\dot{u}' = 0 \quad (2)$$

and corresponding boundary conditions can be obtained. The excitation can be found in the boundary conditions. Now the partial differential equation is directly solved using perturbation techniques to obtain the solution ([1]). If the quadratic terms are considered to be of the same order as the cubic ones, they will not appear in the solution. Hence in the first step, the quadratic terms are considered to be of the order ε while the damping, cubic terms and the excitation terms will be considered to be of the order ε^2. Using the coordinate transformation $\xi = \frac{2x}{l}$ and $\frac{\partial}{\partial x} = \frac{2}{l}\frac{\partial}{\partial \xi}$ and rewriting the above partial differential equation results in

$$-\frac{\pi^2}{4}\ddot{u} + \omega_0^2 u'' + \varepsilon\alpha_1^* u'u'' + \varepsilon^2\alpha_1 u'^2u'' + \varepsilon^2 k\dot{u}'' + \varepsilon^2\alpha_3 u'^2\dot{u}'' + 2\varepsilon^2\alpha_3 u'u''\dot{u}' + \varepsilon^2\alpha_5 u''\dot{u}' + \varepsilon^2\alpha_5 u'\dot{u}'' = 0. \quad (3)$$

Using the perturbation method with the expansion

$$u(\xi,t) = u_0(\xi,t) + \varepsilon u_1(\xi,t) + \varepsilon^2 u_2(\xi,t) + ..., \quad \Omega^2 = \omega_0^2 + \varepsilon^2\delta + ...$$

gives the zeroth solution

$$u_0(\xi,t) = A\sin\frac{\pi}{2}\xi\cos\Omega t \quad (4)$$

where the amplitude A can be obtained from vanishing secular terms of the equation of second order.

5 Rayleigh-Ritz method

As an alternative approach the Rayleigh-Ritz method is used to obtain the equation of motion. The following Ritz ansatz is used for discretization

$$u(x,t) = U_k(x)p_k(t) \quad (5)$$

where U_k is the first eigenform of the linear problem. Then, the equation of motion is given as

$$m_k\ddot{p}_k + d_k\dot{p}_k + c_k^{(1)}p_k + c_k^{(2)}p_k^2 + c_{kd}^{(2)}p_k\dot{p}_k + c_k^{(3)}p_k^3 + c_{kd}^{(3)}p_k^2\dot{p}_k = f_k^{(1)}\cos\Omega t. \quad (6)$$

This equation of motion can also be solved approximately using perturbation techniques.

Experiments conducted at one half and one third of the first resonance frequency have revealed, that the quadratic and cubic nonlinearities at the piezoceramics are of comparable order of magnitude. Following these experimental results, both quadratic and cubic nonlinearities should be considered to be of the same order ε. This will result in the fact, that the quadratic nonlinearities will not influence the zeroth approximation of the vibration response.

Hence, in both methods, quadratic nonlinearities are neglected and cubic parameters are determined, which fit the theoretical curves to the experimental ones. The comparison of the two solution methods with the experiment shows a good agreement of all three curves (Figure 3).

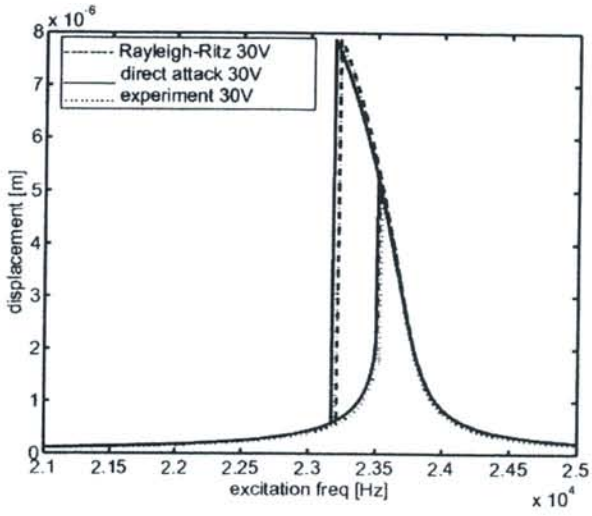

Figure 3: Comparison of amplitude responses from the two methods and the experiment.

6 Conclusions

The nonlinear behavior of a piezoceramic actuator is modeled by introducing quadratic and cubic nonlinearities in constitutive equations. Due to experimental observations, both dissipative and nondissipative terms are used. The resulting equations of motion are solved using perturbation techniques by directly attacking the field equation or by solving equations which are discretized via Rayleigh-Ritz. Using parameters identified for the piezoceramics, a good coincidence between the experimental and the two theoretical results can be observed.

References

[1] A. H. Nayfeh and W. Lacarbonara 1997 *Nonlinear Dynamics* 13, 203-220. On the discretization of distributed parameter systems with quadratic and cubic nonlinearities.

[2] U. v. Wagner 2003 *International Journal of Non-Linear Mechanics* 38(4), 565-574. Non-linear longitudinal vibrations of piezoceramics excited by weak electric fields.

Friction–Induced Instabilities in a Disk Brake Model Including Heat Effects

Jörg Wauer and Jürgen Heilig
Institut für Technische Mechanik, Universität Karlsruhe
Kaiserstraße 12, D–76128 Karlsruhe, Germany
E–mail: wauer@itm.uni-karlsruhe.de

Abstract: The dynamics of a structural car brake model is examined to explain brake noise by friction–induced instabilities including thermal effects. After discretizing the governing boundary value problem by a modal expansion technique, a highly nonlinear system of ordinary differential equations is obtained. A stability analysis is performed which shows instabilities for high and for low driving speed responsible for brake noise. Several suggestions are made to obtain stable operation conditions without noise.

Introduction

Automotive brake noise has become an increasingly important issue for both vehicle quietness and comfort. Several distinct mechanisms have been investigated which provoke instabilities in the brake system assumed to be responsible for this brake noise [1]. A detailed survey of past and recent developments is given by Nishiwaki [2] and Yang and Gibson [3]. All previous theoretical investigations can be divided in two categories. The first one uses large–scaled finite–element models for the whole brake system and will not be discussed in the following. In contrast, the second category deals with closed–form analytical or semi–analytical approaches [4] where simple disk and pad models are introduced and, as an important detail, relative motion between disk and pad is included.

In the present contribution, a structural brake model is introduced characterized by pad motion in circumferential direction and both friction and heating at the contact points between pads and disk. While in two earlier papers [5,6] of the authors the main interest was focused on the detection of instabilities for higher vehicle speed, here the considerations are extended to the range of low speed when stick–slip motions cannot longer be avoided. Additionally, thermal effects will be included considering the heat production by the friction contact between pads and thermoelastic ring. The objective is to find a conclusive explanation for brake squeal and hot spotting within a realistic speed range of the vehicle. Therefore, the stability of the steady state response of the disk brake model is proven to identify growing thermoelastic vibrations of the ring and interacting pad oscillations.

Modeling

Dynamic simulations of an expensive FEM brake model demonstrate that the axial vibrations of the brake disk are dominant compared to the oscillations found in radial and circumferential direction. Therefore, an analytical model for the brake system is established. The brake disk is approximated by a slender thermoelastic ring of mass density ρ, Young's modulus E and damping coefficients $d_{1,2}$. The ring of mean radius R, thickness h and radial dimension b rotates with constant angular velocity Ω. k is the thermal conductivity, α the linear thermal expansion coefficient and c_v the specific heat; β denotes the heat transfer coefficient between ring and surroundings. The two stationary brake pads are connected to the rotating ring by two separate one–point contacts assuming that the pads have identical physical properties. Each pad is modeled as a rigid body of mass M viscoelastically (spring constants $c_{y,z}$ and damping coefficients $d_{y,z}$) suspended in axial and circumferential direction and loaded by an external axial brake force $F_{1,2}$ such that a separation of pads and ring in axial direction is avoided.

Between the rotating ring and the sliding pads, dry so–called Stribeck friction is assumed. Typically, the friction coefficient is a function of the relative (angular) velocity between the contacting parts and exhibits different stick and sliding friction coefficients μ_h and μ_g, respectively. At the two contact points between pads and ring, heat is fed into the ring which is proportional to the power of the friction forces.

Formulation

It seems to be adequate to formulate the model equations applying a stationary reference frame to avoid parametric vibrations. Then, a time–invariant boundary value problem results with the complication that it appears as a highly nonlinear system of differential equations. The transformation $\varphi = \Omega t + \phi$ (time t) connects the Euler variable φ and the material coordinate ϕ. There are bending vibrations $w(\varphi, t)$ of the ring and the temperature field $\vartheta(\varphi, z, t)$ (axial thickness coordinate $-\frac{h}{2} \leq z \leq +\frac{h}{2}$) in it interacting with the circumferential pad oscillations $R\psi_k(t)$ $(k = 1, 2)$. With respect to the axial pad vibrations it is assumed that there is a permanent contact to the ring at the location $\varphi_{ck} = \psi_k(t)$ $(k = 1, 2)$ so that the corresponding displacements coincide with $w(\varphi_{ck}, t)$. Identifying the relative (angular) velocity $\Omega_{rel} = \Omega - \dot{\psi}_k(t)$ (superior dots denote derivatives with respect to time t) between the contacting parts, an analytic description of the friction characteristic can be given. Assuming that the temperature field is a linear function of z (taking into consideration that, in particular, in–plane circumferential deformations are not permitted), the thermoelastic field equations of the ring as a system of two coupled partial differential equations together with two additional integro–differential equations describing the circumferential pad motion can be written.

The initial–boundary value problem obtained is highly nonlinear and, in general, cannot exactly be solved. In a first solution step which can be performed analytically, the steady–state response is calculated assuming that the brake forces are identical on both sides. Observing then the brake system's dynamics about the operating stationary state, inserting a superposition of steady–state solutions and small perturbations into the equations of motion and transforming the position coordinate into the operating state, the governing equations for the perturbations can be given. As the next solution step, the expansion theorem is applied to discretize the ring. A Fourier series for ring displacement and temperature (fulfilling all conditions of periodicity) and applying Galerkin's approach to the ring equations as well evaluating the integro–differential equations lead to a set of $4(n + 1 - j_0) + 2$ homogeneous nonlinear ordinary differential equations.

The stability of the steady state response of the disk brake model is proven by an eigenvalue analysis of the corresponding variational equations about the stationary solution supplemented by the computation of the top–Lyapunov exponent corresponding to the discretized strongly nonlinear equations of motion. While for high operating speed rates, the dynamics is smooth and the suggested linearization obviously leads to correct results, the eigenvalue analysis (based on the variational equations) becomes questionable for low speed range because the stationary operation state in that case may be close to the discontinuity at $\Omega_{rel} = 0$. Now it is appropriate to verify the results of the eigenvalue analysis by the computation of the largest Lyapunov exponent. But for nonlinear systems with discontinuities, there is no mathematical proof of any definition of λ_L so that also this approach is problematic, however, in most cases satisfying results are obtained from an engineering point of view.

Results and Discussion

First, a reference case neglecting thermal effects is discussed. Based on a calculation of the maximum real part of the eigenvalues λ_i of the system matrix, for a three–term truncation of the ring $(j_0 = 1, n = 3)$, a stability chart is presented for the undercritical speed range $\eta < 1$ and for different "circular frequencies" $\omega_y = \sqrt{\zeta_y/m}$ of the pads in circumferential direction. It is assumed that η is sufficiently high so that stick slip phenomena, first of all, cannot occur and Coulomb's friction law with a constant sliding friction coefficient μ_g in the considered speed range can be assumed. A comparison with the normalized eigenfrequencies ω_i $(i = 1, 2, \ldots)$

of the rotating ring (neglecting the circumferential pad dynamics) shows that the instabilities may occur if $\omega_y \approx \omega_i$, i.e., the nonlinear interaction of ring and pad dynamics (together with gyroscopic effects) leads to so–called internal resonance which gives rise to the appearing instabilities. A detailed parameter study can be found in the thesis [7].

Now taking into consideration the Stribeck friction characteristic and activating stick–slip in a speed range $0 \leq \eta \leq 2.4 \cdot 10^{-4}$, the corresponding stability chart is given next. Obviously (as well–known), the stick–slip vibrations in form of a limit cycle destabilize the steady operation state of the brake system for every value ω_y, the instability bands shown earlier are slightly modified. Since, in particular, the results originating from an eigenvalue analysis of the variational equations are questionable, they are compared for the special case $\omega_y = 1$ with those obtained from a computation of λ_L associated with the original nonlinear equation set. Considering the stability boundaries, a good agreement of the results of the two methods can be stated.

In a last supplement, thermal effects are included which modify the results only quantitatively.

Conclusions

Friction–induced instabilities in a structural disk brake model have been examined to explain brake noise and hot spotting for high but also low vehicle speed. The stability analysis of the linearized originally strongly nonlinear model equations (supported by a computation of the top–Lyapunov exponent of the nonlinear equations) clearly shows that instabilities of the system due to internal resonances and accompanied by gyroscopic effects occur. For a realistic choice of all the system parameters as mass, stiffness, damping, friction coefficients, brake force, etc., these instabilities may appear in realistic speed ranges from about 100 – 150 km/h until very low values for which stick–slip phenomena have to be taken into consideration. It can be supposed that thermal effects modify the instability regions but not substantially and only in such a form that the increasing disk/pad vibrations are coupled with an increasingly oscillating temperature field which might be responsible for hot spotting in the brake disk. Additional instability ranges originating from the thermoelastic properties of the ring and the heat feeding at the contact points between pads and disk seem not to be generated.

To avoid these friction–induced instabilities, a specific tuning of the parameters can be suggested. Since a decreased brake force or friction coefficient – which would stabilize the system – cannot be recommended because of safety reasons, only increased damping coefficients (realized, for instance, by ceramic brake components) are really helpful within all speed ranges. A certain choice of the different stiffness parameters may shift instability domains to higher or lower speed ranges but in most engineering applications this is not helpful because for a car, braking can be required for every speed.

References

1. Ibrahim, R.A., Friction–induced vibrations, chatter, squeal and chaos, Part I and II, *Appl. Mech. Rev.* **47**, No. 7, 1994.
2. Nishiwaki, M., Review of study on brake squeal, *JSAE Review* **11**, No 4, 48–54, 1990.
3. Yang, S., Gibson, R.F., Brake vibration and noise reviews, comments and proposals, *Int. J. Materials & Product Technology* **12**, Nos. 4–6, 496–513, 1997.
4. Mottershead, J.E., Vibration and friction–induced instability in disks, *Shock & Vibration Digest* **30**, No. 1, 14–31, 1998.
5. Heilig, J., Wauer, J., Dynamics and Stabilty of a Nonlinear Brake Model. In: *Proc. DETC'01*, Pittsburgh, USA, DETC01/VIB–21579, 2001.
6. Heilig. J., Wauer, J. Stability of a Nonlinear Brake System at High Operating Speed, *Nonlinear Dynamics*, 2002 (to appear).
7. Heilig, J., Instabilitäten in Scheibenbremsen durch dynamischen Reibkontakt. *Diss. Universität Karlsruhe*, 2002.

ANALOGOUS BEHAVIOUR OF TRANSCENDENTAL AND LINEAR EIGENSOLUTIONS FOR FREE VIBRATION OF STRUCTURES

F. W. Williams
Department of Building and Construction, City University of Hong Kong, Kowloon, HONG KONG

D. Kennedy
Cardiff School of Engineering, Cardiff University, Cardiff CF24 0YF, UK

Let a member be hypothetically represented by an infinite number of finite elements, with its internal freedoms $\mathbf{d}_i$ numbered first and those of its connection nodes, $\mathbf{d}_c$, numbered last. For vibration (buckling can be dealt with similarly) the dynamic stiffness matrix of order $n \to \infty$ can be partitioned as

$$\begin{bmatrix} \mathbf{k}_{ii} - \omega^2 \mathbf{m}_{ii} & \mathbf{k}_{ic} - \omega^2 \mathbf{m}_{ic} \\ \mathbf{k}_{ic}^t - \omega^2 \mathbf{m}_{ic}^t & \mathbf{k}_{cc} - \omega^2 \mathbf{m}_{cc} \end{bmatrix} \tag{1}$$

where ω = circular frequency, $\mathbf{k}$ = the static stiffness matrix and $\mathbf{m}$ = the mass matrix.

Eliminating $\mathbf{d}_i$ by the usual static FEM substructuring procedure gives

$$\mathbf{k}_c = \mathbf{k}_{cc} - \omega^2 \mathbf{m}_{cc} - \left(\mathbf{k}_{ic}^t - \omega^2 \mathbf{m}_{ic}^t\right)\left(\mathbf{k}_{ii} - \omega^2 \mathbf{m}_{ii}\right)^{-1}\left(\mathbf{k}_{ic} - \omega^2 \mathbf{m}_{ic}\right). \tag{2}$$

Inversion by Cramer's rule shows that all elements (i, j) of $\mathbf{k}_c$ have the same denominator Δ_m and that it and the numerators k_{cij}^n are given by Eq. (3), in which $\mathrm{fn}\left(\omega^2\right)$ indicates functions consisting of only even powers of ω.

$$\Delta_m = \det\{\mathbf{k}_{ii} - \omega^2 \mathbf{m}_{ii}\} = \mathrm{fn}\left(\omega^2\right), \quad k_{cij}^n = \mathrm{fn}\left(\omega^2\right). \tag{3}$$

Clearly if any values of k_{cij}^n which are zero for all values of ω (e.g. due to lack of flexural and axial coupling) are excluded, neither Δ_m nor the k_{cij}^n can be zero at $\omega = 0$, and so normalising them by dividing by their values there gives

$$\overline{\Delta}_m = 1 + a_2\omega^2 + a_4\omega^4 + \ldots \qquad \overline{k}_{cij}^n = 1 + b_2\omega^2 + b_4\omega^4 + \ldots \tag{4}$$

in which the crucial point is that the first term is unity.

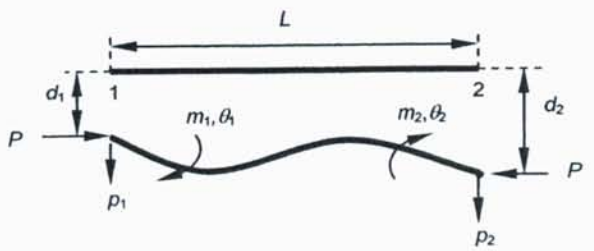

Figure 1. Member end forces and displacements.

Figure 1 shows d, θ, p and m, the displacement, rotation, force and moment amplitudes at ends 1 and 2 of a Bernoulli-Euler member, which are all multiplied by $\sin \omega t$. The member has length L, flexural rigidity EI, mass per unit length μ and axial force P. For Bernoulli-Euler beams, $P = 0$ and the transcendental flexural stiffnesses are given (Williams and Wittrick, 1970), using $k = EI/L$ and the λ of Eq. (7), by Eqs (5)-(8).

$$\begin{bmatrix} \gamma k/L^2 & \xi k/L & -\varepsilon k/L^2 & \delta k/L \\ & \alpha k & -\delta k/L & \beta k \\ \text{Symmetric} & & \gamma k/L^2 & -\xi k/L \\ & & & \alpha k \end{bmatrix} \begin{bmatrix} d_1 \\ \theta_1 \\ d_2 \\ \theta_2 \end{bmatrix} = \begin{bmatrix} p_1 \\ m_1 \\ p_2 \\ m_2 \end{bmatrix} \tag{5}$$

$$\left.\begin{aligned} \alpha &= (SC' - CS')\lambda/\sigma & \beta &= (S' - S)\lambda/\sigma & \gamma &= (SC' + CS')\lambda^3/\sigma \\ \delta &= (C' - C)\lambda^2/\sigma & \varepsilon &= (S + S')\lambda^3/\sigma & \xi &= (S\,S')\lambda^2/\sigma \end{aligned}\right\} \tag{6}$$

$$\lambda^4 = \omega^2 L^4 \mu/EI \qquad \sigma = (1 - CC') \tag{7}$$

$$S = \sin\lambda \quad C = \cos\lambda \quad S' = \sinh\lambda \quad C' = \cosh\lambda \tag{8}$$

The above notation is standard except for the abbreviations of Eq. (8). Because Eqs (5) – (8) include ω only *via* λ, Eq. (4) gives

$$\bar{\Delta}_m = 1 + c_4\lambda^4 + c_8\lambda^8 + \ldots \qquad \bar{k}^n_{cij} = 1 + d_4\lambda^4 + d_8\lambda^8 + \ldots \tag{9}$$

However substituting the expansions of the trigonometric and hyperbolic functions of Eq. (8) into the σ of Eq. (7) and into the six numerators of Eq. (6) gives, in every case, polynomials which satisfy Eq. (9) except that they start with a term in λ^4 instead of with 1. Hence dividing σ and all the numerators by the first term in the expansion for σ $(=\lambda^4/6)$ gives $\bar{\Delta}_m$ and the replacement for Eq. (6) as

$$\left.\begin{aligned} \alpha &= \left\{6\,(SC' - CS')/\lambda^3\right\}/\bar{\Delta}_m & \beta &= \left\{6\,(S' - S)/\lambda^3\right\}/\bar{\Delta}_m \\ \gamma &= \left\{6\,(SC' + CS')/\lambda\ \right\}/\bar{\Delta}_m & \delta &= \left\{6\,(C' - C)/\lambda^2\right\}/\bar{\Delta}_m \\ \varepsilon &= \left\{6\,(S + S')/\lambda\ \right\}/\bar{\Delta}_m & \xi &= \left\{6\,(S\,S')/\lambda^2\right\}/\bar{\Delta}_m \end{aligned}\right\} \qquad \bar{\Delta}_m = 6\,(1 - CC')/\lambda^4 \tag{10}$$

Here the brackets $\{\ \}$ contain the numerators, which may be denoted as α^n, β^n, γ^n, δ^n, ε^n and ξ^n and have the first term in their polynomials as, respectively, 4, 2, 12, 6, 12 and 6. Hence normalising them to become $\overline{\alpha^n}$, $\overline{\beta^n}$ etc, by dividing by their values at $\omega = 0$, which implies that $\mathbf{k}_c$ of Eq. (2) is normalised by using its value when $\omega = 0$, gives

$$\left.\begin{aligned} \bar{k}^n_{c11} &= \bar{k}^n_{c33} = \overline{\gamma^n} = \gamma^n/12 & \bar{k}^n_{c12} &= -\bar{k}^n_{c34} = \overline{\xi^n} = \xi^n/6 & \bar{k}^n_{c13} &= -\overline{\varepsilon^n} = -\varepsilon^n/12 \\ \bar{k}^n_{c14} &= -\bar{k}^n_{c23} = \overline{\delta^n} = \delta^n/6 & \bar{k}^n_{c22} &= \bar{k}^n_{c44} = \overline{\alpha^n} = \alpha^n/4 & \bar{k}^n_{c24} &= \overline{\beta^n} = \beta^n/2 \end{aligned}\right\} \tag{11}$$

Hence the stiffness matrix of Eq. (5) can alternatively be written as

$$\begin{bmatrix} 12k\bar{\gamma}/L^2 & 6k\bar{\xi}/L & -12k\bar{\varepsilon}/L^2 & 6k\bar{\delta}/L \\ & 4k\bar{\alpha} & -6k\bar{\delta}/L & 2k\bar{\beta} \\ \text{Symmetric} & & 12k\bar{\gamma}/L^2 & -6k\bar{\xi}/L \\ & & & 4k\bar{\alpha} \end{bmatrix} \tag{12}$$

where $\bar{\alpha} = \alpha^n / \bar{\Delta}_m$, etc. Hence the $\bar{\alpha}$, etc, become modification factors acting on the well-known stiffnesses of the slope-deflection equations, to which the Bernoulli-Euler equations limit when $\omega = 0$.

The transcendental formulations of Eqs (10)-(12) have fundamental importance because they represent the exact equivalence with the hypothetical infinite order FEM representation of Eqs (1)-(3). Hence the conventional Eqs (6) and (7) can be regarded as simplifications of Eq. (10) for use when computing because they are faster. In particular, although the above derivation lacks the mathematical rigour of the original proof that Eq. (10) gives the FEM $\bar{\Delta}_m$ it has appealing simplicity and elegance and it also establishes a very satisfyingly comprehensive equivalence with the infinite order FEM solution. Incidentally, Eq.(11) can be viewed as giving the coefficients of the matrix $\bar{\mathbf{k}}_c^n$, which is also given by normalising the $\mathbf{k}_c^n$ which follows from Eq.(2) as

$$\mathbf{k}_c^n = \det\{\mathbf{k}_{ii} - \omega^2 \mathbf{m}_{ii}\} \times (\mathbf{k}_{cc} - \omega^2 \mathbf{m}_{cc}) - (\mathbf{k}_{ic}^t - \omega^2 \mathbf{m}_{ic}^t)\mathbf{k}^* (\mathbf{k}_{ic} - \omega^2 \mathbf{m}_{ic}) \tag{13}$$

where $\mathbf{k}^*$ is the matrix containing the co-factors when Cramer's rule is applied.

The $\bar{\Delta}_m$ of Eq. (10) was only discovered recently and was named the *member stiffness determinant*. This is the first method developed for deriving it because previously it was found by trial and error and then verified by an appropriate procedure.

It is easily seen that ω^2 rather than ω is fundamental to the transcendental eigensolution, both because the FEM analogy given above uses ω^2 and also because the expressions of Eq (6) and the σ of Eq (7) contain only even powers of ω in their expansions. This will seem natural to those with an FEM background, but those working with transcendental eigenvalue problems have usually thought of ω (or even λ, implying $\sqrt{\omega}$) as being the eigenparameter. Switching to ω^2 has practical advantages. For example a recent recursive adaptation of standard inverse iteration to enable, for the first time, (almost) machine accuracy modes to be found for the transcendental eigenproblem has been shown, both theoretically and by numerical experiments, to converge faster when formulated in terms of ω^2 instead of in terms of ω.

Acknowledgements

The work forms part of EPSRC Grant number GR/R05406/01 and the first author will return to his chair at Cardiff University when his present appointment ends.

References

Williams, F. W. and Wittrick, W. H. (1970). "An automatic computational procedure for calculating natural frequencies of skeletal structures", *Int. J. of Mechanical Sciences*, **12** (9), 781-791.

EXACT MULTI-LEVEL TRANSCENDENTAL EIGENVALUE SOLUTION METHOD BY ANALOGY WITH THE NATURAL FREQUENCIES OF STRUCTURES

F.W. Williams
Department of Building and Construction, City University of Hong Kong, Kowloon, Hong Kong

W.P. Howson and A. Watson
Cardiff School of Engineering, Cardiff University, Cardiff, CF24 0YF, UK

Many disciplines involve eigenvalue problems and these often give spectra with alternating populated and void bands, e.g. pass- and stop-bands. The topical mathematics application reported here involves the tree topology shown in Figure 1. It illustrates the truly exceptional power of the Wittrick-Williams (W-W) algorithm[1,2], originally developed for structural mechanics, in order to stimulate its use in other disciplines, particularly those requiring exact solutions of transcendental eigenproblems.

Specifically, a single component at level 1 branches into b identical components at level 2 which themselves branch similarly, etc., to n levels. The components have their end conditions linked where branching occurs. The band spectrum shown in Figure 1 is for increasing values of n when all components obey the same simple second order Sturm-Liouville differential equation $-y'' = \lambda y$. The identical bullet-shaped curves bound the populated bands and repeat to infinity with the intermediate gaps void except for extremely high multiplicity eigenvalues at $i\pi$ (i = 1,2, ...).

A very recent mathematical study of this problem for n infinite[3] (n finite is more probable in other disciplines) could not obtain confirmatory numerical results for n large. This deficiency is currently being very successfully rectified by transfer from structural mechanics of the powerful multi-level substructuring[4] corollary of the W-W algorithm for solving such transcendental eigenproblems. Briefly, if λ_t is any value of λ, the W-W algorithm calculates J, the number of eigenvalues below λ_t. This has spawned many totally reliable eigenvalue computation methods. Alternatively, the eigenvalue count for an interval $(\lambda_\ell, \lambda_u]$ equals $J_u - J_\ell$. Hence: using successive intervals reveals the eigenvalue distribution, or *modal density*, plot; this incidentally reveals the band structure shown and; using almost infinitesimal intervals identifies multiple eigenvalues and their multiplicity.

The multi-level W-W corollary is most powerful when groups of components repeat frequently. Hence for the present problem a subsystem consisting of a set of b identical members at level n and their linked member at level (n-1) was analysed first to obtain equations relating solely to the left-hand end of the subsystem. b such subsystems and a member at level (n-2) were then similarly analysed, etc., until the complete tree was formed. For n = 43 and b = 2, a SUN Ultra 10 333 MHz computer using double precision arithmetic ($\cong$ 16 significant figures) gave J in 0.000071 seconds without ill-conditioning, despite there being $\cong 10^{12}$ components and no refinements such as pivoting. Eigenvalue multiplicities of N_T divided by 2, 6, 14, 30 etc. (i.e. with multiplicities of order $\cong 10^{11}$) were found extremely straightforwardly, where N_T = total number of eigenvalues in $(0, \pi]$. These multiplicities agreed with formulas for any b or n derived theoretically from an analogous structural mechanics problem, as described further below.

The tree with n = 4 and b = 3 of Figure 2 has been drawn and lettered to aid the following discussion of the behaviour of the structures, which assumes that all members are co-linear although clarity prevents them being shown as such. The structure is always clamped at node A and at all 27 of the nodes denoted by O-W. Each of O-W denotes three nodes, which are differentiated from each other by using subscripts t, m and b for, respectively, the top, middle and bottom nodes. Attention is confined below to consideration of the multiplicity of eigenvalues, by establishing a set of independent but not necessarily orthogonal modes.

Consider first the possible modes of vibration for which $\alpha = i\pi$, where $\alpha = \lambda^{\frac{1}{4}}$. These correspond to the clamped/clamped natural frequencies of each bar. Now consider any one of the 27 *paths* from any of nodes O-W to node A. The path contains four members and it is clearly possible for each of these to vibrate in-phase with each other and with equal amplitudes, while none of the other members vibrate. This is because there is no displacement at the three nodes at which the four members meet, since the frequency is a clamped/clamped natural frequency, and there is clearly force equilibrium at the three joints due to the amplitudes being equal. These 27 modes are clearly independent of each other, because each of them involves a different one of the 27 members at level 3, but are readily seen not to be mutually orthogonal. Other modes are easily visualised, but are readily shown to be combinations of two or more of these 27. For example, if the two members of the path Q_tHQ_b (or Q_tHQ_m) vibrate in anti-phase they give y = 0 (i.e. zero axial displacement) and equilibrium at H, but can be obtained by subtracting the mode for the path Q_bHCBA (or Q_mHCBA) from that of equal amplitude for the path Q_tHCBA. Similarly the mode for path $O_mFCBDJS_t$ can be obtained by subtraction of those for O_mFCBA and S_tJDBA, etc. Hence there are only 27 independent modes for this example. Since this is the number of members at level n-1 it follows by generalisation to any b or n that M_1, the number of independent modes of vibration for which $\alpha = i\pi$, is equal to b^{n-1}.

It is readily shown that eigenvalues at $\alpha = (i-\frac{1}{2})\pi$ correspond to clamped/free vibrations of a single member. Hence any path originating from all three nodes at any one of O-W, going to the node two levels to its left and returning to all three nodes at a different one of O-W defines a possible mode as follows. A typical such path is P*GCHQ* where the asterisk denotes the paths P_tG, P_mG and P_bG are all present, etc. Hence, so long as all members vibrate with equal amplitudes, compatibility (i.e. y is shared) is guaranteed at G and H if each of the six members represented by P*G and Q*H vibrate in-phase with their right-hand ends clamped and their left-hand ends free, while CG and CH vibrate in anti-phase with these six members and with their right-hand ends free and C clamped. So long as the paths CGP* and CHQ* vibrate with equal amplitudes in anti-phase to each other there is force equilibrium at C. Hence this mode satisfies all necessary compatibility and equilibrium conditions and so is one possible mode of the entire structure of Figure 2. Clearly b-1 independent modes of this type exist for each of C, D and E, i.e. in general there are $(b-1)b^{(n-3)}$ such modes. However in addition the four members AB, BC, BD and BE form a similar pattern to the one just discussed and so contribute one further mode only, since member AB is at level zero. In general for higher n, i.e. n>5, there are $(b-1)b^{(n-5)}$ of these, noting that the equilibrating force at C comes from one (or more) of CFO*, CGP* and CHQ* vibrating in-phase with ABC and that the equilibrating forces at D and E arise similarly. Hence if n is even M_2, the total number of independent modes at $\alpha = (i-\frac{1}{2})\pi$, is $(b-1)\{b^{(n-3)}+b^{(n-5)}+\ldots+b\} + 1$ whereas if n is odd the member at level 0 will not participate so we can neglect the 'extra mode' which occurs when there is an even number of levels, giving $(b-1)\{b^{n-3}+b^{n-5}+\ldots+1\}$ independent modes. Summing these series gives

$$\left.\begin{aligned} M_2 &= (b^{(n-1)}+1)/(b+1) \qquad \text{(n even)} \\ &= (b^{(n-1)}-1)/(b+1) \qquad \text{(n odd)} \end{aligned}\right\} (1)$$

The above arguments can be extended to obtain the mode multiplicities M_k for any k. In effect such modes are clamped at node levels n-ik (i=1,2,...,int(n/k)) and hence

$$\left.\begin{aligned} M_k &= (b-1)(b^{(n-1)} - b^{(t-1)})/(b^k - 1) + \text{int}(t/k) \qquad (k = 1,2....) \\ t &= n - k \ \text{int}\{(n-1)/k\} \end{aligned}\right\} (2)$$

Note that when k=2 equation (2) gives both the n even and n odd cases of equation (1).

Current studies include: fragmentation of all of the above multiple eigenvalues due to the introduction of a potential, which modifies the Sturm-Liouville equation to $-y'' + qy = \lambda y$ and; trees of fourth and higher order Sturm-Liouville equations. In structures, these repectively correspond to axial vibration of trees of tapered bars and to flexural vibration of trees of beams.

REFERENCES

1. F.W.Williams and W.H.Wittrick, An automatic computational procedure for calculating natural frequencies of skeletal structures, *Int. J. Mech. Sci.*, **12:9**, 1970, 781–791.

2. W.H.Wittrick and F.W.Williams, An algorithm for computing critical buckling loads of elastic structures, *J. Struct. Mech.* **1:4**, 1973, 497-518.

3. A.V.Sobolev and M.Solomyak, Schrodinger operator on homogenous metric trees: Spectrum in gaps, *Revs. Math. Phys.*, **14:5**, 2002, 421-467.

4. F.W.Williams, Natural frequencies of repetitive structures, *Q. J. Mech. Appl. Math.*, **24:3**, 1971, 285–310.

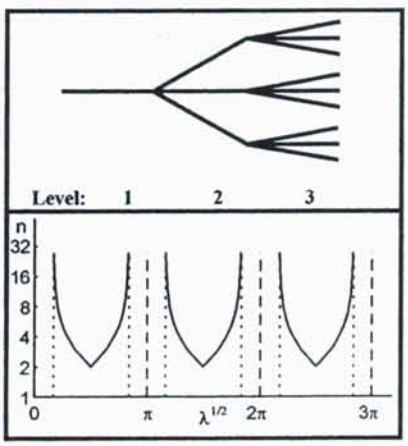

Figure 1. A tree with b=3 and n=3 and its spectrum for b=3 and $2 \le n \le 27$ (short dashed lines are limits of band as $n \to \infty$).

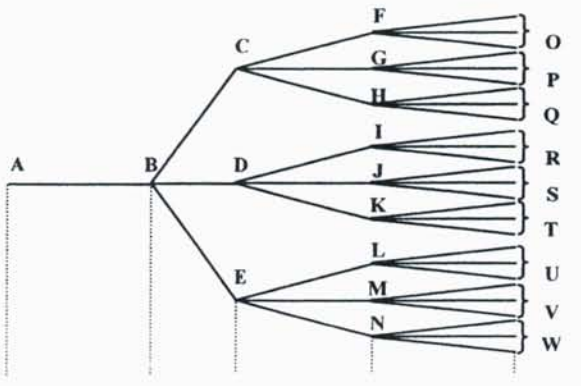

Member/edge:
0 1 2 3 (=n-1)
Node/vertex:
0 1 2 3 4 (=n)

Figure 2. Four level tree with b=3

ON THE FREE VIBRATION OF FULLY-FREE AND PINNED SPHERICAL SHELLS

Philippe Young
School of Engineering and Computer Science, University of Exeter

The free vibration of both fluid-filled and empty multi-layered hollow spherical shells has been studied with a focus on understanding the response of the human head to impact.

For the fully free case the emphasis was placed on the behaviour of the first ovalling (n = 2) mode of spheroidal oscillation as material and geometric parameters are varied. The motivation for focusing our attention on this mode is a parametric study (Young and Morfey [1]) on the response of a fluid-filled shell to a radially applied force, which has shown that both the onset of dynamic pressure effects in a fluid-filled shell and the magnitude of the observed pressures can be very accurately predicted by the ratio of the impact duration to the period of oscillation of the first ovalling mode. Numerical results obtained using the full three dimensional elasticity equations are compared with results obtained using simpler membrane and shell theories to explore the range of applicability of these theories. It is shown that for a remarkably wide range of geometric and material parameters, which encompass values typical for the human head, the first ovalling mode of a fluid-filled shell behaves like a membrane filled with incompressible fluid and a simple closed form expression is derived which closely approximates the natural frequencies obtained using the exact three dimensional equations.

The period of oscillation of the first few axi-symmetric modes of vibration of a pinned fluid-filled shell were then explored. The motivation for this was the prediction of impact duration for blunt unprotected head impact. Again a number of interesting results were obtained and will be discussed.

1. Young, P.G. and Morfey, C.L., 1998, "Intra-cranial pressure transients caused by head impacts," Proceedings of the 1998 IRCOBI Conference on the Biomechanics of Impact, pp.391-403.

AN EXACT DYNAMIC STIFFNESS METHOD FOR THE FREE VIBRATION PROBLEM OF NON-UNIFORM BEAMS

Si Yuan*, Cheng Xiao*, Kangsheng Ye* and F. W. Williams**

** Dept of Civil Engineering, Tsinghua University, Beijing, 100084, China*

*** Dept of Building and Construction, City University of Hong Kong, Kowloon, Hong Kong*

INTRODUCTION

When exact dynamic stiffnesses are used for solving free vibration problems of skeletal structures, continuous systems are reduced to the transcendental matrix eigenproblem

$$\mathbf{K}(\omega)\mathbf{D} = \mathbf{0} \tag{1}$$

where ω is the circular frequency, $\mathbf{K}(\omega)$ is the global dynamic stiffness matrix and $\mathbf{D}$ is the joint displacement amplitude vector, which becomes the mode vector at the natural frequencies.

The most successful and reliable methods for computation of the natural frequencies from (1) are those based on the Wittrick-Williams (WW) algorithm[1], which gives the total number of frequencies below an arbitrary trial value as being

$$J = J_0(\omega^*) + s\{\mathbf{K}(\omega^*)\} \tag{2}$$

Here $s\{\mathbf{K}\}$ is the sign count of $\mathbf{K}$, which equals the number of negative leading diagonal elements of the upper triangular matrix $\mathbf{K}^{\Delta}$ obtained from $\mathbf{K}$ by ordinary Gaussian elimination, and J_0 is the total number of so-called member fixed-end natural frequencies $\omega_{\mathrm{F},i}$ that are below ω^*. Repeating (2) for different ω^* yields several alternative iterative methods[3] that effectively narrowly bound the sought frequency to the desired accuracy.

The above dynamic stiffness method (DSM) is considered to be exact if: (a) the exact dynamic stiffnesses are used in $\mathbf{K}(\omega)$ and; (b) J_0 can be exactly counted, which in turn implies the exact evaluation of the $\omega_{\mathrm{F},i}$ for each individual member. For uniform members in skeletal structures, this can be achieved conveniently, whereas great difficulty exists for non-uniform members, i.e. for members with variable cross-sections. Therefore this paper considers the exact calculation of the fixed-end natural frequencies $\omega_{\mathrm{F},i}$ of non-uniform beams and their associated vibration modes.

THE MAIN IDEA

The vibration problem of fixed-end non-uniform beams can be expressed as the fourth order ODE eigenproblem

$$\begin{aligned} &(EI(x)v'')'' - \lambda m(x)v = 0, \qquad EI, m > 0, \quad 0 < x < L \\ &v(0) = 0, \quad v'(0) = 0, \quad v(L) = 0, \quad v'(L) = 0 \end{aligned} \tag{3}$$

where: $\lambda = \omega^2$; $EI(x)$ and $m(x)$ show that the flexural rigidity and mass per unit length vary with x and; v is the mode function. Problem (3) is a special case of the fourth order Sturm-Liouville (SL) problem, which can be solved by any general code for solving fourth order SL problems. However, the fourth order SL problem is very challenging and to the authors' best knowledge, the only recent code that directly and specially solves such problems is SLEUTH[2]. The present paper, however, presents an alternative solution method, which uses the exact dynamic stiffness method and any of the available standard adaptive linear ODE solvers.

The main idea of the proposed method is based on the fact that the WW algorithm (2) becomes particularly simple if all $\omega_{\mathrm{F},i} > \omega^*$ (i.e. $J_0 = 0$). This can be achieved by appropriately subdividing members into sufficient sub-members to give the following simple solution strategy.

(1) *Mesh Generation*: divide the beam into sufficient sub-members for every $\lambda_{F,i}$ of them all to exceed the trial value λ^*, thus eliminating the difficult need to calculate J_0;

(2) *Calculation of Stiffnesses*: calculate exact dynamic stiffnesses by solving the governing ODEs using a standard adaptive linear ODE solver, so that the variable cross-sections are exactly modelled, which virtually eliminates any discretisation errors;

(3) The rest is the same as in the usual DSM and the most recent method[3] has been used in this paper, which can quickly produce highly accurate frequencies and mode vectors.

ADDITIONAL DETAIL

In the following, some key treatments are explained in greater detail.

(1) Mesh Generation

The mesh to be generated should be sufficiently fine to raise the minimum $\lambda_{F,1}$ in each sub-member high enough to exceed the upper bound of the group of sought eigenvalues, but should not be unnecessarily fine, so as to avoid excessively increasing the computational effort.

a) ***Initial mesh***. The initial goal is aimed at finding a set of appropriate bounds for the sought frequencies. Since there is not much information provided, a uniform mesh (say N uniform sub-members) can be used for simplicity, even though more sophisticated approaches exist. Then two models of piecewise constant cross-sections are considered as shown in Fig. 1, where the lower/upper bound model uses the m and EI values at which m/EI is maximum/minimum for the considered sub-member. Then the usual DSM is applied to the two models to roughly determine (say by using bisection) two sets of the sought eigenvalues, which form both lower and upper bounds for each natural frequency required.

b) ***Optimum mesh***. When initial bounds have been obtained by a), more accurate frequencies and mode vectors are computed one by one by using the exact model and an optimum mesh, which should use a minimum number of sub-members for which all $\lambda_{F,i}$ are greater than the upper bound λ_u of the largest eigenvalue being sought. This can easily be done by using the fact that, for a uniform beam, the minimum dimensionless $\lambda_{F,1}$ can be directly calculated in a straightforward way, and therefore each sub-member length l can be determined by $l \le 4.73004 \Big/ \sqrt[4]{\lambda_u \max\left(m/EI\right)}$. Repeated use of this formula from one end of the beam to the other generates an optimum mesh.

(2) Stiffness Calculation

For optimum meshes, the exact dynamic stiffnesses are used, the calculation of which, taking k_{i1} as an example, can be achieved by solving the following linear ODE problem

$$(EI(x)v'')'' - \lambda^* m(x)v = 0 \text{ with } v(0) = 1, \quad v'(0) = 0, \quad v(l) = 0, \quad v'(l) = 0 \tag{4}$$

Then k_{i1} can be obtained from the above solution v by simple calculations. In addition, the derivative k'_{i1} with respect to λ, which is used to form the exact mass matrix[3], can also be obtained by solving the different linear ODE problem

$$(EI(x)\tilde{v}'')'' - \lambda^* m(x)\tilde{v} = m(x)v \text{ with } \tilde{v}(0) = 0, \ \tilde{v}'(0) = 0, \ \tilde{v}(l) = 0, \ \tilde{v}'(l) = 0 \tag{5}$$

Hence numerically exact dynamic stiffnesses and their derivatives can be obtained conveniently and reliably by using any standard adaptive linear ODE solver

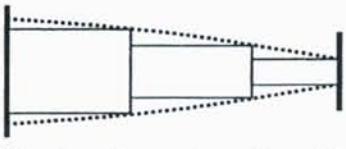

Fig. 1a Lower bound model

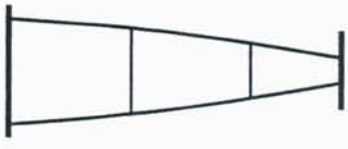

Fig. 1b Exact model

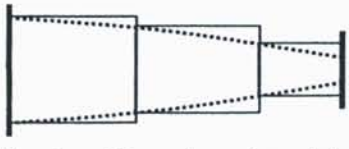

Fig. 1c Upper bound model

Table 1 Results for Example 1

Frequency Index	This Paper		SLEUTH [2]	
	ω	Time (Sec)	ω	Time (Sec)
1	31.67264485	0.070	31.67264514	0.040
5	378.1937270	0.050	378.1937293	0.060
10	1388.283922	0.080	1388.283936	0.120
⋮	⋮	⋮	⋮	⋮
40	20747.72295	0.270	20747.72313	1.192
45	26188.78994	0.310	26188.79018	1.091
50	32262.54698	0.340	32262.54728	1.603
Total Time		9.293		30.92

Table 2 Results for Example 2

Frequency Index	This Paper		SLEUTH [2]	
	ω	Time (Sec)	ω	Time (Sec)
50	10587.28984	0.411	10587.28995	0.691
55	12787.56186	0.451	12787.56199	1.011
60	15195.40670	0.501	15195.40685	0.901
⋮	⋮	⋮	⋮	⋮
85	30348.22327	0.701	30348.22355	1.472
90	34001.50504	0.731	34001.50538	1.602
95	37862.35965	0.771	37862.36003	1.763
Total Time		29.89		61.00

NUMERICAL EXAMPLES

Two examples are shown in this section to exhibit the efficiency and validity of the proposed method. The solutions are compared with those obtained using SLEUTH[2]. For both examples and for both the present method and SLEUTH, the error tolerance was set as $Tol = 10^{-8}$. The exact dynamic stiffnesses were calculated by using the ODE solver COLSYS[4].

Example 1. $EI(x) = 3 + \sin(x)$, $m(x) = 2 + \sin(10x)$, $L = 1$

The first 50 natural frequencies and mode functions were computed and the natural frequencies are shown in Table 1, in which both the time needed to find individual natural frequencies and the total time taken are given.

Example 2. $EI(x) = (x+1)^3/12$, $m(x) = x + 1$, $L = 1$

The 50th to 99th frequencies and mode functions were computed, see Table 2.

SUMMARY AND ACKNOWLEDGEMENTS

Although the proposed method is only at a preliminary stage, so far it works very well and is much faster than the general code SLEUTH. This suggests great potential for further development.

This work was jointly supported by the National Natural Science Foundation of China, Ministry of Education of China and by grant GR/R05437/01 from the Engineering and Physical Sciences Research Council of the UK.

REFERENCES

1. W. H. Wittrick and F. W. Williams, A general algorithm for computing natural frequencies of elastic structures, *Q. J. Mech. Appl. Math.* 24(1971), 263-284.
2. L. Greenberg and M. Marletta, The code SLEUTH for solving fourth order Sturm-Liouville problems, *ACM Trans. Math. Software* 23(1997), 453-497.
3. Si Yuan, Kangsheng Ye, F. W. Williams and D. Kennedy, Recursive second order convergence method for natural frequencies and modes when using dynamic stiffness matrices, *Int. J. Num. Meth. Eng.*, accepted in 2002.
4. U. Ascher, J. Christiansen and R. D. Russell, Algorithm 569, COLSYS: Collocation software for boundary value ODEs[D2], *ACM Trans. Math. Software* 7(1981), 223-229.